Resonances in the $\pi^+\pi^-$ mass spectrum in hadronic decays of Z^0

Diplomarbeit

zur Erlangung des akademisches Grades

Magister rer. nat.

an der

Naturwissenschaftlichen Fakultät

der

Leopold-Franzens-Universität Innsbruck

eingereicht von: **Krebs Wolfgang**

geboren am 19.November 1973

in Innsbruck

Innsbruck, am 23.6.2000

Contents

List of Figures

List of Tables

Acknowledgements

I would like to thank Prof. Dietmar Kuhn for inviting me into the High Energy Physics group of Innsbruck, I have enjoyed the work tremendously. Special thank to my supervisor Univ. Doz. Gerald Rudolph for his support and guidance throughout the whole time working on my diploma thesis.

I would also like to thank Dr. Emmerich Kneringer for his help on computing problems and for his continued interest and discussion. Thanks also to Vasile Ghete and Armin Nairz for discussions and being friends.

Thankyou also to my parents for the support and the understanding during my whole study.

Last, I thank my wife Karin for her understanding during the whole time I was working on this diploma thesis and my study, having less time and for her love.

Chapter 1

Introduction

Es ist meine innere Überzeugung,
dass die Entwicklung der Wissenschaften
sich in der Hauptsache auf die Bedürfnisse
der reinen Erkenntnis gründet.
1920; Einstein A

The notion that a fundamental simplicity lies below the observed diversity of our world has carried physics far. In the past decades many different concepts for forces and for the particles have been developed. During the last 50 years many ideas converged to one theory and it seems that a final solution gets closer and closer.
Today particles physics tries to find models which describe the interaction between the smallest particles of our world. A fast look into the Particles Data Tables reveals the richness and variety of the hadron spectrum. This number increased dramatically with the use of the first high energy accelerators. Whereas the LEP collider is one of them, the first task of the LEP was the production of the Z^0. The hadronic decays of the Z are of special interest since they help to understand how the production of particles works out of a $q\bar{q}$ pair. The idea of the quarks has its origin in the early 60's and with the group-theoretical model of Gell-Mann and Zweig ([29, 17] it was possible to categorize the whole particle zoo built of the fundamental particles. The hadrons form so called multipletts with different angular momentum and particles of three different multipletts (Scalar- ,Vector- ,Tensor- mesons) have been treated within this work. The forces that act within this small dimensions are the electro-magnetic, strong and weak interactions. Whereas the weak and the electro-magnetic can be described with an adequate theory and many processes can be calculated, the strong interactions are not that easy to handle since the concept

of pertubation theory works in certain circumstances and fails at low momentum transfer. Therefore it is necessary to develop models which describe the experimental situation as best as possible. These models need to be tuned to real data and need particle characteristics as input. Exactly this input is the motivation of this work and the aim should be to measure all particles available.

The ρ^0 has been analyzed by ALEPH in the past only with low statistics and therefore this measurements have been repeated. Additionally the f_2 and the f_0 have been included into this analysis too since both haven't been measured by ALEPH up to now. The multiplicity and the fragmentation functions have been extracted.

It is also a fact that the theory includes many phenomena of which not all consequences have been studied. The Bose Einstein correlations are such a phenomenon. The concept of BE correlation has been used in this analysis to explain some distortion in the data. The results have been compared to other measurements and also to existing models.

The work starts with a short introduction into the theory behind and a explanation of the processes that have been treated. A brief discussion of the used Monte Carlo model is also provided by the theory section. The second part of the work deals with experimental details and introduces at first the accelerator and the detector. The following chapter describes the analysis itself with most of the technical details. The last step is the presentation of the results and its discussion.

Chapter 2

Theoretical foundations and motivation

Within the scope of this work I will, as already mentioned in the introduction, analyze the production of light, neutral mesons ($\rho(770)$,$f_0(980)$,$f_2(1270)$), which can be observed in the $\pi^+\pi^-$ mass spectrum. These resonances are produced in the process $e^+e^- \rightarrow Z^0 \rightarrow q\bar{q}$, for the description of which a fundamental understanding of the theory behind is crucial. In the following sections I will therefore discuss the central formulations.

2.1 $e^+e^- \rightarrow$ hadrons

In an annihilation of e^+ and e^-, in which the centre of mass energy E_{cm} reaches at least the value of 91.2 GeV the production of the Z^0 dominates the cross- section [26]. With the given probability of 69% the Z^0 turns into a hadronic final state. Another possible decay, but ignored in this treatment because its irrelevancy for this analysis, is the leptonic channel. Schematically the whole process $e^+e^- \rightarrow$ hadrons can be depicted in the following manner (fig. 2.1). This picture we should keep in mind for our further considerations.

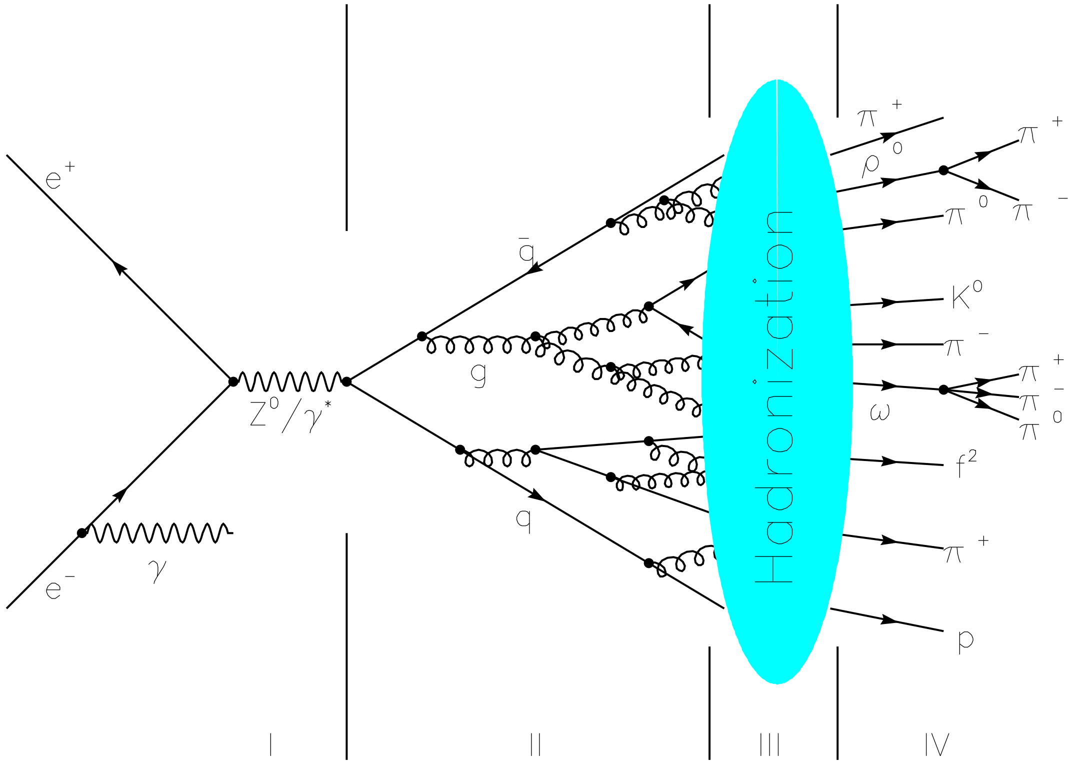

Figure 2.1: $e^+e^- \rightarrow$ hadrons

We can subdivide this process into 4 sections.

I. e^+e^- annihilates into a Z^0- resonance which propagates corresponding to its lifetime $\tau \sim 10^{-25}$ until it decays into a highly virtual quark-antiquark pair. One problem which must not be neglected is the emission of photons by the incoming electron (positron), (i.e. the initial state radiation), because this radiation reduces the available energy in the CM - system and affects the final cross - section. The correct description for this stage is provided by the electroweak theory.

II. The emission of gluons by the primary quarks respectively the splitting of gluons into $q\bar{q}$-pairs follows the laws of the perturbative QCD down to a certain virtuality limit. (The limit is fixed by the requirements for validity of perturbation theory.) This part of the process is called **parton- shower**.

III. Beyond this limit the hadronization starts. Within this phase the colored partons turn into white hadrons. Since perturbative Ansätze do not work any longer we have to switch to completely phenomenological models - which of course have to be tuned in order to get the best approximation to the data.

IV. The decay of the unstable hadrons into lighter particles that can be registered by a detector completes the process -chain. We find pions, kaons, protons, leptons, photons and neutrons.

However, there are several ideas (theories) appropriate to describe the underlying physics. Most of them have been implemented in the so called **standard-model**.

2.2 The Standard-model

The standard-model embodies our knowledge about the strong- as well as the electro- weak interactions. As fundamental constituents the model has implemented spin $\frac{1}{2}$particles, categorized into three families and provides a description for the force mediating spin 1 gauge bosons. To explain the masses of these weak gauge bosons a scalar Higgsfield necessarily has to be introduced. The latter field causes the spontaneous symmetry breaking which is a central concept of the electroweak standard-model. Up to now the standard-model requires 19 parameters [1] that can't be explained by the model itself and must be determined through experiments. By the way it has to be stressed that various Ansätze made to unify all forces could not reach the high quality of the standard model.

2.2.1 The electroweak theory

In 1967, Glashow, Salam and Weinberg [35] have introduced the theory of electroweak interaction and have so unified the two theories considered independent up to this date: the theory of electromagnetic- and that of weak- forces. The final result has been a renormalizeable gauge invariant theory which is based on the gauge group $SU(2) \times U(1)$. Gauge invariance related to $SU(2)$ and $U(1)$ can be obtained by introducing the gauge fields W_μ^i $i = 1, 2, 3$ respectively B_μ.
Fermions form weak isospin doublets but according to the non conservation of parity in weak interactions only the left-handed part of the eigenstate can contribute. Consequently the remaining right handed states form singlets. According to the weak hyper-charge $Y = Q - I_3$ that connects the electric charge Q and the third component of the isospin I it is possible to characterize the elementary fermions as shown in Tab.2.1.

As shown in Table 2.1 the eigenstates d'_L,s'_L,b'_L are specially marked because they are no mass -eigenstates:

[1] 3 weak mixing angles Θ_1, Θ_2, Θ_3, m_H, 12 masses of the quarks(leptons), 3 coupling-constants - α_1, α_2, α_3

fermions			Q	I_3	Y	
ν_{e_L}	ν_{μ_L}	ν_{τ_L}	0	$\frac{1}{2}$	-1	leptons
e_L^-	μ_L^-	τ_L^-	-1	-$\frac{1}{2}$	-1	
e_R^-	μ_R^-	τ_R^-	-1	0	-2	
u_L	c_L	t_L	$\frac{2}{3}$	$\frac{1}{2}$	$\frac{1}{3}$	quarks
d'_L	s'_L	b'_L	-$\frac{1}{3}$	-$\frac{1}{2}$	$\frac{1}{3}$	
u_R	c_R	t_R	$\frac{2}{3}$	0	$\frac{4}{3}$	
d_R	s_R	b_R	-$\frac{1}{3}$	0	-$\frac{2}{3}$	

Table 2.1: fundamental fermions as categorized in the standard electroweak model; left-handed doublet-states (indexed with L) and right-handed singlet- states (indexed with R) with their characteristic quantum numbers of isospin and hyper-charge;

In order to explain the transition from an u to a s- quark ($K^+ \rightarrow \mu^+\bar{\nu}_\mu$), the Cabibbo - angle has been introduced. Additional studies and results made the extension of this angle to the full CKM (Cabibbo-Kobayashi-Maskawa)-mixing matrix V_{ij} [30] necessary, which is the connection between the lagrangian eigenstates d',s',b' and the mass eigenstates d,s,b via the relation $q'_i = \sum_i V_{ij} \cdot q_j$.

The components of the CKM matrix are composed of up to 4 parameters (3 angles θ_1,θ_2,θ_3 and 1 phase δ) in which the phase δ includes an option for CP-violation.[21]

To introduce the last missing constituent of the theory we have to treat the gauge bosons. The eigenstates of the two W bosons can be deduced directly from SU(2) invariance and require two gauge fields (Equ.2.1) for their construction.

$$W_\mu^\pm := \frac{1}{\sqrt{2}}(W_\mu^1 \mp iW_\mu^2) \tag{2.1}$$

If we include U(1) invariance it is possible to derive two further neutral gauge bosons, the Z^0 and the photon. Therefore we must first introduce the weak mixing angle θ_W, and second combine this with the two remaining fields (W_μ^3,B_μ), so we can define this new bosons Equ.2.2 - 2.3.

$$A_\mu := W_\mu^3 \sin\theta_W + B_\mu \cos\theta_w \tag{2.2}$$

$$Z_\mu := W_\mu^3 \cos\theta_W - B_\mu \sin\theta_W \tag{2.3}$$

Originally the theory was based on the idea of massless bosons as it is valid for the photon. In order to explain the short-ranged weak forces , however the bosons of weak interaction are demanded to have mass. Only by introducing a complex higgs-doublet $\phi = \begin{pmatrix} \phi^+ \\ \phi^0 \end{pmatrix}$ that leaves the theory still gauge invariant, through the interaction of the bosons with this field, a mass can be assigned to the gauge bosons. The quantum of this field is the Higgs particle. Its mass is unknown and the discovery of this particle is one of most important tasks for the future. Due to a nonzero expectation value ρ_0 of the Higgs field however, the symmetry of the theory is spontaneously broken. The requirement that the photon and the neutrino remain massless fix the orientation of the Higgs field within the SU(2). Thus we obtain $m_W = \frac{g\rho^0}{2}$ and $m_Z = \sqrt{g^2 + g'^2}\frac{\rho^0}{2}$ (where g and g' represent the coupling constants of the electroweak theory.) Summarising all these thoughts, we obtain following lagrangian.

$$\begin{aligned}
\mathcal{L}_{\mathcal{F}} &= \sum_i \bar{\psi}_i \left(i\gamma^\mu \partial_\mu - m_i - \frac{g m_i H}{2M_W} \right) \psi_i \\
&\quad - \frac{g}{2\sqrt{2}} \sum_i \bar{\psi}_i \gamma^\mu (1 - \gamma^5)(T^+ W_\mu^+ + T^- W_\mu^-)\psi_i \\
&\quad - e \sum_i q_i \bar{\psi}_i \gamma^\mu \psi_i A_\mu \\
&\quad - \frac{g}{2\cos\theta_W} \sum_i \bar{\psi}_i \gamma^\mu (v^i - a^1 \gamma^5) \psi_i Z_\mu
\end{aligned} \tag{2.4}$$

g ang g' are the coupling constants belonging to SU(2) and U(1) respectively. Since it's a unifying theory, all coupling constants fulfil the relations.

$$e = g \sin\theta_W = g' \cos\theta_W \qquad with \quad \tan\theta_W = \frac{g'}{g} \tag{2.5}$$

The second and the third term correspond to the interaction of the charged weak current respectively the electro-magnetic interaction. T^+ and T^- are the ladder - operators of the weak isospin. Recalling the introductory picture (Fig.2.1) we see that for our problem mainly the 4th term, of Eqn. 2.4 (the interaction of neutral weak currents) is of interest. Namely in this term we identify the vector and the axial coupling:

$$v^i = I_3(i) - 2Q_i \sin^2\theta_w \tag{2.6}$$

$$a^i = I_3(i) \tag{2.7}$$

To recognise the implications of these coupling terms, we have to write down the cross section for the process $e^+e^- \to Z^0/\gamma^* \to q\bar{q}$ [41].

$$\sigma_0 = \frac{4\pi\alpha^2\kappa^2}{3\Gamma_Z^2}(a_e^2 + v_e^2)(a_f^2 + v_f^2) \tag{2.8}$$

$$\Gamma_Z = \frac{\alpha M_Z}{3}(\sum_l (v_l^2 + a_l^2) + N_C(1+\frac{\alpha_S}{\pi})\sum_q (v_q^2 + a_q^2)) = 2.5GeV \tag{2.9}$$
$$\kappa = \frac{\sqrt{2}G_F M_Z^2}{16\pi\alpha}$$

This formula (eqn. 2.8) is valid as long as the center of mass energy is near the Z pole because only in this range we can neglect the contribution of annihilation into a photon. When calculating the vector-, axial-couplings for the quarks with the given values of I_3 and Y (see tab. 2.1) we see that at $E_{CMS} = M_Z$ the production of d-quarks is preferred. (production-probabilities: u,c $\sim$ 17%;d,s,b$\sim$ 22%) By the way in contrast to the Z^0 the photon couples stronger to the u-quark. This happens due to the larger charge which gets important above the Z mass. Summed up for all quark flavours we get a $\sigma = 41.469 \pm 0.016$ nbarn [20]. Taking into account the initial state radiation this value is corrected and reduced to $\sigma = 30.5 \pm 0.1$ nbarn. In the following section we have to treat the next step in fig 2.1 , the parton- shower, which is part of the QCD calculations.

2.2.2 The theory of strong interactions - QCD

Quantum **C**hromo **D**ynamics (QCD), the theory of the strong forces [21, 22, 40], can explain - at least qualitatively - all measurements of strong interaction. The non abelian theory of colour charges is based on the gauge group $SU(3)_C$.

Originally the quark model, developed by Gell-Mann and Zweig [29] in the early 60's, has been introduced to resolve the problem of the large number of new particles on a fundamental level. This theory is the theoretical basis to explain many of the observed phenomena and enables us to categorize the particles into mesons (quark- antiquark states)and baryons (3 quark states) which than build octets, nonnets and decuplets.

On the other hand the theory failed in explaining the wave-function of the Δ^{++}, because fermion spin statistics forbids a totally symmetric wave-function for the Δ^{++} ($= u^\uparrow u^\uparrow u^\uparrow$) as it would be predicted by the theory. A further degree of freedom (the colour) has been introduced, to ensure a total antisymmetric wave-function for the Δ^{++}. Therefore we need at least three different colours (**R**ed, **G**reen, **B**lue) which lead to the following wave-function $\Delta^{++} = \frac{1}{\sqrt{6}}\epsilon^{\alpha\beta\gamma}|u_\alpha^\uparrow u_\beta^\uparrow u_\gamma^\uparrow\rangle$.

Since no colored hadrons have been observed, all states must be singlet states (singlets under rotations in the colour space).

$$\begin{aligned} |Baryons\rangle &= \frac{1}{\sqrt{6}}\epsilon^{\alpha\beta\gamma}|q_\alpha q_\beta q_\gamma\rangle && (2.10) \\ |Mesons\rangle &= \frac{1}{\sqrt{3}}\delta^{\alpha\beta}|q_\alpha \bar{q}_\beta\rangle && (2.11) \end{aligned}$$

Also the attempt to find free colored quarks has not been successful, which is taken into account by the theory with the concept of **confinement**.
As stated before it is not possible to measure the colour directly and so several tests have been made to prove and establish this new quantum number. The measurement of the ratio $R = \frac{\sigma_{ee\rightarrow hadrons}}{\sigma_{ee\rightarrow \mu\mu}}$ and also the decay of the π^0 into 2 γ confirmed the number of colours (N_C)= 3.

The force mediating particles (gluons) couple to the colour charge, but in contrast to the other theories (e.g. QED) also the gauge bosons carry colour and can therefore interact with each other. The gluons are a consequence of local SU(3) gauge invariance. To receive this invariance we have to introduce, corresponding to the 8 generators, 8 gauge fields. Using their fundamental representation we can describe the fields of matter; for the gauge bosons (gluons) we have to apply the adjoint representation. Both representations are related to the Casimir operators (C_A, C_F) defined through (2.12, 2.13) which we should keep in mind for later considerations.

$$\begin{aligned} \sum_{r=1}^{8} t^r_{ij} t^r_{jk} &= C_F \delta_{ik} = \\ &= \frac{n^2-1}{2n}\delta_{ik} = \frac{4}{3} && (2.12) \\ \sum_{r,s=1}^{n^2-1} f^{rst}\cdot f^{rsu} &= C_A \delta^{tu} = 3 && (2.13) \end{aligned}$$

Combining all stated requirements we can write the QCD - Lagrangian in the following manner:

$$\begin{aligned} \mathcal{L}_{QCD} &= -\frac{1}{4}F^r_{\mu\nu}F^{r\mu\nu} + \sum_q \bar{\psi}^a_q(i\gamma^\mu D_{\mu ab} - m^q\delta_{ab})\psi_{qb} && (2.14) \\ D_{\mu ab} &= \partial_\mu \delta_{ab} + ig_s t^r_{ab} G^r_\mu(x) && (2.15) \\ F^A_{\mu\nu} &= \partial_\mu G^r_\nu(x) - \partial_\nu G^r_\mu(x) - g_s f^{rst} G^s_\mu G^t_\nu && (2.16) \end{aligned}$$

G_μ are the gluon fields; ψ_K represents the quark spinors with the flavour K;
The lagrangian gets complete with additional gauge fixing- and ghost- terms I omit here. Of special interest is the third term of the field strength tensor $F^{\mu\nu}$: $g_s f^{rst} G^s_\mu G^t_\nu$
With this expression the theory takes into account the self coupling of the gluons which is the basis for the asymptotic freedom. (Asymptotic freedom is the behaviour of quarks at high momentum transfer in which they act as free particles within the hadrons .) The total antisymmetric

structure constant of the SU(3), f^{rst} has to full-fill the commutation relations 2.17 together with the generators of the group t^r_{ij}

$$[t^r, t^r] \;=\; i f^{rst} t^t \tag{2.17}$$

$g_S(=\sqrt{(2\alpha_S hc)}$ is the coupling constant for strong interactions. As already known from QED it is not constant , but it is running with the energy. Since we have to remove ultraviolet divergences coming from (higher order) loop diagrams, we must renormalize the field and also the couplings. Therefore using one of the resummation schemes ($\bar{M}S$,MS,...) dimensional regularisation is applied and results in a running QCD coupling constant. With one loop calculations we obtain:

$$\alpha(Q^2) \;=\; \frac{\alpha(\mu^2)}{1-\frac{\beta_1\alpha(\mu^2)}{2\pi}\ln\left(\frac{Q^2}{\mu^2}\right)} \tag{2.18}$$

$$\beta_1 \;=\; \frac{2N_f - 11N_C}{6} \tag{2.19}$$

The beta function coefficient β_1 (2.19) and the scale μ are components of the renormalization group equation (see [21]). The behaviour of α_S with increasing energy is Eqn. 2.20.

$$\lim_{Q^2\to\infty} \alpha_S(Q^2) \;=\; 0 \tag{2.20}$$

This behaviour, known as asymptotic freedom, enables us to do perturbative calculations. This freedom results from the self coupling of the gluons which causes an anti- screening effect instead of screening as already known from QED. Equation 2.18 we can be rewritten if we substitute the scale μ with the Λ_{QCD} parameter. This parameter defines the limit below which non perturbative effects are important. If we desire more accurate results, we must in any case include higher order calculations which in most of the cases can be stopped at second order.

A further property of QCD is the confinement which solves the problem of the non observable free quarks. Up to now only the qualitative explanation, used in several **M**onte **C**arlo models, exists according to which an assumed potential $V(r) = kr$, makes it impossible for quarks to escape. Due to the running coupling which allows the use of perturbation theory only for small distances (high momentum transfer) its difficult to do calculations at large distances. ——————- MC ——————————————————-

2.3 Monte Carlo - Perturbative QCD and Hadronization

To complete the chapter of strong interactions I will discuss the perturbative QCD and the hadronization. Due to the high multiplicity and the complex event structure in hadronic Z^0 decays its difficult to perform analytical calculations. That is one reason why **M**onte **C**arlo computations are an essential part of high energy physics.

perturbative QCD:	This is the part of QCD where α_S is small enough that the perturbation theory applicable. The MC works with several analytical and semi-analytical Ansätze. In this case the main reason for using a MC method are the high multiplicities which we have to deal with.
non perturbative QCD:	Due to the too large perturbative evolution parameter (the coupling) we can't use for these calculations, also known as hadronization or fragmentation, the perturbation theory. Therefore we must rely on phenomenological models.

2.3.1 Perturbative QCD

As shown in fig. 2.1, phase II, the two primary produced quarks can radiate gluons and can initialize a subsequent parton cascade.
For a theoretical approach the following two methods can be used:

(1) Matrix Element Method
This method is based on an exact order by order calculations (all contributing Feynman diagrams must be taken into account). Due to its increasing computational effort, this method is available only up to $\mathcal{O}(\alpha_S^2)$.

The cross section for the tree level has already been given during the discussion of the standard-model. (see eqn. 2.8). Adding single gluon radiation to the Born level cross-section we obtain [41]:

$$\frac{d^2\sigma}{dx_q dx_{\bar{q}}} = \sigma_0 \frac{C_F \alpha_S}{2\pi} \frac{x_q^2 + x_{\bar{q}}^2}{(1-x_q)(1-x_{\bar{q}})} \tag{2.21}$$

$$\sigma_0 = \frac{4\pi\alpha^2}{3s} N_C \sum_{f=1}^{N_f} Q_f^2 \tag{2.22}$$

x_q, $x_{\bar{q}}$ and $x_g = 2 - x_q - x_{\bar{q}}$ correspond to the parton momenta divided by the total energy; $C_F = \frac{4}{3}$ is the colour factor related to the transition $q \to qg$;
This cross- section 2.21 becomes divergent for $x_g \to 0$ (soft gluon radiation) and for collinear gluons ($x_q \to 1$; $x_{\bar{q}}$ and x_g are collinear). Since assigning a mass to the gluons, the singularity can be removed. This divergence is also known as mass- divergence.

Of course these divergences are not of physical nature but arise from the breakdown of fixed order perturbation theory. We need the divergences of the loop diagrams to the $e^+e^- \to q\bar{q}g$ cross-section to cancel the $\mathcal{O}(\alpha_S)$ infrared divergences when calculating the total cross- section (eqn. 2.23).

$$\sigma(e^+e^- \to q\bar{q}) + \sigma(e^+e^- \to q\bar{q}g) + ... = \sigma_0(1 + \frac{\alpha_S}{\pi} + ...) \tag{2.23}$$

The ME- method is meaningful, only for a small number of partons in the final state. Otherwise we have to find alternatives of which the parton shower method is the preferred one.

(2) Parton- shower

For the PS (parton- shower) method only dominant terms are taken into account. It is a leading logarithm approximation (LLA) which receive its name from the perturbative expansion in terms of $\alpha_S \ln(\frac{Q^2}{\Lambda^2})$. Λ is the scale at which non perturbative effects become important. This method in its pure form is not that suitable for Monte Carlo calculations a more appropriate approach is the LUND-scheme which is a successive usage of probabilistic parton transitions. Each parton receives a virtuality $t = ln(Q^2/\Lambda^2)$ (often Q^2 is replaced with the transverse momenta p_t^2) in which this evolution- variable t is reduced in every transition. The probability for such a transition or splitting of a parton is given by the Sudakov- formfactor $S_a(t)$. This function uses the GLAP (Gribov-Lipatov-Altarelli-Parisi)- splitting- kernels $P_{a\to bc}$ which contain the relative probability $\mathcal{P}$ (eqn. 2.24) for a transition $a \to bc$.

$$\frac{d\mathcal{P}}{dt} = \int dz \frac{\alpha_{abc}(t)}{2\pi} P_{a\to bc}(t) \tag{2.24}$$

α_{abc} depends on the type of the transition:

QCD $\to \alpha_S$

electromagnetic $\to \alpha_{em}$

The splitting kernels $P_{a\to bc}$ are defined as follows: [21]:

$$P_{q\to qg} = C_F \frac{1+z^2}{1-z} \tag{2.25}$$

$$P_{g\to gg} = C_A \left(\frac{z}{1-z} + \frac{1-z}{z} + z(1-z) \right) \tag{2.26}$$

$$P_{g\to q\bar{q}} = T_R(z^2 + (1-z)^2) \tag{2.27}$$

As mentioned briefly in the previous section, the color factor (eqn.2.13,2.12) can be assigned to specific processes, because they control their probability The primary parton splits up corresponding to $S_a(t)$ [[36]] as long as the minimal cut off t_0 (Q $\sim \mathcal{O}(1GeV)$ = effective quark masses) has been reached. This limit is given by the breakdown of perturbation theory caused by the large α_S in this energy region. At this point we have to proceed to the hadronization-process.

2.4 Hadronization

The fragmentation contains the conversion of colored quarks and gluons into hadrons as shown by the 4^{th} phase of figure 2.1. The produced unstable hadrons decay into lighter particles which then can be detected. As stated above it is impossible to use perturbation theory at these large distances, but generally it must be remarked that the hadronization process in its details up to now couldn't be exactly understood. Therefore it is necessary to use fragmentation- models, of which we have three important possibilities:

- independent fragmentation
- cluster fragmentation
- string fragmentation

Since in this work I only use the QCD generator Jetset, which is based on the Lund string concept I will restrict my discussion on the latter model.

2.4.1 String fragmentation

Confinement is the motivation for this model. This concept uses a color flux tube (string) stretched along the line between two oppositely colored quarks which has transverse dimensions of typical hadronic size. A with the distance linearly rising potential V(r)$\sim \kappa r$ along the string ensures that quarks cannot escape ($\kappa = 1GeV/fm$). If quarks move apart, the energy stored in the string gets higher. The massless relativistic string breaks up when the stored energy is high enough to build a new $q\bar{q}$-pair. In the case of gluon emission the flux tube connects the quark with the gluon and the second gluon colour charge enables the string also to couple to the antiquark. For the further treatment of the string- fragments exist several interpretations, like continuous mass fragments, clusters, and discrete mass hadrons as used in the Lund scheme [2] In the latter fragmentation model, developed by the Lund - group [Sjostrand:93], the string- fragments build new $q\bar{q}$ pairs until the invariant mass of the string reaches the order of hadronic masses. The final fragments are interpreted as discrete mass hadrons. Due to the fact that it is impossible to produce such a quark- antiquark- pair in a space- time- point without violating the energy conservation, this production can be seen as a tunneling process. The distance d needed for production is given by the field strength and the mass of the new pair ($d = \frac{2m}{\kappa}$).

We can see that heavy quark production (charm, bottom) is strongly suppressed in hadronization ($u : d : s : c \sim 1 : 1 : 0.3 : 10^{-13}$). When all fragments have reached the mass limit this algorithm stops.

These QCD generators contain a lot of parameters, specially for the hadronization- part. To describe the data as well as possible it is necessary to tune the MC with several fits of eventshape and single charged particle observables. The parameters for Jetset which have been used in this analysis are shown in Tab. 2.2 ([33, 15, 36]).

[2]Reviews on this schemes can be found in [27].

Parameter	Value	Description
MSTJ 1	1	fragmentation scheme (string)
MSTJ 11	3	hybrid fragmentation
MSTJ 12	3	first baryon suppression(on)
MSTJ 26	0	no $b\bar{b}$ mixing
MSTJ 41	1	FSR off (=1) on (=2)
MSTJ 42	2	coherent branching for time like showers
MSTJ 43	4	z definition in branching; energy fraction in c.m. frame of the showering partons
MSTJ 44	2	α_S scale; running with $z(1-z)m^2$
MSTJ 46	0	no azimuthal correlations
MSTJ 47	3	corrections to the lowest order $q\bar{q}g$
MSTJ 101	5	parton shower is allowed to develop from an original $q\bar{q}$ pair
MSTJ 105	1	perform fragm. & decay within one step
PARJ 1	0.1079	qq/q
PARJ 2	0.2855	s/u
PARJ 3	0.6908	su/du
PARJ 11	0.5529	Vud
PARJ 12	0.4699	Vs
PARJ 13	0.65	Vcb
PARJ 14	0.12	$J^P = 1^+$
PARJ 15	0.04	$J^P = 0^+$
PARJ 16	0.12	$J^P = 1^+$
PARJ 17	0.20	L=1 $J^P = 2^+$
PARJ 19	0.5371	suppression factor for 1^{st} rank baryons
PARJ 21	0.3652	σ
PARJ 26	0.276	η' suppression factor
PARJ 41	0.40	a
PARJ 42	0.9058	b
PARJ 54	-0.040	ϵ_c
PARJ 55	-0.0035	ϵ_b
PARJ 81	0.3145	LLA
PARJ 82	1.4616	M_{min}
PARU 45	0.04	JADE ycut
MSTU 41	1	use all particles in the event analysis routines

Table 2.2: Jetset parameters

name	mass (MeV)	width (MeV)	L,S	I,$J^{P,C}$	description
ρ^0	770	150.7	0,1	$1,1^{--}$	Vektormeson
f_2	1270	185.5	1,1	$0,2^{++}$	Tensormeson
f_0	980	40 to 100	1,1	$0,0^{++}$	Scalarmeson

Table 2.3: Characteristics of light mesons

2.5 Hadrons - Mesons

In the quark model bound states of $q\bar{q}$ pairs are denoted as mesons. At LEP I we find 5 different contributing flavours (u,d,c,s,b), according to the available phase space. The variety of mesons contains orbital and radial excited states as well as simple ground states. Taking into account only the lightest quarks (u,d,s) the $SU(3)_F$ delivers a valuable classification scheme which of course must be extended when facing more quarks. (SU(4),...) The nine possible $q\bar{q}$ combinations can be grouped according to: $3 \otimes \bar{3} = 1 \oplus 8$

Each of the mesons has its given quantum- numbers: Isospin (I),angular momentum (J),parity ($P = -(-1)^L$) When a state is formed by a quark and the same antiquark this is also an eigenstate of the C operator with the eigenvalue $C = (-1)^{L+S}$. Within the framework of my analysis I have to deal with three differently excited mesons as shown in table 2.3.

$q\bar{q}$ states, which have the same quantum numbers, can mix when building physical states (fixed by the mixing angle). For the vector mesons we obtain an angle $\Theta = 35.3$ with the assumption of ideal mixing for the states ω^0 and ϕ. The ρ^0 with $I = 1$ cannot contain a $s\bar{s}$ contribution and this is why it is not affected by the mixing. So we get:

$$\rho \quad = \quad \frac{1}{\sqrt{2}}(u\bar{u} - d\bar{d}) \tag{2.28}$$

For the f_2 we can also do such a parametrization but due to the mass dependence of the mixing angle we find $\Theta \sim 28°$.

$$f_2 \quad \sim \quad (u\bar{u} + d\bar{d}) \tag{2.29}$$

The most problematic resonance is the f_0 because it is not clear of what the particle consists of. A short summary of this discussion can be found in [20].

All these 3 resonances decay strongly inter alia into a $\pi^+\pi^-$ pair according to their ratios [20]. The $\pi^+\pi^-$ spectrum contains several other contributions which will be treated in the experimental part. These decays can be influenced by interactions, correlations e.g. the BEC which is the most important one - I will discuss it in the following section.

2.6 Bose- Einstein Correlation

Bose- **E**instein **C**orrelation (BEC) is an effect which is known since the late 50´s and has been topic of several studies [18, 14, 13, 9, 23, 4]. Originally this correlation, also known as GGLP- effect, has been used to determine the space time structure of particle sources in high energy collisions. This kind of measurement was first done by Goldhaber, Goldhaber, Lee, Pais [19] in $p\bar{p}$ collisions which is still an important application of the interference effects . Nowadays BECs appear also in other analyses. In the following section I want to treat the classical basics [39, 42, 43, 34, 39] of BECs which nowadays appear also in other analysis. [6, 3, 12]

To understand the cause for the BE- correlations, we consider two identical bosons (e.g. pions) emitted simultaneously within a region with the radius R_0. For the description of these two particles we have to impose Bose- Einstein statistics which demand a wave function symmetric upon exchange of two particles.(This necessity results of the fact that each of the particles can travel along two possible ways and these both amplitudes interfere.)

Let's first consider the production- probability of two particles (p_1, r_1),(p_2, r_2)...

$$\begin{aligned} P(p_1, p_2) &= \int_\Omega \int_\Omega dr_1 dr_2 |\psi_{12}|^2 = \\ &= \int \int dr_1 dr_2 \rho(r_1)\rho(r_2)|\psi_{12}|^2 \end{aligned} \tag{2.30}$$

...with the 2 particle wave function...

$$\psi_{12} = < p_1 p_2 | r_1 r_2 > \; = \; \frac{1}{V} \exp^{i(p_1 r_1 + p_2 r_2)} \tag{2.31}$$

$$\tag{2.32}$$

...which after the symmetrization looks like:

$$\bar{\psi}_{12} = \frac{1}{\sqrt{2}V} \left[\exp^{i(p_1 r_1 + p_2 r_2)} + \exp^{i(p_2 r_1 + p_1 r_2)} \right] \tag{2.33}$$

$$\tag{2.34}$$

In eqn. 2.30 $\rho(r)$ corresponds to the distribution of the sources within the region. In general we know nothing about the density distribution of the sources but it has been shown that with the parameterisation as a symmetric or a a Gaussian distribution one obtains a good description for the data. Using the Gaussian parametrisation I follow the previous measurements [[9], [12]]. If we apply this in 2.30 we get:

$$P(p_1, p_2) = \int \int |\bar{\psi}_{12}|^2 \frac{1}{(\pi\lambda)^{\frac{3}{2}}} \exp \frac{-(r_1^2 + r_2^2)}{2\lambda} \tag{2.35}$$

It is noteworthy that λ is not the radius of the source but connected to it via the relation: $R = 2.15\lambda^{\frac{1}{2}}$. To enable the measurement of the correlation, a correlation function $C(p_1, p_2)$ must be introduced:

$$C(p_1, p_2) \quad = \quad \frac{P(p_1, p_2)}{P(p_1)P(p_2)} \tag{2.36}$$

$P(p_1, p_2)$ denotes the two particles production probability; $P(p_1)$,$P(p_2)$ represents the production probability for a single particle;
Often the denominator is replaced (in measurements) with the fictive two particle function $P_0(p_1, p_2)$ without BEC (event mixing, ...)[9, 4]. Calculations of the Eqn. 2.36 give:

$$\begin{aligned} C_{12}(p_1, p_2) &= 1 + F(\rho(r_1, r_2)) = 1 + \exp^{-\lambda^2|p1-p2|^2} \\ \rightarrow \quad C_{12}(q) &= 1 + \exp^{-\lambda^2 q^2} \end{aligned} \tag{2.37}$$

Out of that we would expect a value of $C_{12} = 2$ at $Q \rightarrow 0$. In practice however the observed numbers were much smaller than 2 - a result which has been interpreted in the following way: Not all particles in the final state have been affected by BEC as it can happen, if the sources are not completely incoherent, one of the basic assumptions for the sources. To take this into account, an additional parameter λ (different to the λ in Eqn.2.37) is introduced which controls the strength of the effect respectively the coherence of the sources. By this parameter the Eqn.2.37 is changed in the following manner:

$$C(Q) \quad = \quad 1 + \lambda \exp^{-Q^2 R_G^2} \tag{2.38}$$

$Q^2 = (p_1 - p_2)^2 - (E_1 - E_2)^2 = M^2 - 4m_\pi^2$. is the negative squared 4- momentum difference;R_G is the radius of the production volume. These correlations cause an enhancement of the number of like-sign pion pairs at low values of Q. Consequently we can observe preferential production of identical bosons with a small distance in phase-space. (similar momentum, close to each other, ...)
This importance of this effect for my work can be seen if we consider the conditions of the process:

- high multiplicity
- most of the particle are bosons
- the emission region is small in space (0.5-1fm)

Due to the BEC, the invariant mass spectrum of $\pi^\pm\pi^\pm$ is enhanced at low masses and furthermore the unlike-sign mass spectrum ($\pi^+\pi^-$) is affected. Long time it was assumed that the unlike-sign mass spectrum would stay unaffected ([19]) which was the reason for its use as a reference sample $P_0(p_1, p_2)$. Later however it has been shown that at higher energies and for higher multiplicities also the unlike-sign invariant mass spectrum is affected by BECs ([28]).

Because the effect arises from the symmetrization of the like-sign particle pairs it is known as "residual" BEC. (Depletion above, enhancement below the central mass - both result in a shift of the nominal mass and a broadening of the shape of a resonance.)

To do measurements one needs a Monte Carlo calculation to compare with - a procedure which up to now can only be done with the JETSET- generator ([36]) because this is the only one which has such a model implemented. With its calculation it does not change the production mechanism but works as a final state interaction between the hadrons:

> In this simplified BEC model the correlations are simulated by shifting the momenta of the like-sign boson pairs until they fulfill the given distribution of Q. Thus the phase-space which is assumed to be spherical ($\frac{d^3p}{E} \sim \frac{Q^2 dQ}{\sqrt{Q^2+4m^2}}$) is changed via the correlation function $C_{12} = 1 + \lambda \exp^{-Q^2\sigma^2}$. From this we get the equation for Q´.
>
> $$\int_0^{Q_{ij}} \frac{Q^2 dQ}{\sqrt{Q^2 + 4m^2}} = \int_0^{Q'_{ij}} C_{12}(Q) \frac{Q^2 dQ}{\sqrt{Q^2 + 4m^2}} \tag{2.39}$$
>
> To recover the violations of the energy-momentum-conservation done by this method a rescaling becomes necessary. To describe some of the effects seen we have to apply sometimes unphysical values for the parameters, a necessity which could be explained by the final state like implementation of the effect or other correlations. The whole BEC algorithm is provided by the JETSET - subroutine LUBOEI and needs 5 parameters which are listed in the table 2.4 .

parameter	default-value	used value	description
MSTJ(51)	D=0	1	inclusion of BEC or not (0) and the shape of the distribution. (2=gausian)
MSTJ(52)	D=3	9	number of particles species affected by BEC (9=π^+,π^-,π^0,K^+, K^-,K_L^0,K_S^0,η,η'
PARJ(91)	D=0.020	0.1	minimum particle width - gives the minimum width for which particles are allowed to contribute to the BEC.
PAR(92)	D=1	~2.1	λ gives the nominal strength for the BE- effect
PAR(93)	D=0.20	~0.3	$\frac{1}{\sigma}$ inverse region size - it measures the size and is related to the radius via $R = h/PARJ(93) = 0.2fmGeV/PARJ(93)$

Table 2.4: Bose-einstein correlation parameters of Jetset

Chapter 3

Experimental Setup

This analysis is based on data collected by the ALEPH detector. ALEPH (**A**pparatus for **LEP** p**H**ysics) is one of four experiments located around the LEP (**L**arge **E**lectron **P**ositron) collider at CERN. In the following the explanation is subdivided into two stages: the event-production induced by LEP and the data-taking of the ALEPH detector.

3.1 The Large Electron Positron collider (LEP)

LEP is designed to accelerate, store and collide electrons and positrons in order to make it possible to do precise tests and studies of the Standard model. The machine is a circular synchrotron with a circumference of 26.67 km, embedded in a tunnel with a diameter of 3.8 m, positioned 50 – 170 m below the surface as shown in Figure 3.1. More precisely, it is a octagonal polygon consisting of eight straight, 500 m long acceleration sections which are connected by eight circular arcs with a radius of curvature of 3300 m.
These dimensions are imperative because otherwise the losses due to synchrotron radiation would become too large. The energy loss per turn is proportional to $\frac{E^4}{m^4\rho}$ where E is the energy of the electron, m the mass of the electron and ρ the radius of curvature. From that one obtains for electrons with an energy of 45.6 GeV (LEP 1) an energy loss of 0.11 GeV which must be provided by the accelerator to hold the energy. In order to achieve this high energy and to hold it, LEP uses RF cavities for the acceleration (final stage of LEP 1: 120 copper and 60 super-conducting cavities). The energy has been measured with a method based on resonant depolarisation. The leptons are bound to their orbits with the help of 3368 dipole magnets. For the focusing 816

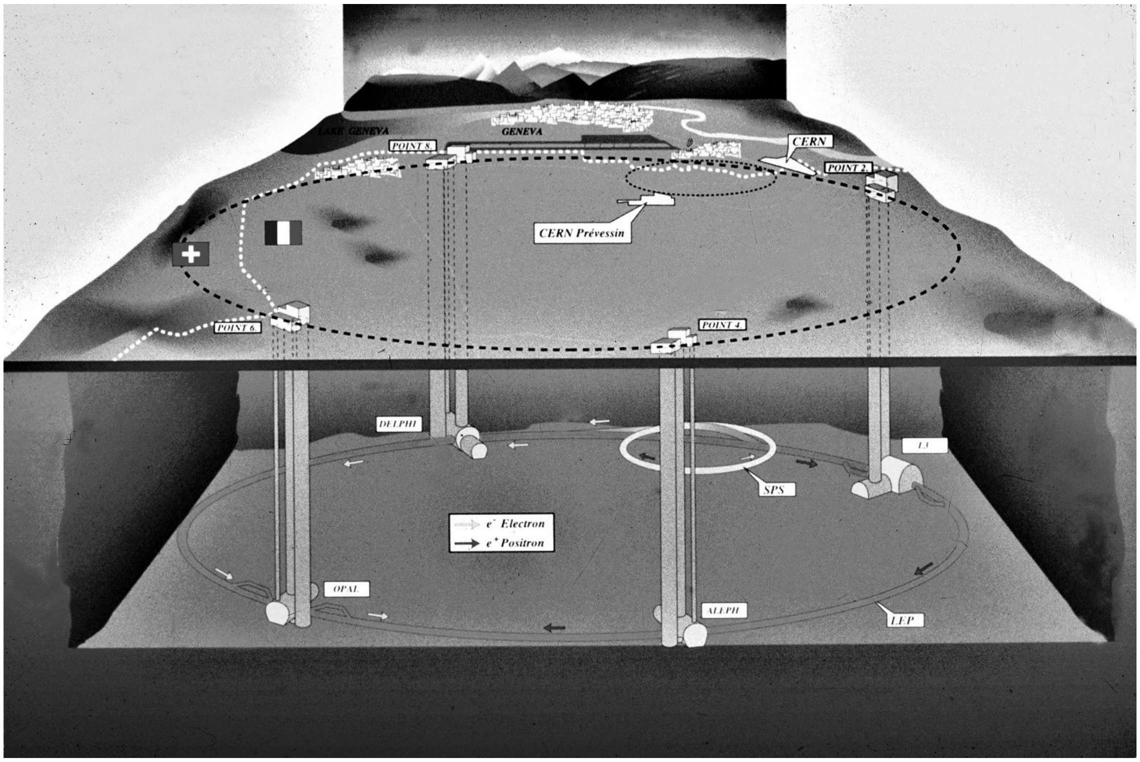

Figure 3.1: The LEP ring and the location of the four experiments.

quadrupole and 504 sextupole magnets have been installed.
The high energies provided by LEP cannot be produced directly, they are the results of an acceleration chain of which the LEP storage ring is the final stage. The electrons produced by the electron gun are accelerated to 200 MeV and some of them are directed on a tungsten target to generate the positrons. In the following both types are speeded up to 600 MeV before they enter into the Proton Synchrotron (PS) where they obtain an energy of 2.2 GeV. The following SPS with a final energy of 22 GeV is the last acceleration stage before they are injected into the LEP.

In the LEP ring tunnel the electron and positron beams circulate in opposite directions with a frequency of 11.246 Hz and a life time of about eight hours. These beams contain up to four bunches of particles which are about 15000 μm long, 250 μm wide in the horizontal direction and 10 μm in the vertical direction. Both beams are forced to collide every 22 μs in four (ALEPH, DELPHI, L3, OPAL) of the eight collision- points. In the years 1992-1995 an integrated luminosity of $179.1 pb^{-1}$ at an energy of 91.2 GeV (+ sidebands) has been achieved. A detailed list is given in Table 3.1.

year	luminosity (pb^-1)
1992	28.6
1993	40.0
1994	64.4
1995	46.1
total	179.1

Table 3.1: Integrated luminosity seen by each year

3.2 The ALEPH detector

The ALEPH (Apparatus for LEP pHysics) detector is designed to perform high precision measurements for different types of Standard model processes. The detector has a cylindrical structure arranged around the beam pipe with the collision point in the center. The detector collects data for almost the full solid angle with a high granularity. This information is transported to the reconstruction computers via 500.000 electronic channels. The data are recorded by several subdetectors as shown in Figure 3.2. Particular emphasis has been given to the momentum and position measurement of charged tracks, for which three tracking detectors are at our disposal.

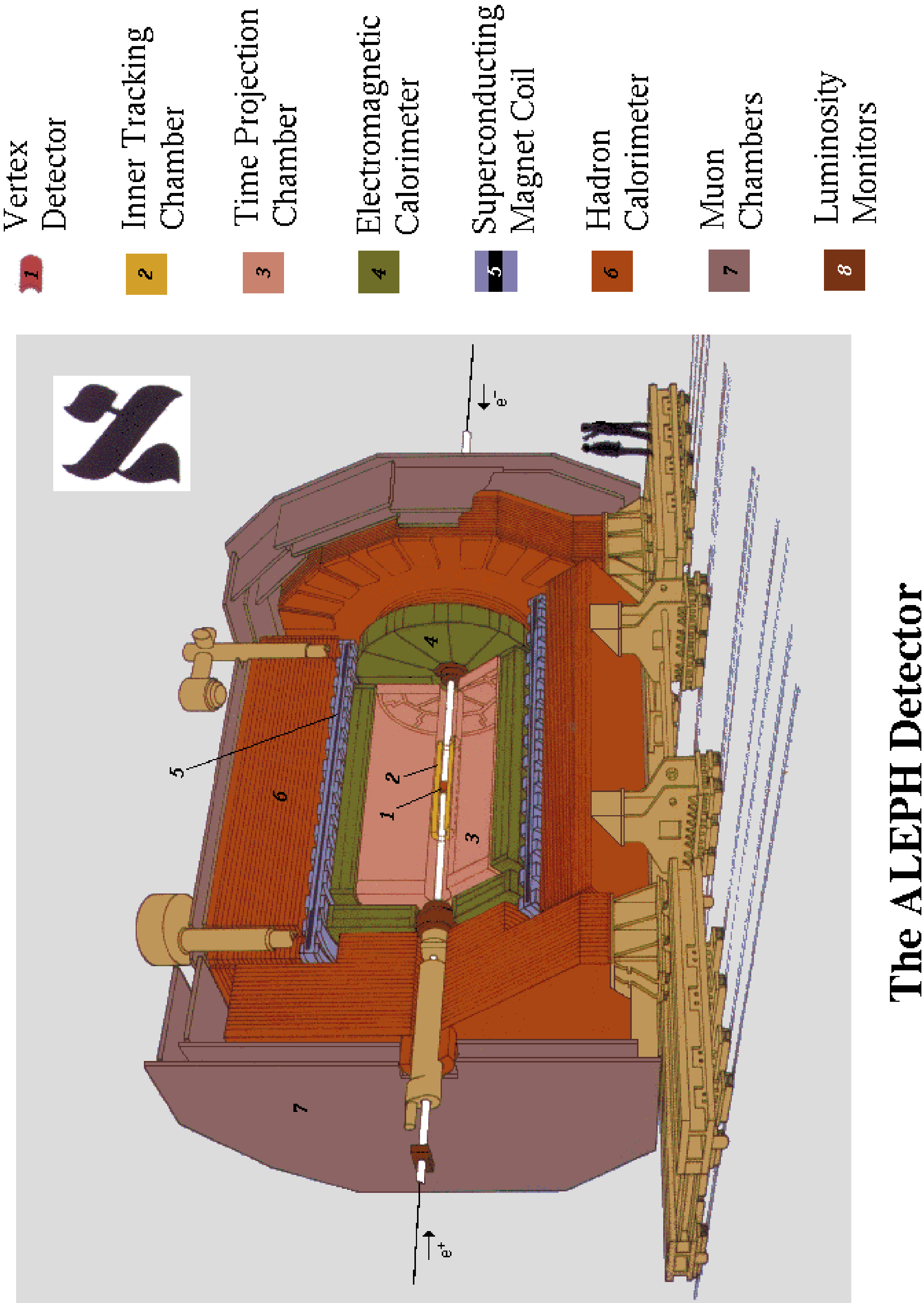

Figure 3.2: The ALEPH detector

The innermost detector, the silicon Vertex DETector (VDET) and the Inner Tracking Chamber (ITC) provide precise data for the positions close to the beam pipe - which is most important for short-living particles like b and c hadrons or τ- leptons. The main tracking device, the TPC, measures the exact course of the charged particle trajectories and also their energy loss. To enable momentum measurements, a 1.5 Tesla magnetic field immerses the inner tracking devices in axial direction and causes a momentum dependent curvature to all charged tracks. With the aid of calorimeters the energy of charged and neutral particles can be measured. The calorimeters can be subdivided into two parts:
(1) The electro-magnetic calorimeter (ECAL) which is located within the super-conducting coil and is mainly used for energy measurements of photons and electrons;
(2) The hadronic calorimeter (HCAL) positioned outside the coil forms together with the muon chambers the outermost part of the detector and is responsible for the energy measurements of hadrons and muons. For luminosity measurements some additional calorimeter have been installed around the beam pipe (LCAL, SICAL, BCAL). The whole detector is 11 m long and has a diameter of 10 m and a weight of 2800 tons. In the following sections some of the detector parts will be discussed. Further details can be found in [11].

3.2.1 The ALEPH coordinate system

The coordinate system used by the ALEPH detector is defined by the theoretical interaction point. (This is the midpoint along the straight section between the two nearest quadrupoles.) The positive z direction is along the e^- beam line but due to the inclination of LEP the axis shows an angle of 3.587 mrad to the horizontal. The positive x axis points towards the center of LEP and the positive y axis is orthogonal to the two others and points skywards (They form a right-handed system). As an alternative one can use the representation in cylindric coordinates (r, ϕ,z) - defined by

$$\begin{aligned} r(x,y) &= \sqrt{x^2+y^2} \\ \phi(x,y) &= acos(y/x) \end{aligned} \tag{3.1}$$

3.2.2 VDET and ITC

Located near the interaction point, the Silicon Vertex detector (VDET) is used to obtain as much information as possible about the origin of each track. Thereby it becomes possible to reconstruct details about the decay topologies of short living particles. The detector consists of 112 double sided silicon strip detectors which are arranged in two layers around the beam pipe. The surfaces of the layers form two concentric barrels, whereas the inner one has a dodecagonal structure with a radius of 95 mm and the hexadecagonal outer barrel has a radius of 114 mm. On one side of the wafer the strips are oriented perpendicularly to the beam-pipe to enable the measurements of the z coordinate. The strips on the other side of the layer are oriented parallel for the measurement of the ϕ coordinate. Between two strips a pitch of 25 μm restricts the resolution for the r, ϕ measurement. For the z coordinate a pitch of 100 μm determines the limit.

Performance: The point resolution is $\sigma_{r\phi} = 13\mu m$ and $\sigma_z = 20\mu m$. Two tracks can be resolved up to 200 μm in r,ϕ and 400 μm in z.

The crossing of the inner tracking chamber (ITC) is the next important stage for charged tracks. This sub-detector serves as a support device for the TPC but more important is its task as the main part of the level 1 trigger. The ITC is a cylindrical multi-wire tube which measures the position of tracks with the help of eight concentric arranged drift cells. The resolution for the r, ϕ direction is given by the drift time (2 dim $\rightarrow$ 1/2μs). A little bit longer takes the determination of the z coordinate because it is measured by the difference of the arrival-times on the two opposite sides (3 dimensions $\rightarrow$ 2 μs). This is the determinant time factor of the level 1 trigger decision. Of course the uncertainty of the z-coordinate is larger than the others.

Performance: Only tracks with $|\cos\phi| < 0.97$ can transverse all layers and can be measured with a resolution in r, ϕ of 150 μs and in z with a resolution of 5 cm.

3.2.3 The Time Projection Chamber (TPC)

The TPC, a cylindrical drift tube with a inner radius of 0.31 m and an outer radius of 1.8 m, represents the main tracking device of the ALEPH detector. This device provides high precision information about the momentum and the position of charged particles, allowing to identify particles by measuring their energy loss (dE/dx). For tracks that cross the whole TPC it is possible to obtain up to 21 three dimensional space points. The chamber is filled with a mixture of argon (91%) providing good ionization properties, and methane (9%) which controls the ionization avalanche. The electric field extends from each plate towards the central membrane that divides the chamber into two halves and is held on a potential of -27 kV. Each created electron moves with a drift velocity of 5.2 cm/μs along a tight helix towards the end-plate and there it hits one of the 21 multi-wire chambers of which 3 different types (K, L, M - type) exist. With this method all trajectories can be projected as circular arcs onto the x-y (r- ϕ) plane. The necessary ionization avalanche is initiated between the cathode grid held on zero potential and the sense grid held on 1250 V. The beyond lying cathode-pads collect the signals and make it possible to do a precise measurement of the position (r, ϕ) by the means of interpolation between several pads. The z coordinate is deduced from the drift time (= difference between arrival time and beam crossing) and the well known drift velocity. The precision of this measurement depends on the knowledge about the drift behavior and the inhomogeneities of the magnetic and the electric field. By the means of the impulse height one gains information about the energy loss of the crossing particle. The calibration of the TPC is done with a Laser system with three equidistant beams. A further important part is the gating system which controls the acceptance of tracks. Due to this gating system it is possible to select the data corresponding to the last event. (For details see [11])

Performance: The r-ϕ resolution for isolated tracks is $\sigma = 173\mu m$ and the resolution in z direction is $\sigma = 740\mu m$. Using only the TPC for the transverse momentum measurement one obtains a resolution of $\sigma(1/p_t) = 1.2 \times 10^{-3}$ $(GeV/c)^{-1}$ with additional ITC measurements the resolution can be improved up to $\sigma(1/p_t) = 0.8 \times 10^{-3}$ $(GeV/c)^{-1}$

3.2.4 Calorimeter

3.2.4.1 The Electromagnetic CALorimeter (ECAL)

The ECAL, consisting of a barrel and two end-caps, surrounds the TPC but is still located within the coil. Built up of 45 layers of lead and proportional chambers each part can be subdivided into 12 modules which cover a angular range of $|\cos\theta| < 0.98$. This composition corresponds to a thickness of 22 radiation length. The ECAL stops most of the electrons and photons and measures their energies. Due to cracks, 2% of the barrel surface and 6% of the end-cap surface are insensitive for particles. To prevent a coincidence of the cracks of the barrel and the end-caps, they are rotated 15° against each other. The cathode pads of the chambers are wired in such a way that they build towers pointing towards the interaction point. Totally the readout of the ECAL knows 73.728 towers with a granularity of $0.9° \times 0.9°$ and a solid angle coverage of 3.9 π

Performance: The energy resolution of the ECAL is $\sigma(E)/E = 0.178/\sqrt{E/GeV} \oplus 0.009$ (using a quadratic form for the fit to the energy resolution distribution) and it achieves an angular resolution of $\sigma_{\theta,\phi} = (2.5/\sqrt{E/GeV} + 0.25)$mrad

3.2.4.2 Hadronic calorimeter and Muon chambers

The hadronic calorimeter (HCAL) is a large sampling calorimeter designed to measure the energy and the position of hadronic showers. Like the ECAL, also the HCAL consists of a barrel and two end-caps and is located outside of the coil. 23 layers of plastic streamer tubes separated by 5cm thick iron slabs form a detector with a thickness of 7.7 interaction lengths. This part of the detector is composed of 24 modules (six per end-cap and twelve in the barrel) which are packed into 4788 projective tower units. The HCAL is part of the load bearing structure of the detector and serves as the return yoke of the super-conducting solenoid. Outside the hadronic calorimeter additional streamer tubes are located which form the muon chambers. Together with the HCAL they provide a good muon identification and a good energy measurement.
Performance: The HCAL provides for pions at normal incidence a energy resolution of $\sigma(E)/E = 0.85/\sqrt(E/GeV)$.

All other detectors like the SICAL, LCAL and BCAL have no major importance for this analysis and won't be treated in this summary. For details to all parts of ALEPH look up [11]

3.2.5 Trigger and Data acquisition

The data collected by the detector must be prepared for further usage which is the task of the **D**ata **A**c**Q**uisition system (DAQ). A simplified view of the complete DAQ system is presented in Figure 3.3, illustrating the flow of data from the front-end electronics to the final stage of event reconstruction.

The DAQ system starts with the trigger system that has to decide if an event can be used for an analysis or if it has to be rejected. Therefore three trigger levels are employed by the system to decrease the number of 'bad' events and to reduce the frequency of events to a rate that can be written to tape. Since the first trigger must decide very quickly so that no events get lost, this level uses only information based on the combined data from the ITC (number of fired wires), ECAL (energy threshold) and HCAL (number of fired chambers). The decision is available after 5 μs and in the case of acceptance it prevents the TPC from closing the gate and initiates a complete read out of the detector data.

The second trigger level uses mainly the information of the TPC and due to the drift time this decision takes about 50 μs. After this stage the events are submitted to the event builder which has to deal with a frequency of 10 Hz. In the case of a "no" after the first or the second trigger level the detector buffers are cleared. The last level decision is a software trigger is based on part of the reconstructed data. After a positive decision an event is written on the tape which happens with a frequency of 1-2 Hz.

The connection of these stages starting from the front end electronics up to the reconstruction computer and storage devices is the second task of the DAQ. It provides the correct control signals, protocols and data on the right location at the right time. A complete list of all signals and controls can be found in [11].

After all decisions a complete reconstruction of the events with the program JULIA is initiated on a FALCON cluster. These events are stored in the POT format and prepared for analysis. Also other formats are available, like the DST, MINIDST, NANODST,..., which represents a reduced data format containing only specific information and the precision which is absolute necessary for an analysis. For this work a MINIDST has been used.

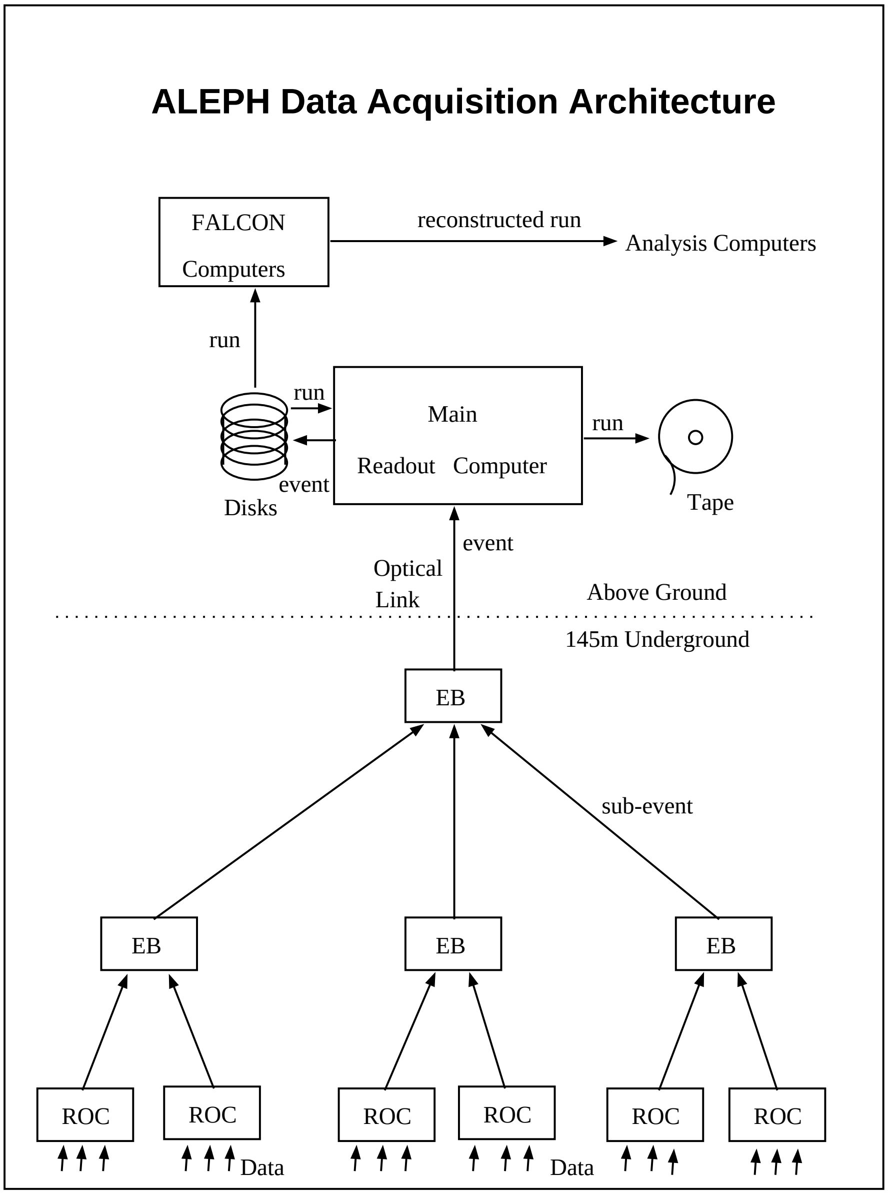

Figure 3.3: Simplified scheme of the DAQ system. ROC = Readout Controller; EB = Event builder; FALCON = computer system for event reconstruction;

Chapter 4

Analysis

4.1 General remarks

It's the aim of the following chapter to explain in detail the procedures that happened to the $\pi^+\pi^-$ mass spectrum. The spectrum contains several resonances of which the three neutral states ρ^0, f_0 and f_2 have been chosen to be of interest for this work. Each of these particles represents another state of angular momentum (scalar, vector and tensor) and therefore the fragmentation functions can be important for the tuning of hadronization models.
It is the primary task to get the differential cross section (Eqn.4.1) normalized

$$\frac{1}{\sigma_{had}}\frac{d\sigma}{dx_p} \tag{4.1}$$

to the number of events for each of those three particles - where x_p=p_{meson}/p_{beam} represents the momentum of the meson normalized to the momentum of the beam. The cross- sections are extracted from the invariant mass distribution of the daughters.

All three particles decay via the strong interaction into their pseudo-scalar partners the pions. While the ρ^0 decays at 100% into the $\pi^+\pi^-$ channel, the two other mesons have only fractions into this channel. Nevertheless it is the dominant channel for all three particles. The detailed decay characteristics and some other particle data have been listed in Table 4.1.

Additionally to the branching ratios different charge states can occur according to isospin conservation. In view of this fact one obtains a final branching ratio into $\pi^+\pi^-$ for the f_2 of 56.4% and for the f_0 a value of 52.1%.

At least 79% of the resonances are produced by the initial string - the missing fraction originates

Particle	Decay mode	Fraction
$\rho^0(770)$	$\pi\pi$	$\sim 100\%$
$f_0(980)^1$	$\pi\pi$	$78.1 \pm 2.4\%$
	$\mathrm{K\bar{K}}$	$21.9 \pm 2.4\%$
$f_2(1270)$	$\pi\pi$	$84.6^{+2.5}_{-1.3}\%$
	$\pi^+\pi^-2\pi^0$	$7.2^{+1.5}_{-2.7}\%$
	$\mathrm{K\bar{K}}$	$4.6 \pm 0.4\ \%$
	$2\pi^+2\pi^-$	$2.8 \pm 0.4\ \%$

Table 4.1: Decay characteristics of ρ^0, f_0 and f_2

from the decay of heavier particles. The short lifetime or rather the short travel distance is common to all three particles and this provides a good starting point for the definition of the selection criteria. Such cuts, additionally to standard cuts, as described in the following section are highly important, because the $\pi^+\pi^-$ mass spectrum is crowded by reflections and some other particles in the interested region. A quick look on Figure 4.5 can help to visualize this situation. From this picture the disturbing contributions can be easily recognized as there are the 3 pion decay of the omega, the $K\pi$ decay - with misidentified K - of the K^{*0} and the two pion decay of the K^0_S.

The whole analysis can be subdivided into several steps until the final results are known. A short overview of this procedure is given by Figure 4.1. The details of each stage will be explained and completed in the according chapter.

It will be the first task to select those events which can be identified as hadronic ones in order to form the base for this analysis. This step will be described in the following section.

4.2 Event selection

Looking on Table 4.2 it can be seen that the Z decays into several channels. Although 70% of all events can be identified as hadronic events, it is necessary to reject the others to achieve an applicable result.

Therefore the high multiplicity common to all hadronic events is used to identify them. Furthermore the outgoing charged particles in hadronic events carry a large fraction of the center of mass energy which also helps to classify this event type.

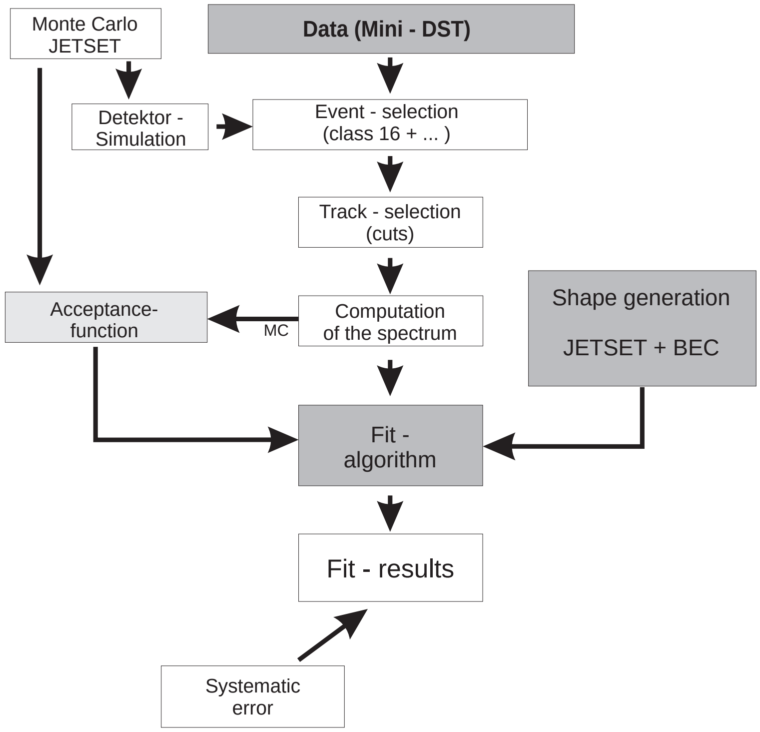

Figure 4.1: Flow-diagram of this analysis

The standard ALEPH criteria for hadronic events are based on charged tracks which must be well reconstructed - so called 'good' tracks. Such a 'good' track must have:

- ⋆ at least 4 TPC coordinates
- ⋆ a polar angle θ such that $|\cos\theta| < 0.95$
- ⋆ a transverse impact-parameter $|d_0| < 2cm$

Z decay mode	Fraction (%)
e^+e^-	3.366 ± 0.008
$\mu^+\mu^-$	3.367 ± 0.013
$\tau^+\tau^-$	3.360 ± 0.015
invisible	20.01 ± 0.16
hadrons	69.90 ± 0.15

Table 4.2: Decay modes of the Z

- ⋆ a longitudinal impact-parameter $|z_0| < 10cm$
- ⋆ a transverse momentum $p_t < 200$ MeV/c (this criterion is not part of the standard selection - it will be applied afterwards)

With these good tracks the next step can be started which selects hadronic events. It requires:

- ⋆ a minimum of 5 good charged tracks
- ⋆ the sum of the energy carried by the charged tracks must be greater then 10% of the center of mass energy

These cuts become clear from Figure 4.2 where we can identify the hadronic events as a broad bump in the above dedicated range.

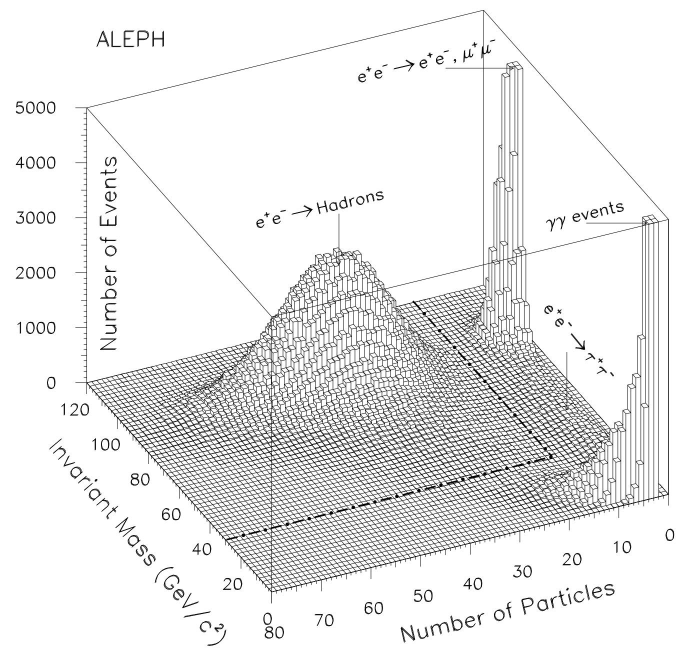

Figure 4.2: Invariant mass versus number of particles for all the events with at least two charged particle tracks. [11]

The cuts can be applied directly to the data by setting the 'CLASS 16' flag in the data cards of the analysis routine. I've used the ALEPH data from the years 1992 to 1995 at a center of mass energy of $\sqrt{s} = 91.2$GeV, whereas the data are marked as PERF or MAYB in the offline event - database. Events selected according to above criteria contain still a small fraction of $\gamma\gamma$ and $e^+e^- \rightarrow \tau\tau$ events. To further clean the sample the number of energy flow objects has to be larger than 15 and the total visible energy has to exceed 45.6 GeV. This ensures that the contamination is reduced to 0.6%. Backgrounds arising from other processes such as the T channel scattering, beam gas and cosmic rays are small but resides in the sample.

Furthermore the polar angle of the thrust axis is required to be within the range $30° < \theta < 150°$ which makes sure that the selected events are well contained with the detector. In which the thrust axis is defined as follows:

$$T = max_{\vec{n}_{Thrust}} \frac{\sum_{i=1}^{N_{particle}} |\vec{p}_i \cdot \vec{n}_{Thrust}|}{\sum_{i=1}^{N_{particle}} |\vec{p}_i|} \tag{4.2}$$

Finally after all selections a sample of **2.76 Mio** events has been obtained.

To correct effects arising from the detector or the selections cuts, a Monte Carlo (MC) simulation has been used. Therefore events have been generated with HVFL which stands for the parton shower model JETSET 7.4 with modified bottom and charm decay and a modified generation for ISR photon with the DYMU3 program [25]. The HVFL sample has been produced nearly each year with different parameters according to the different geometries used in the real detector.

For this analysis the HVFL 03 for 1992 geometry and the HFVL 04 for 1994/1995 have been used.

These MC events have been processed through a full detector simulation, reconstruction and have been analyzed in the same way as the data. In the following full MC corresponds to the HVFL sample.

4.3 Track selection

The standard ALEPH cuts defined in class 16 are too weak for this analysis. Since we are only interested in charged pions originating close from interaction point, additional cuts have been applied. That means that all cuts which have been used for the 'good' track selection with added p_t cut are reused and additionally tighter restrictions to the impact parameter have been applied, namely $|d_0| < 0.3$ cm and $|z_0| < 3.0$ cm. This cut rejects decay products from weakly decaying particles and photon conversions and reduces the combinatorial background by a large amount. The effectiveness of all cuts is shown in Table 4.3, in which for reasons of simplicity all cuts have been shown although some cuts will be discussed later. Starting from the total number before any additional cut has been applied each number gives the reduction of this particle due to this cut referring to the previous one. The numbers in the brackets in the last column represent the percentage of the total number of the particle that remain after all these cuts.

Particle	$p_t > 0.2GeV$	$\|d_0\| < 0.3$cm + $\|z_0\| < 3$ cm	after dE/dx	hemisphere cut
ρ^0	-3.3 %	-34.2%	-15.7 %	-8.4% (49.1%)
f_0	-3.0 %	-30.9%	-19.4%	-3.8% (52.0%)
f_2	-2.97 %	-40.1%	-16.2%	-2.03% (47.7%)
K_S^0	-3.33 %	-59.1%	-24.4%	-3.89% (28.7%)
K^{*0}	-1.64 %	-33.2%	-36.3%	-2.74% (40.7%)
ω	-5.76%	-34.3%	-16.2%	-3.03% (50.31%)

Table 4.3: Effects of the cuts to different particles where the number of particles after the class 16 selections is defined as 100%

The cuts above and the cuts which are discussed below are optimized to reject particles such as the e, μ, p, K and the result is shown in Table 4.4.

The percentage number for each cut in Table 4.4 represents the fraction of the particle in the sample after applying the cut. The numbers in the brackets correspond to the summed up reduction of the particle fraction caused by the cuts.

To further reduce the combinatorial background it is useful to identify the particles. A tool for direct particle identification is the simultaneous measurement of momentum and ionization energy loss. Therefore ALEPH detector uses information of the TPC sense wires providing up to 338 measurements for tracks which traverse the whole TPC.

particle name	after class 16	strong d0,z0 cuts	dE/dx cut	after all cuts
e	7.024%	5.8% (-51.6%)	0.9% (-95.2%)	0.9% (-97.3%)
μ	3.03%	3.0% (-42.4%)	3.3% (-58.9%)	1.27% (-91.1%)
π	75.2 %	76.0% (-40.6%)	83.7% (-57.6%)	85.5% (-75.8%)
K	10.4 %	10.9% (-38.4%)	9.6% (-64.6%)	9.70% (-80.1%)
p	4.34%	4.4% (-59.4%)	2.53% (-77.8%)	2.59% (-87.3%

Table 4.4: Fractions in percent for different particles in hadronic events (In brackets the total reduction in percent is given)

All particles originating from the collision point are considered as pions and the ionization measurement if available must be compatible with the pion hypothesis.

The deviation from an assumed hypothesis is expressed as $\chi(dE/dx)$:

$$\chi(dE/dx) \quad = \quad \frac{(\frac{dE}{dx})_{measured} - (\frac{dE}{dx})_{expected}}{\sigma_{dE/dx}} \tag{4.3}$$

where $\sigma_{dE/dx}$ is the expected dE/dx resolution normalized with a sample of minimum ionization pions [11].

For each track it is required to fulfil $\chi(dE/dx) < 3$. This cut rejects mainly protons and electrons and in the low momentum region also an acceptable pion/kaon separation is given - an observation which is confirmed by the numbers in Table 4.4. If we consider the number of the electrons, we can see that the fraction in the sample is reduced to less then one percent and also for the kaons a reduction can be seen.

As already mentioned in the previous section also the full MC events have to pass the same criteria as the data to provide the information which is necessary to calculate the efficiencies and limits.

4.4 The $\pi^+\pi^-$ mass spectrum

The two particle $\pi^+\pi^-$ mass spectrum is built of combinations of the previous selected pion candidates. Most of the combinations are random and therefore contribute to a large combinatorial background.It is useful to require for each combination of the pions to lie in the same hemisphere as defined by the thrust axis (Eqn 4.2) to reduce this background. The hemisphere itself is given by a plane that is perpendicular to the thrust axis.

Although the strong cuts on the impact parameter in addition to the dE/dx and the hemisphere cut improve the signal to background ratio from 1/140 to 1/45 [2] the combinatorial background dominates the spectrum as it can be seen in Figure 4.3.

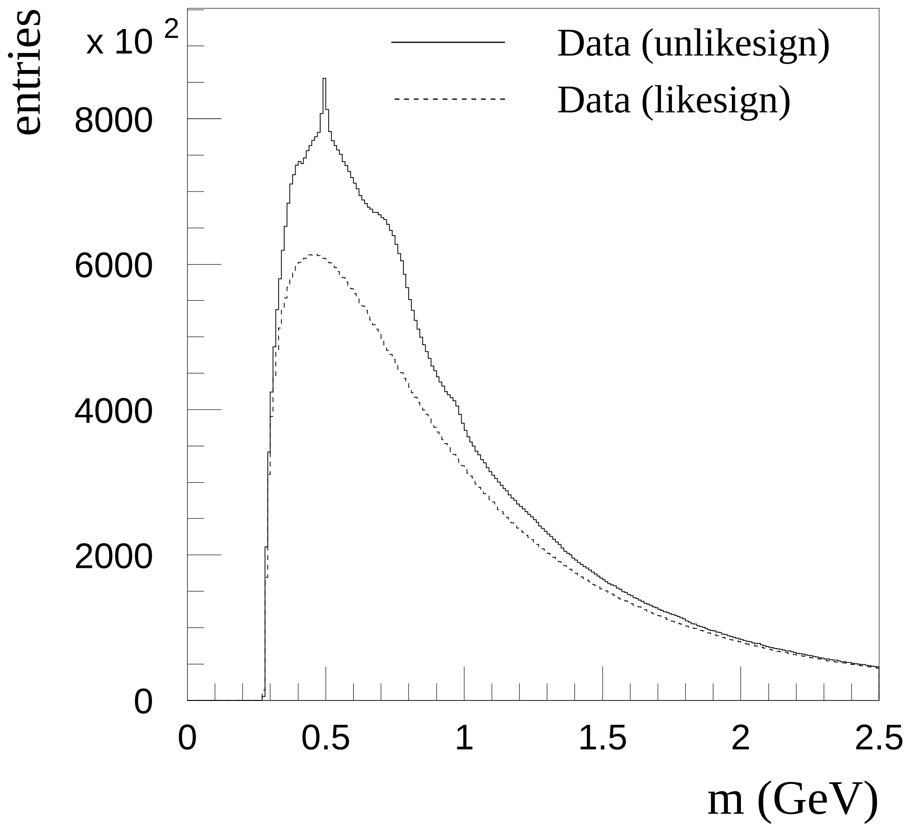

Figure 4.3: It shows the dominating combinatorial background of the $\pi^+\pi^-$ mass spectrum

While the ρ^0 can be easily identified and the f_0 is also recognizable the f_2 is not that easy to identify. Therefore most of the following procedures are dictated and motivated by the aim to reduce this large combinatorial background.

One possibility to improve the situation is to further optimize the cuts but it's a more efficient method to subtract the like-sign mass spectrum from the unlike - sign one [12]. This procedure reduces systematics common to both pion mass spectra and due to the fact that the like-sign spectrum has a similar structure than the unlike - sign combinatorial background, this background

[2] The signal to background ratio has been calculated for the ρ^0. The improvement of the rate for f_0 and the f_2 is not that good as the one of the ρ^0 but comparable

is reduced to a minimum.Hence the $\pi^{\pm}\pi^{\pm}$ mass spectrum must be calculated as well, in the same manner as the $\pi^+\pi^-$ but this time only equal charged combinations are considered.

The results of this procedure are presented in Fig. 4.4. The three resonances (ρ^0 , f_2 , f_0) can be identified easiernow. The fact that this method introduces some problems as it will be discussed in the following sections, does not overwhelm the afford of visualizing (amplifying) the resonance peaks.

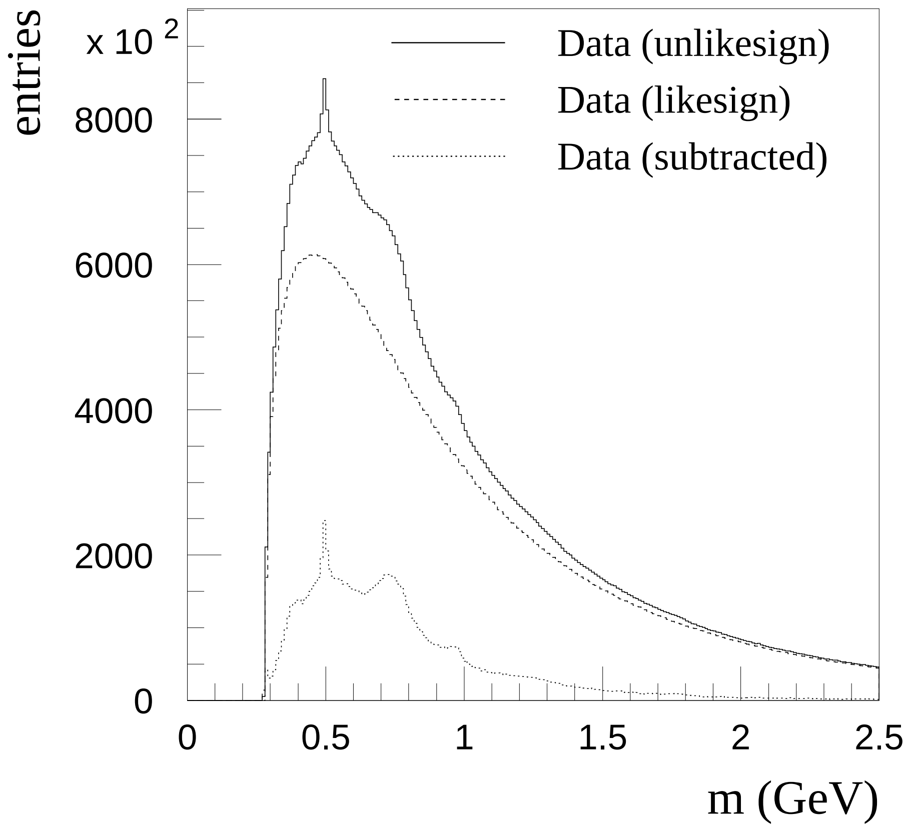

Figure 4.4: The unsubtracted $\pi^+\pi^-$ mass spectrum together with the like- sign spectrum and the result after the subtraction.

As one can see from the latter figures the bin size has been chosen to be 10 MeV per bin. This particular small bin size is driven by the idea to have at least 3 points for each resonance shape. The decisive particle is the f_0 of which the width is around 50 MeV. The lower limit is given by the mass resolution of the analysis. First the detector has only a certain mass resolution for this type of analysis, which is around 3 MeV and second the precision of the data in the Mini-DST is also limited of which the value is also around the mass resolution. Both restrictions give a natural

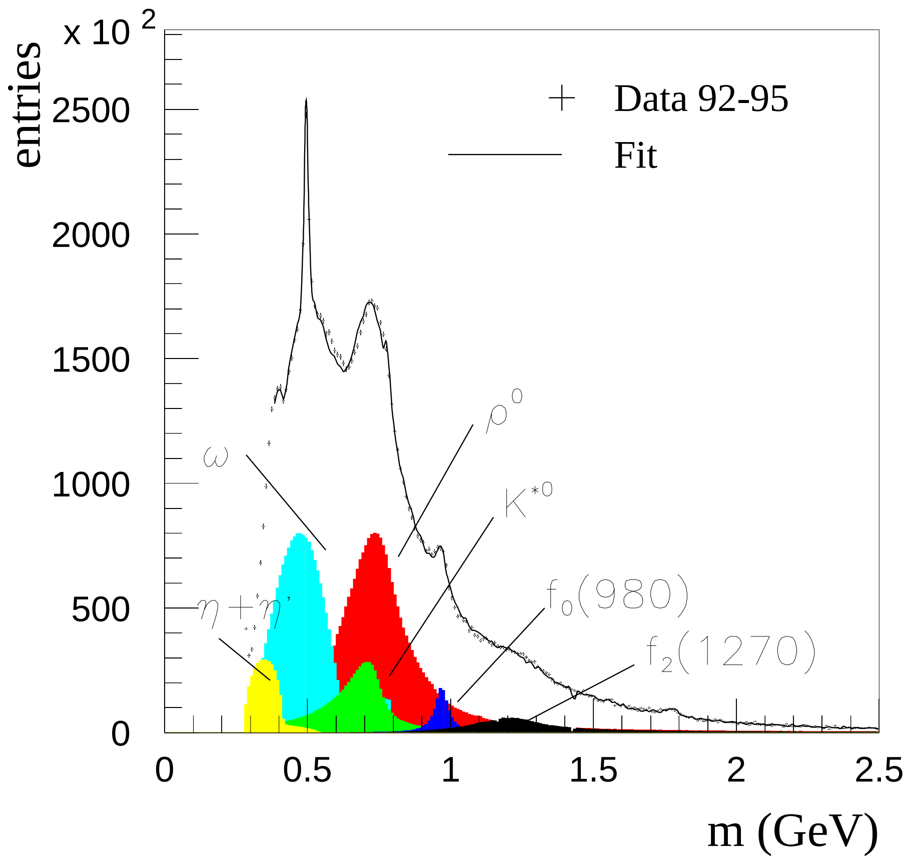

Figure 4.5: The like-sign subtracted $\pi^+\pi^-$ mass spectrum together with the most important components indicated

limit for the bin size.

A comparison of the subtracted $\pi^+\pi^-$ mass spectrum obtained from the data and the same spectrum calculated from fully simulated MC events, shows large discrepancies between them - Fig. 4.6. While for masses higher then the ρ^0- mass the MC exceeds the data, the situation is the other way around below the ρ peak. Also in the region below the K_S^0 the data differ from the simulated events. As a consequence of these distortions the ρ^0 peak of the data seems to be shifted towards lower masses and also its width has increased. The origin for these effects can be found in the like - sign mass spectrum and in the unsubtracted unlike - sign mass spectrum. In the subtracted $\pi^+\pi^-$ mass distribution we observe a mixture of both phenomena, introduced by the subtraction. All these effects described above have been already reported several times for high energies [7, 28, 8, 12, 6] as well as for lower energies [1]. Several explanation exist for these discrepancies which I will not discuss in detail - but the listing below should give a short overview.

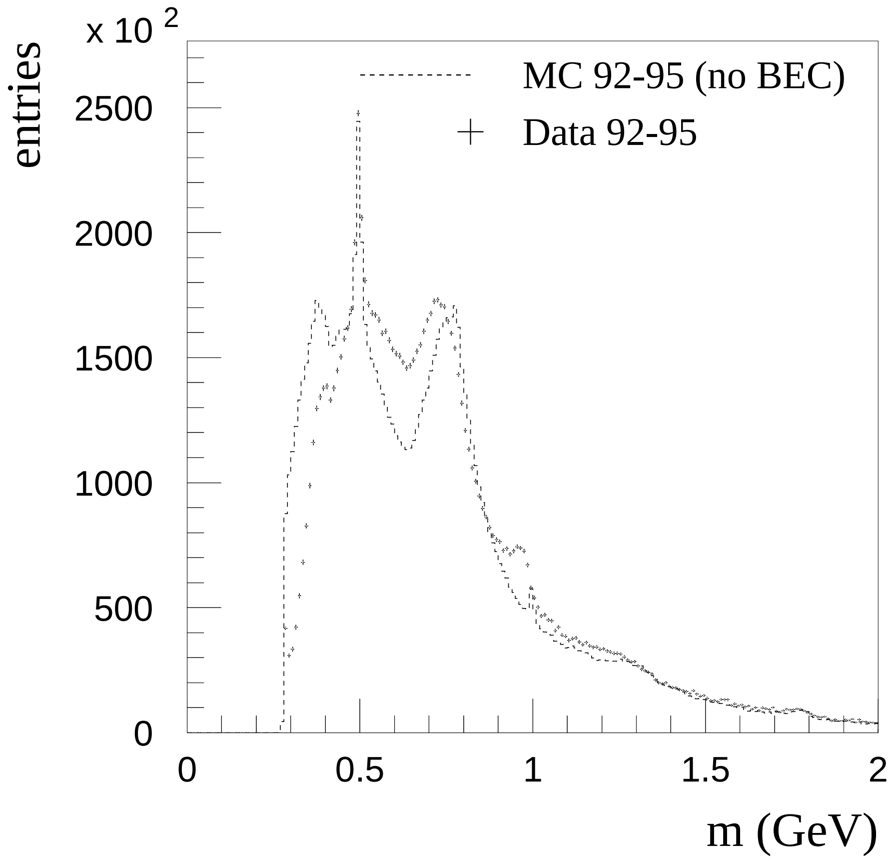

Figure 4.6: Differences in the mass spectrum between for the data and the MC.

The three most popular are:

- ρ^0 **-** ω **interference:** The idea is motivated from the G - parity violating electromagnetic mixing of the ρ^0 and ω states. The violation opens a decay channel for the ω into $\pi^+\pi^-$ with a branching ratio $B_{\omega\rightarrow\pi^+\pi^-} = 2.21 \pm 0.3\%$. Since this state and the ρ^0 are almost degenerated in mass interference can happen. This can change the shapes of the spectrum in particular the shape of the ρ^0 resonance. For more details see [28]

- **Interference with non resonant background:** This effect belongs to the idea of the Söding model [28] which contains an additional Drell type diagram as an extra component to the total amplitude. The diagram describes the dissociation of a photon directly into pions and this may be followed by a rescattering of these pion via a ρ^0 state. The result of the interference with such a ρ^0 is again an enhancement below the nominal ρ^0 mass and a depletion above of it. Again, for details see [28].

- **Bose - Einstein - Correlations:** The theoretical foundations for these correlations which act between identical pions and change their phase space I have already discussed in chapter 2.6 .

In principle it is not clear which of these effects is responsible for the discrepancies or if it is a mixture of all three. Nevertheless in earlier measurements [4, 9, 8, 32, 3, 12, 10, 5] it has been shown that the inclusion of BE correlations into the analysis can cure the problem. In the following I will use these BE correlations for an improvement of the description. Only these BEC effects can be simulated by a MC generator - namely the JETSET 7.4 model. Hence, for my analysis I have to use this generator. The inclusion of BEC's needs some special modification of the standard tools which are normaly used for analysis like this as we will see in the following.
Remark: Although a new JETSET routine exists for the calculation of BEC [37] for this analysis the original LUBOEI routine has been used since the new one hasn't been established when I started to build my algorithms.

The standard JETSET implementation of BE effects uses the following defining function, as already mentioned in theory part (Eqn.2.38), for the phase space parameterization.

$$C(Q) \quad = \quad 1 + \lambda \exp^{-Q^2 R_G^2}$$

with its parameters λ which gives the strength of the effect and σ $(= \hbar/R_G)$ which defines the size of the pion source.

The latter parameter causes problems if the value for $1/\sigma$ exceeds 0.35 GeV [31]. Beyond this limit the output of the LUBOEI routine is not related to the input as far as the inverse region size is concerned. I stumbled over this problem since my fit routine Eqn.4.4 delivered absolute nonsense when I used values for $1/\sigma$ larger then 0.35 GeV/$\hbar$c. This means that the inverse region size $1/\sigma$ which has been measured after the event-production with JETSET (BEC on) differs from the input value which has been given in the configuration file (**jeset.par**). This difference increases the more the input value exceeds the limit. Based on the work of [31], who discusses the whole topic more detailed, I started a simplified test for an estimate of the consequence for my analysis. For this test I produced 10^6 events with different BE parameter sets and calculated the ratio $C(Q)$ = ($Q-$ distribution with BEC)/($Q-$distribution without BEC).

This distribution which has been produced with λ = 1.0 has been fitted with Eqn. 2.38. The results of this procedure are shown in Table 4.5, where it can be seen that the routine crashes for values higher than 0.35 GeV.

Input value $(1/\sigma)$ $[GeV]$	measured $(1/\sigma)$ $[GeV]$
0.1	0.107
0.35	0.345
0.5	0.397

Table 4.5: Input values and the corresponding measured values for the inverse region size $1/\sigma$

Since the typical hadron size is close to this value it is necessary to provide a method that supports also higher values than this limit. Since JETSET cannot do this, only values lower than 0.35 GeV are produced and extrapolated to higher values. [3]

The inclusion of BEC cures the problem as it can be seen from Fig.4.4. The fit (solid line) agrees very well with the data for the like-sign subtracted $\pi^+\pi^-$ as well as for the like-sign spectrum Fig.4.7. However the inclusion of BEC makes the extraction procedure more sophisticated and increases the computational efford by a factor of five.

Furthermore it should be mentioned that the tuning of the models does not include BEC up to now. If one tries to retune JETSET with BEC included, some of the QCD parameters change and the quality of the fit to inclusive distributions gets worse.[33] All tuned parameters for the models used within this work are tuned to the normal data.

4.5 Signal extraction procedure

To extract the cross section for the production of the ρ^0 , f_0 and f_2 , the invariant mass spectrum is fitted as the sum of the signal and a background function. The decision how these fit functions should look like is dictated by the following factors:

- the huge combinatorial background
- broad resonances
- many reflections

[3] A further test which could be of interest within the scope of this problem would be a study of the λ-value in dependence of the input parameter.

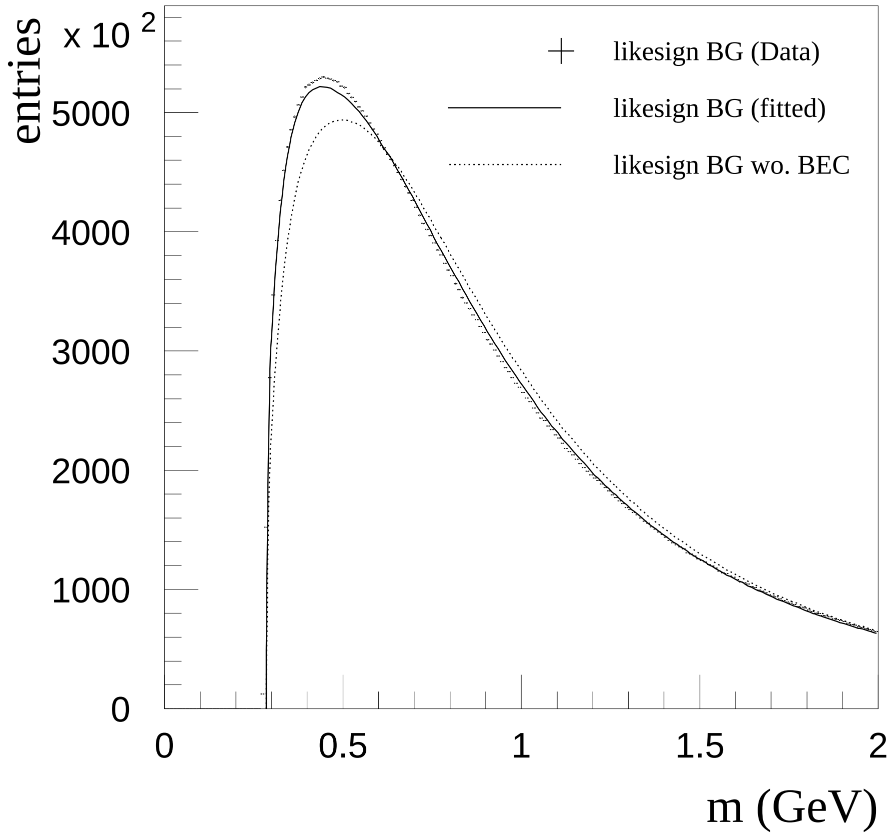

Figure 4.7: Fit to the like-sign invariant mass distribution

- Bose- Einstein- Correlations

As already mentioned, the most important factor are the BE correlations which heavily distort the spectrum as discussed before. To parameterize these changes of the resonance shapes and the corresponding discrepancies in the background shapes due to the BE effects two popular methods exist.

Phasespacefactor: The BE effects will be included with an additional phase space factor which has to be applied to the shapes. The advantage is the possibility of using analytical functions for the BG since the distortions are parameterized and can be added during the fit. The phasespace-factors are created with JETSET which supports BE correlations. For more details see [7]

Shapes with BEC: This method uses the generated full shapes, instead of analytical functions, for parameterizing the signals with BE correlations included. These shapes are produced according to the defining functions (e.g. Breit Wigner) with the JETSET 7.4 MC model including the LUBOEI BE correlation routine. This procedure affects all resonances which are assumed to be distorted by BEC as the ρ^0 , f_0 [4] , f_2 and the background shapes.

Although both methods deliver the same quality the latter method needs less computation time which is, as it can be seen later on, an important factor within this work. The parameters that have been used for the generation are listed in Table 2.4. I already mentioned that these parameters are the result of an extensive tuning of the model to reality [33] except the BE parameters. PARJ(91) controls, whether the decay products of a resonance are allowed to be affected by BEC or not. This decision is realized by a artificial minimum resonance width which rejects particles with a width smaller than this limit. The value for this analysis (100 MeV) is motivated by the idea to keep the K^{*0} which has a $\Gamma = 50.8 \pm 0.6$MeV unaffected by BEC. Both strength controlling parameter PARJ(92) and PARJ(93) are not fixed during the extraction procedure they are implemented as free fit-parameters. They vary freely in the range from 0 to 2.5 for PARJ(92) and between 0 to 0.35 for PARJ(93).

To achieve useful results it is necessary to parameterize the BG in such a way that it describes the data as good as possible. Of course this step is again biased by the inclusion of BEC but independent of that there are two established methods for the parameterization of the BG.

An often used tool is the analytical function, in particular a polynomial of 4^{th},5^{th} degree or sometimes higher in combination with a threshold function which accounts for the $\pi\pi$ threshold.

It works well as long as enough knowledge about the shape of the background is available and as long as the mass spectrum contains only well separated contributions with significant content. For a small test I generated 1 million standard[5] JETSET events, calculated the subtracted invariant mass spectrum and started a least squares fit to the subtracted $\pi^+\pi^-$ mass spectrum with the following fit function:

$$\begin{aligned} f(M) &= \alpha_7 \cdot BW(\rho^0) + \alpha_8 \cdot BW(f_2) + Reflection(\omega, ...) + BG \\ BG(M) &= \alpha_1 \cdot (M - M_{th})^{\alpha_2} \cdot \exp(\alpha_3 \cdot M + \alpha_4 \cdot M^2 + \alpha_5 \cdot M^3 + \alpha_6 \cdot M^4) \end{aligned}$$

where M_{th} is the $\pi\pi$ threshold and BW stands for a non relativistic Breit Wigner as it is implemented in standard JETSET MC. The f_0 has not been added since JETSET implements this resonance only with zero width and therefore cannot be treated within this test. The first term

[4]The f_0 is not affected by BEC although this has been assumed in the beginning

[5]Standard refers to normal JETSET 7.4 package with the parameters mentioned before but without BEC)

in the BG function causes a steep rise after the threshold as it can be also seen in the spectrum and the exponential term provides the long tail of the mass distribution. This fit reproduces the input values of the model as expected with an acceptable χ^2 (around 1) - but only as long as the initial values for the background (α_1....α_6) are close to the final values. To achieve this I fitted the BG, which I filtered out of JETSET with help of the history, with the BG function and used the fit results as input for the final fit. Without this trick it can happen, especially in the lower momentum region, that the f_2 disappears from the fit results because the background function compensates its peak due to its high number of degrees of freedom. This circumstances forced me to find another parameterization for the background which is not that sensitive to the initial values because the real data includes more uncertainties and therefore more destabilizes the procedure. Specially the overlap of so many resonances (ρ^0 , f_2 , f_0) which is forbidden in JETSET, can result in the suppression of a weak resonance such as the f_2 .

The alternative method relies completely on the MC in particular on JETSET. The idea is it to produce a background shape which is as close as possible to the real one as far as the knowledge about the processes behind is available. The MC produces a fixed shape according to the hadronization model and decay tables and is not very sensitive to initial values because only the normalization is a free parameter. A fit procedure using this background either fails totally ($\chi^2 > 10$) since no acceptable parameter set can be found or it fits the background well, but it is nearly safe against failing partly, as it can happen in the other model. Since the resonances ρ^0 , f_0 and f_2 are assumed to be affected by BE correlations it is the most adequate way to use JETSET for the generation. Some other reasons exist for using the JETSET shapes but these facts will be discussed in the section for the resonances.

It is an important task of the BG, to act as determining indicator for BEC parameter. Since the background experiences large changes and modifies the whole spectrum in a significant manner the BE parameters of the fit routine depend strongly on the BG.

For the signal (resonance) and the reflection - shape the same as for the background is valid. The next important factor is the large number of contributions in the spectrum. If we recall Fig 4.5 we recognize that the following shapes must be included.

- Background like-sign, unlike-sign
- ρ^0 , f_0 , f_2
- K^{*0}, η, η', ω, K^0_S

- other decay-modes of f_2 ,f_0 ,....

Each signal introduces at least one free parameter. To restrict the total number of degrees of freedom in order to achieve a reliable result fixed shapes (fixed width and mass) for the signals have been used. Furthermore the BEC requires the use of fixed shapes as we will see.

All four resonance shapes and the BG shapes are assumed to be affected by BEC and these shapes are generated with JETSET without detector. The remaining shapes (ω, η,...) have been taken directly out of the fully simulated standard MC (HVFL+Detekt), shown in Fig. 4.8–4.11 except the K^{*0} which also has been generated with JETSET although it is not affected by BEC.

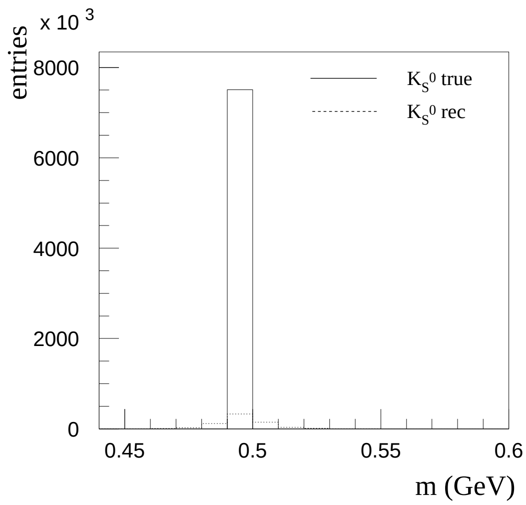

Figure 4.8: Shape of theK_S^0 extracted from full MC

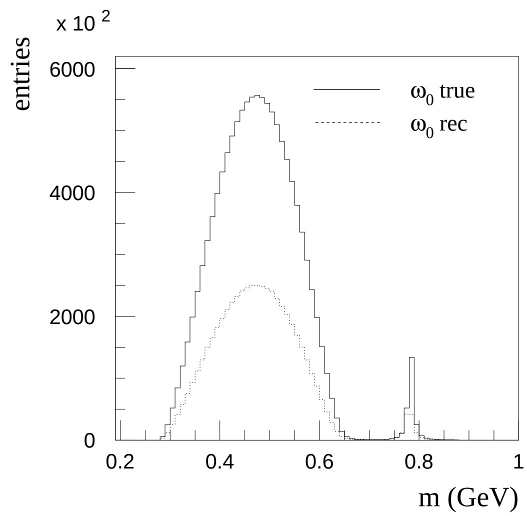

Figure 4.9: Shape of the ω extracted from full MC

Taking the shapes from full MC is possible since all four particles above have been measured extensively during all the years and their characteristics are rather good known and implemented with high quality into the MC.

For the extraction of the shapes 10^7 full MC events, belonging to the years 1992-1994, have been used. To filter the reflections out of the total spectrum the ALPHA routine MCMATCH together with the MC history has been applied . Further details to this matching routine and the procedure will be discussed in acceptance section. These forms can be used as they are, except

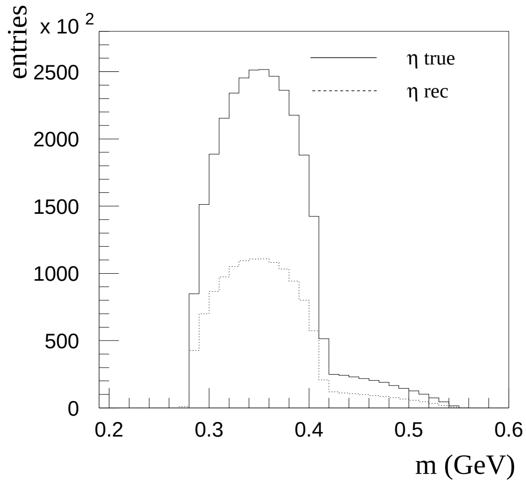

Figure 4.10: Shape of the η extracted from full MC

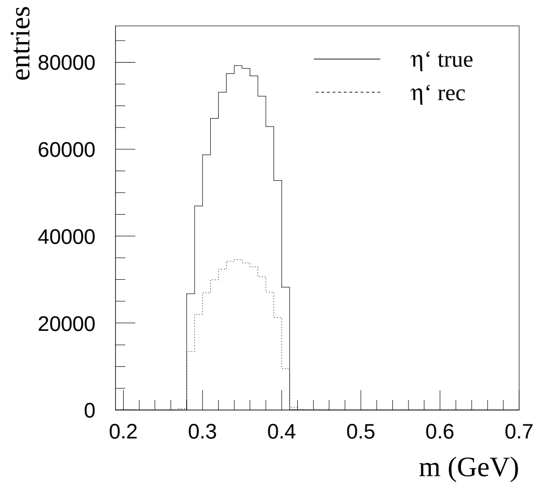

Figure 4.11: Shape of the η' extracted from full MC

their normalization.

This is different for the signals that have been produced by JETSET since they do not include the distortions due to the detector and selection cuts. The change of the signal makes itself felt in reducing the total normalization and in distorting the overall shape as it has been shown for the ω (Fig. 4.9). To take this changes into account acceptance functions have been introduced and this mechanism will be discussed in the acceptance section.

Summarizing the ideas which are necessary to approach as close as possible to reality we can build up a general fit function:

$$\begin{aligned} f(m, \lambda, \sigma) \quad = \quad & BW_{\rho^0} + BW_{f_2} + BW_{f_0} + \\ & Refl(\omega, \eta, \eta', K_S^0) + BW_{K^{*0}} + \\ & BG \end{aligned} \tag{4.4}$$

The two arguments λ and $1/\sigma$ indicate that the fit handles the two BE parameters as free parameters. Making the usage of BEC possible - samples with different BE parameter sets (Table 4.6)

λ PARJ(92)	$1/\sigma$[GeV] PARJ(93)	statistics
0	0	10^7
0.5	0.1/0.3/0.35	each 10^7
1.0	0.1/0.3/0.35	each 10^7
1.5	0.1/0.3/0.35	each 10^7
2.0	0.1/0.3/0.35	each 10^7
2.1	0.1/0.3/0.35	each 10^7
2.5	0.1/0.3/0.35	each 10^7

Table 4.6: Parameter sets for the production of the JETSET shapes

each with a statistics of 10^7 events have been generated.

Each sample contains the shapes of the resonances (ρ^0 , f_0 , f_2), the background and the K^{*0}. During the fit procedure a interpolation algorithm caculates the missing parameter sets with the according shapes in order to allow a free variation of the BE parameter. Since the JETSET algorithm for BEC is a simple one an additional correction must be applied to the background shapes and this changes the BG contribution to the following:

$$\begin{aligned} BG(m,\lambda,1/\sigma) &= BG_{unlike-sign}(m,\lambda,1/\sigma) - \\ &\quad \alpha_1(1-\alpha_2 Q)\cdot BG_{like-sign}(m,\lambda,1/\sigma) \end{aligned} \tag{4.5}$$

where Q is the four momentum difference. This linear correction in Q accounts for long range effects due to BEC which are not implemented in the LUBOEI routine. A further correction would be the inclusion of Coulomb interactions which affect the lowest Q regions. Since no applicable model exists these effects couldn't be regarded.

4.6 The generation of the shapes

The shapes of the three resonances ρ^0 , f_0 , f_2 and also of the background must be generated with JETSET - especially the f_0 which is completely wrong implemented into the standard MC. (zero width, $m_0 = 1$ GeV). Furthermore the reflection K^{*0} is also generated by this procedure since the shape created by the standard full MC is not adequate. The necessity for the JETSET hadronization model is based on the BEC. This requirement together with the complexity of the resonance shapes [24] which is not supported by standard JETSET requires changes in several

JETSET routines. In the following I will discuss what is required and how it can be achieved.

4.6.1 The ρ^0 (770) Signal

The ρ^0 is a vector-meson (l=1)[6] decaying into two pseudo-scalar Mesons ($\pi^+\pi^-$) with a branching ratio of 100 %. Using a relativistic Breit Wigner approximation we obtain the amplitude for the production of a vector meson:

$$\mathcal{A}_V = \frac{\mathcal{P}_V m_V \sqrt{\Gamma_X \Gamma_V}}{m_V^2 - m^2 - i m_V \Gamma_V} \tag{4.6}$$

where $\mathcal{P}_V$ represents the production amplitude, m_V being the nominal mass and Γ_V the total width and Γ_X is the partial width $(V \to X)$ for the final state X. According to the spin and the Eqn.4.6 the invariant mass distribution can be described with a relativistic p-wave Breit Wigner [24]:

$$BW(m) = \frac{m \cdot m_0 \cdot \Gamma(m)}{(m^2 - m_0^2)^2 + m_0^2 \Gamma(m)^2} \tag{4.7}$$

m_0 is the nominal mass of the ρ^0 (value taken from [20]) and $\Gamma(m)$ is the mass dependent width. For the latter several parameterizations exist (see therefore [28]). For this analysis the width is parameterized as follows:

$$\Gamma(m) = \Gamma_0 \cdot \frac{2 \cdot (\frac{m^2 - 4 \cdot m_\pi^2}{m^2 - 4 \cdot m_\pi^2})^{\frac{l+1}{2}}}{1 + \frac{m^2 - 4 \cdot m_\pi^2}{m_0^2 - 4 \cdot m_\pi^2}} \tag{4.8}$$

Γ_0 is the nominal width of the ρ^0 [20] and l=1 corresponds to the spin; m_π the pion mass according to [20]. It is noted by the authors [28] that no parameterization is more meaningful than the other. (The change of the shape due to the other mentioned parameterizations is the same.) Nevertheless Eqn. 4.8 has been found to fit better then the other as well as in low energy and in the high energy regions. A further advantage of this formula is the restriction to known variables instead of introducing new parameters.

[6] l represents the angular momentum

4.6.2 The f_0 (980) signal

This resonance belongs to a part of high energy physics which is still an almost unsolved riddle - namely the 0^{++} sector. The composition of the f_0 (980) is still under investigation [20] and possible explanations for the structure of the particle are: $q\bar{q}$ resonance, $K\bar{K}$ molecule, a particle with a large gluonic content,... . Also the nominal values for the resonance (mass, width) underlie large uncertainties as well as the branching ratios which lately have been removed from PDG book 1998 [20]. Within this work I assumed that the f_0 corresponds to a $q\bar{q}$ state and the branching ratios have been taken from PDG book 1996. The shape of the f_0 is the next problem since several Ansätze exist. The simplest method is the usage of a relativistic s-wave Breit Wigner. Others studies preferred to use a more complicated model, e.g. the so called Flatte formula [16, 38].
This concept incorporates the fact that the f_0 is positioned just above the KK threshold. It takes into account the change of the shape due to the opening of the KK channel. This method is of special interest if one needs to do a two channel analysis [8]. Following other analysis investigating into the same topic I decided to use the Flatte shape for the parameterization. Additionally to this parameterization of the shape I added BE effects to the form. Whereas the first fit-series with only one BE parameter (λ) incorporated into the fit showed acceptable results. Including both BE parameters let the fit fail. The resonance shape of the f_0 became too broad with a vanishing multiplicity. Since the Flatte model does not allow to access the width directly it is difficult to correct the width in a meaningful manner. For a detailed discussion of the parameters of the Flatte parameterization look up [8, 38] As a consequence I switched off the BE effects and reported an improvement of the situation. Since the χ^2 didn't improve in the affected mass range I decided to use a different shape. The use of a relativistic s-wave Breit Wigner without BEC achieved the best results (small χ^2). Of course I tested again this shape with BEC switched on but the χ^2 started to increase again. This can be interpreted that the f_0 is not affected by BEC. This change from Flatte model to the simpler Breit Wigner function improves the χ^2 from 1.63 to 1.49. The shape has been embedded into the fit procedure as a analytical function according to Eqn. 4.7 and the width Γ has been parameterized in the same manner as the width of the ρ^0 - Eqn. 4.8. Since it is assumed that the f_0 is a scalar meson, the value for the angular momentum is set to $l = 0$. The use of an analytic function allows to vary the nominal mass and width during the fit procedure, as it will be described in detail in the section discussing the fit procedure. Due to large uncertainties of the nominal mass and width [20] it is nearly impossible to proceed with a method that uses fixed values and a variation of the shape is obviously impossible with a fixed one.

In a first fit series the mass and width have been implemented as additional degrees of freedom. The fit to each x_p range delivered a value for the mass and the width listed in Table 4.7.

$x_p - range$	f_0-mass [GeV]	f_0-width [GeV]
0.005 -0.025	0.9609±0.0032	0.0727±0.0249
0.025 -0.05	0,9646±0.0030	0.0601±0.0101
0.05 -0.1	0.9751±0.0024	0.0606±0.0071
0.1 -0.15	0.9661±0.0029	0.0636±0.0084
0.15 -0.2	0.9716±0.0019	0.0479±0.0067
0.2 - 0.3	0.9690±0.0011	0.0436±0.0040
0.3 - 0.5	0.9688±0.0018	0.0315±0.0045
0.5 - 1.0	0.9615±0.0028	0.0287±0.0079

Table 4.7: Measured values for the f_0 mass and width for each x_p interval

From this table averaged values for the mass of the f_0 and for its width have been derived.

$$
\begin{aligned}
m_{f_0} &= 0.97 \pm 0.0025 \\
\Gamma_{f_0} &= 0.051 \pm 0.0111
\end{aligned}
$$

The values agree within one sigma with the PGD values [20]. ($m_{f_0} = 0.98 \pm 0.01$; $\Gamma_{f_0} = 40\text{to}10$ MeV) and therefore I used the averaged values as input for the final fits where they are implemented as fixed parameters. The small width stresses the assumption that the f_0 isn't affected by BEC, as long as we assume that a resonance affected by BEC must have a certain width - in our case larger than 100 MeV. The small width is also the reason that a small bin width (10 MeV) has been chosen for the analysis. Since it is required to have at least three points for the peak of each resonance to get a reasonable fit a adequate bin size must be selected. This requirement excludes a bin width of 20 MeV as it was used in earlier measurements [12]. Since the measurement of the mass and the width is not the main task of this work no systematics have been done due to lack of time.

4.6.3 The f_2 (1270) resonance

This resonance is the highest excited one of the three analyzed particles. The f_2 is a tensor meson with a mass of 1275 ± 1.2 MeV and a width of $185.5^{+3.8}_{-2.7}$MeV and it decays mainly into the $\pi^+\pi^-$ channel with a branching ratio of $84.6^{+2.5}_{-1.3}$ %. Apart the angular momentum (l=2) the f_2 is assumed to behave in the same way as the ρ^0 and therefore is is generated with the same parameterization - Eqn. 4.7. Since the width of the f_2 is larger than the JETSET BE limit (PARJ(91) = 100MeV - look up section 2.6) it is assumed to be affected by BE effects. This means that the resonance has been produced with the same BE parameters as the ρ^0 . The shape differs in principle from the shape of the ρ^0 since the higher excitation causes a longer tail for the f_2 than for the ρ^0 . It has been claimed that this tail is somehow unphysical [44] and therefore other suggestions for the parameterization have been made [44]. A comparison of both parameterizations shows some problems when using the shape defined in [44]. The χ^2 increases from 1,49 (using the parameterization from this work) to $\chi^2 = 1{,}95$ (using the other description).

4.6.4 The K^{*0} reflection

The K^{*0} is a strange vector meson at a mass of $m = 896.1 \pm 0.28$ MeV and a full width $\Gamma = 50.5 \pm 0.6$ MeV. Although it decays into $K\pi$ with nearly 100 % it is part of the $\pi^+\pi^-$ mass spectrum since the K is misidentified. During the analysis the mass of the misidentified K is assigned to the pion mass and that is the reason why the K^{*0} appears at $m \sim 692$MeV in the $\pi^+\pi^-$ mass spectrum. Of course only 2/3 of the particles decay into the $\pi^+\pi^-$ spectrum due to the isospin algebra. Since the peak is positioned just below the ρ^0 resonance it can't be neglected in the analysis and therefore it is necessary to improve the parameterization of this reflection (not truncated, relativistic BW,....) . The reflection has been parameterized with a relativistic p-wave Breit Wigner (Eqn. 4.7), setting l=1. It has been tested by other analysis [3] that it is adequate to use a slightly different parameterization of the width for the K^{*0} than for the ρ^0 .

$$\Gamma_{K^{*0}} = \Gamma_0 \cdot \left(\frac{q}{q_0}\right)^{(2l+1)} \frac{m_0}{m} \tag{4.9}$$

where l=1 is required a for vector meson; m is the invariant mass and m_0 the central mass of the K^{*0}; q is the momentum of the decay products in the rest frame of the parent, and q_0 is the momentum if $m = m_0$. The contribution of this reflection to the $\pi^+\pi^-$ mass spectrum can be seen in Fig. 4.5. It should be noted once again, that the K^{*0} is assumed to be not affected by BE correlations since the χ ($\hat{=}$ minimum particle width - see section 2.6) of the JETSET routine has been set to 100 MeV. The nominal mass and the width have been taken out of [20].

Generation algorithm

All shapes discussed above must be generated with a modified JETSET [36] because the standard JETSET which is used for the full MC generation does not support all these different types of parameterization. In the standard MC as already mentioned only non relativistic Breit Wigner are generated and the shapes are truncated symmetrically around the nominal mass. The truncation width is set individually to a value that ensures that all decay channels are kept open - as well for the decays of the resonance itself as for the particles which contain the resonance as a decay product. Normally the resonances are produced according to:

$$BW(m) \sim \frac{\Gamma^2}{((m - m_0^2)^2 + (m/m_0\Gamma)^2} \tag{4.10}$$

This function can be inverted, integrated and therefore the function can be easily used to distribute the random numbers according to the function. The Breit Wigner functions used for the resonances and reflections in this work cannot be integrated analytically and it is also hard to invert the function specially the width. Because of that a small modification has been applied to the JETSET routine to allow the usage of the formulas required.

As already stated above it is not possible to build a generator that uses an analytical function for the shapes. It is necessary to use a numerical method for the generation. The algorithm is based on the idea of "hit or miss", which always yield to a correct answer. A requirement is the knowledge of the maximum of the function $f(x)$ in the considered range. The maximum for the Breit Wigner function 4.7 is not at $m = m_0$ as someone would expect. Due to the complicated function of the width the peak is positioned a small step below the nominal mass. This maximum has been determined numerically.

The method works as long as only one peak dominates the distribution otherwise one must subdivide the distribution into several parts and calculate each peak for its own. Since this is not necessary in our case the procedure can be described as follows.

1. select an x with even probability in the allowed range; i.e. $x = x_{min} + R(x_{max} - x_{min})$ where R is a random number between 0 and 1

2. compare a new random number R with the ratio $f(x)/f_{max}$; if $f(x)/f_{max} \leq R$ reject the x value and return to point 1 for a new try.

3. otherwise the most recent x value is retained as final answer.

The two random numbers must generated independently. The correct distribution is generated since the probability that $f(x)/f_{max}$ is greater equal than the random number is proportional to $f(x)$. The quality of the procedure increase with the computational efford but this slows down the total generation process. This new generation routine has been implemented into the JETSET subroutine LUMASS which produces the mass distribution of the particle according to their functions. The standard JETSET produces resonances only within a certain mass range which ensures that each decay channel of the resonance can be accessed. To provide a realistic model of the resonances this restriction must be changed. The resonances, the reflections respectively have been produced within a range from the $\pi\pi$ threshold (m=280 MeV) to an upper limit of 3.0 GeV. Beyond the latter the shape contains no significant contributions and it is far enough from the highest nominal mass (m_{f_2} = 1275MeV) so it does not distort any resonance. Only for the K^{*0} the lower starting point has been set to the $K\pi$ threshold.

Of course these modification distort the total rates of the resonances within this production, but this is irrelevant for this usage since the program has been used only for the generation of the shapes neglecting the total normalization. This has been taken into account with normalizing the shapes to unity after their production.

In Fig. 4.12 to Fig. 4.15 the shapes of the resonances (ρ^0 , f_2) are presented with different BE parameter and compared with the standard MC shapes.

As already mentioned in the beginning of the section the BG is also produced with JETSET since the BG is affected by BEC as well. For the BG no modification have been necessary to the JETSET program except the change of the BE parameters.In Fig. 4.17 and Fig. 4.18 one can see the changes that happen due to BEC as described in the theory.

Since it is not affected by BE effects for the f_0 only the shape generated with the Flatte algorithm and the finally used relativistic s-wave Breit Wigner is shown (Fig. 4.16. All effects caused by BE correlations, as described in the previous sections (e.g. broadening of the ρ^0 , shift of the mass peak,...), can be observed in the pictures. Since these shapes do not know anything about the detector they must be corrected for this distortions. This correction does not change only the normalization, it distorts also the shape itself and that's why an acceptance function is needed.

4.7 Acceptance function

The detector and also the cuts change the shape of the signals since the distortions are not uniform over the full mass range. To include this effects into the fit procedure its necessary to define a function which parameterizes all the changes. This function can be applied to the true level shapes which have been produced according to the mechanism explained in the previous section and we

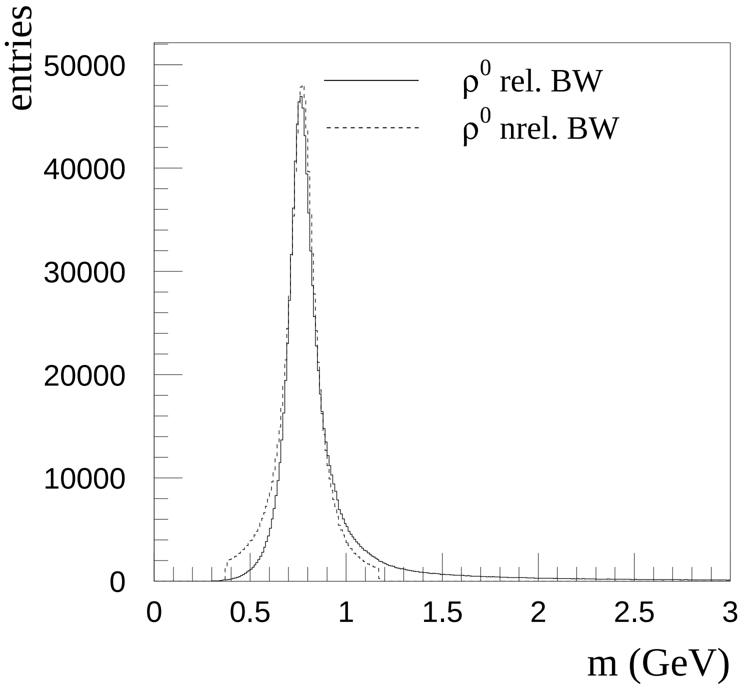

Figure 4.12: The shape of the ρ^0 has been parameterized once with the options set by the standard MC and once with the relativistic parameterization.

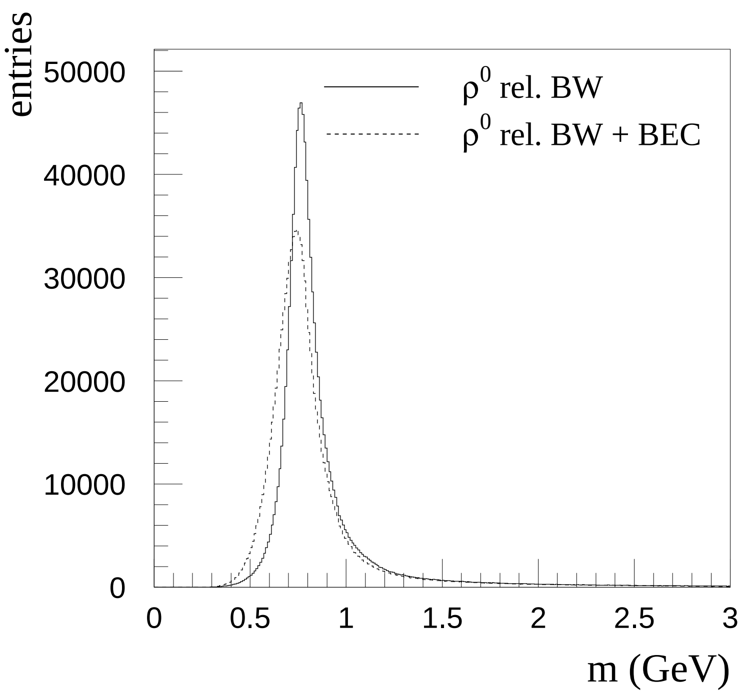

Figure 4.13: Comparison of the shapes of the ρ^0 with and without BEC.

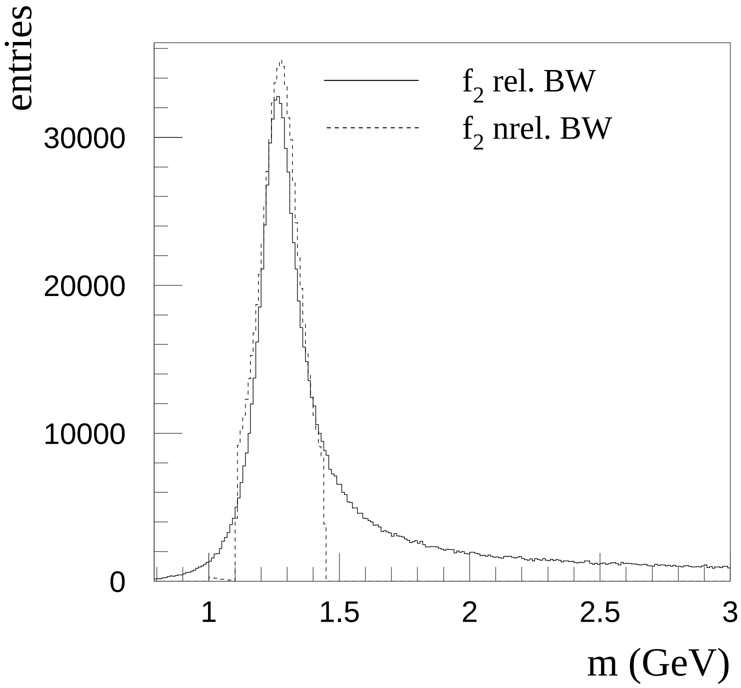

Figure 4.14: The shape of the f_2 has been parameterized once with the options set by the standard MC and once with the relativistic parameterization.

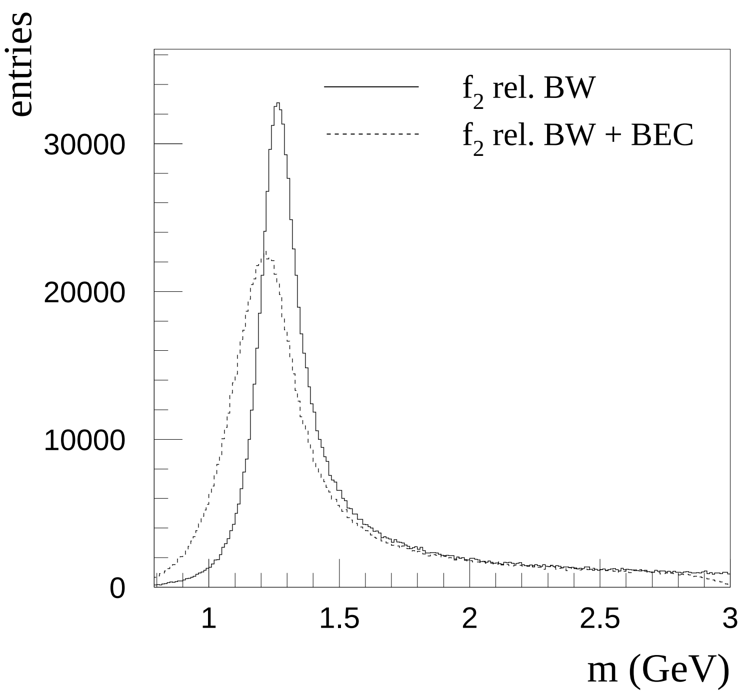

Figure 4.15: Comparison of the shapes of the f_2 with and without BEC.

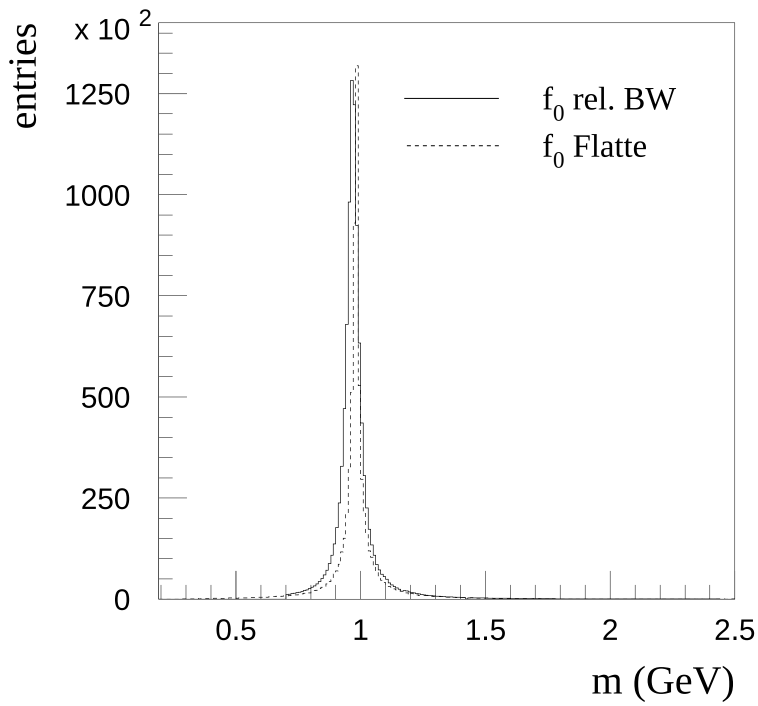

Figure 4.16: The shape of the f_0 has been generated once with the Flatte formula and once with the normal relativistic s-wave Breit Wigner

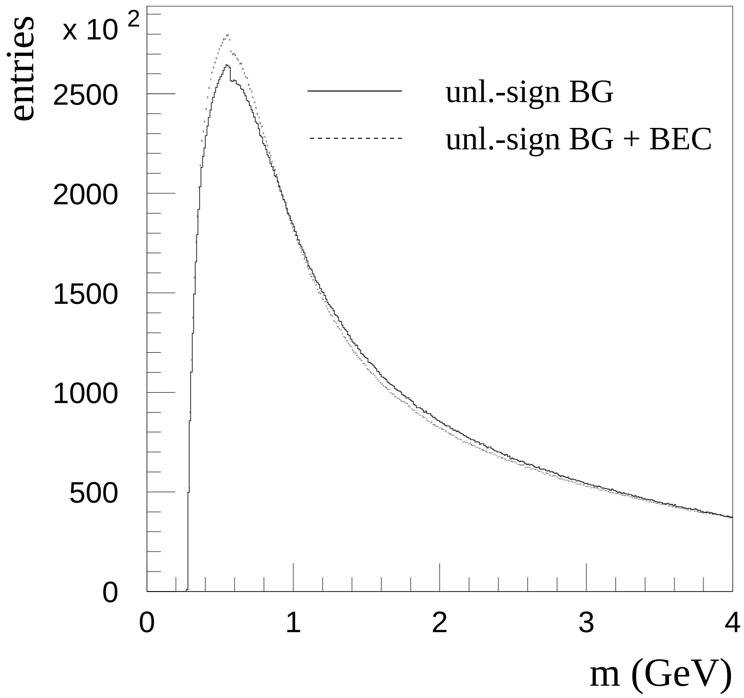

Figure 4.17: The unlike-sign background with and without BEC

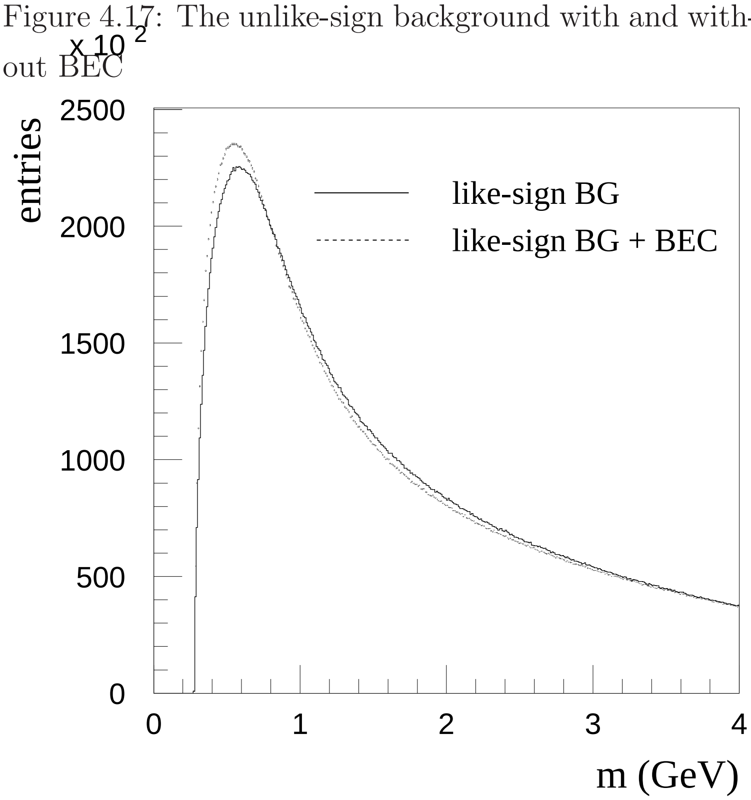

Figure 4.18: The like-sign background with and without BEC

should obtain a sample of shapes equal to the shapes from the full MC but with more features.

This function must parameterize the following distortions:

- detector acceptance
- detector smearing
- selection cuts

This acceptance function has been calculated with a large full MC sample together with the history and the matching information which connects each detected particle with the true particle produced. For the matching between the produced particle and the detected particle the ALPHA routine MCMATCH (which corresponds to the detector acceptance) has been used. The matching has been accepted when the routine returned an unique match. After fulfilling all cuts the detected particle has been stored. For this acceptance-algorithm exist several methods. In the following I will shortly present the two most popular.

- The first method has been favoured, by [8]. Its a more complex method since it splits up this function into three parts: The detector acceptance A_n, a smearing matrix S_{mn} and factor C_m which characterizes the losses due to the cuts. The acceptance function is than defined as follows:

$$\bar{N}_m = C_m \sum S_{mn} A_n \cdot f_n \tag{4.11}$$

  where f_n is the shape to be changed. This method is very time consuming when it is applied during the fit. But if all the resonances which are affected are narrow (¡ 50 MeV) this method should be preferred since then, the smearing matrix delivers better results than the second method.

- The used procedure is simpler than the previous one although within this work no difference can be observed. This method knows only two stages: the particle before it passes the detector and once after all cuts. The acceptance is reduced to a one-dimensional function A_m which works according to the following formula:

$$\bar{N}_m = A_m \cdot f_m \tag{4.12}$$

  where m indicates the number of the mass bin and f_m is the shape of the signal generated by JETSET.

For the following type of signals an acceptance function is needed.

- Resonances: ρ^0 , f_2 , f_0
- Reflections: K^{*0}
- Background like-sign
- Background unlike-sign

For each of the four types above and for each x_p-range two histograms have to be stored. One for the true particle and one for the detected which is related to the truth via MCMATCH as described in the beginning. These two histograms have been used in the following defining function 4.13 to calculate the respective acceptance function.

$$A_m = \frac{dn/dm(MC^{full})_1}{dn/dm(MC^{gen})_i} \qquad (4.13)$$

where i indicates the signal type. Of course both used histograms are normalized to the same number of events. Some particles are produced by interaction with matter (e.g. e,p) which causes problems in MC samples. These particles must be produced already by the generator and therefore they are available also in the MC truth for technical reasons although they should exist only in the reconstructed sample. To achieve a clean sample which contains no such particle in the histograms of MC truth the stability code (**KSTABC**) has been required to be either 1,2 or -3. This requirement rejects all unwanted particles and ensures that the total energy is conserved. If one neglects this option it results in a too high number of protons.

Again each particle has to pass all the cuts which have been applied to the real data. The history of each particle has been used to distinguish between different parent particles (ρ^0 , f_2 ,...) and for each the mass distribution has been stored separately. The truth mass distribution of the particle as well as the reconstructed. The next step is the calculation of the acceptance function according Eqn. 4.13. The whole production process of the acceptance function is illustrated in Fig. 4.19.

As before the truncation of the standard resonance shapes requires an additional investigation to complete the whole procedure. Beyond such a cut off no acceptance function can be calculated for the resonance which goes up to 3.0 GeV. In this analysis the following solution has been found. For the three resonances it can be assumed that all have the same behaviour in the detector and therefore the acceptance-functions of the latter can be put together. With this method the acceptance for the $\pi^+\pi^-$ resonances goes up to 1.45 GeV which is the upper limit of the f_2 . The

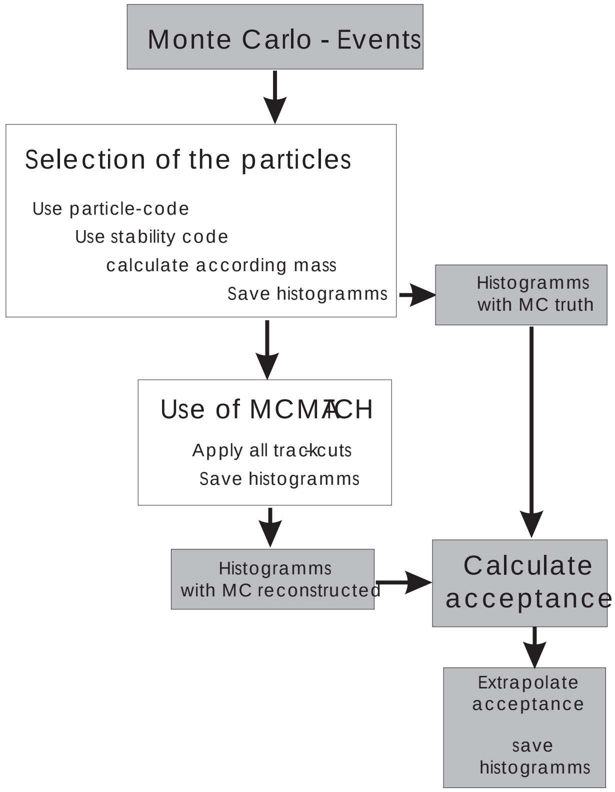

Figure 4.19: The production of the acceptance function.

f_0 does not contribute to this calculation since the implementation in the standard MC is wrong as already mentioned before. A linear extrapolation has been used to provide the required full mass range. The extrapolation uses the last 0.4 GeV (f_2 mass range) to fit the linear function. The influence of the choice of the extrapolation function has been tested in the systematic section. The acceptance functions of the signals for different x_p ranges are shown in Fig. 4.20 - Fig. 4.27. Specially for higher momenta the statistics for the f_2 are rather low due to the low multiplicity. That's why the uncertainties, the fluctuations respectively are larger in this range. The handling of the acceptance for the reflections (K^{*0}) is more difficult since only one signal exist. For the region without signal again the extrapolation has been used. The statistics are low for the reflection and this produces large fluctuations. The acceptance functions of the reflection are presented in Fig. 4.28 - Fig. 4.35.

For the backgrounds these problems are not present since they are available over the full range as shown in Fig. 4.36-4.51. If we compare the acceptance function of the background to the function of the resonances we find that the BG acceptance functions fluctuate less compared to the other, since the number of entries is much higher. This fact is important for the stability of the fit.

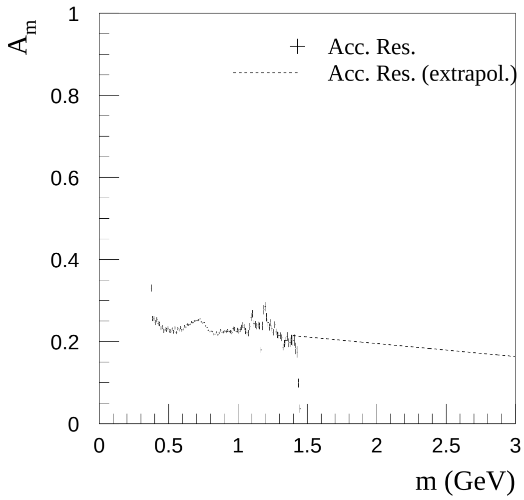

Figure 4.20: Resonance (x_p=0.005-0.025)

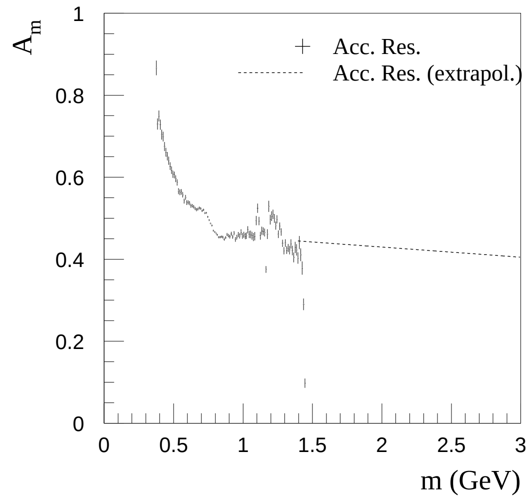

Figure 4.21: Resonance (x_p=0.025-0.05)

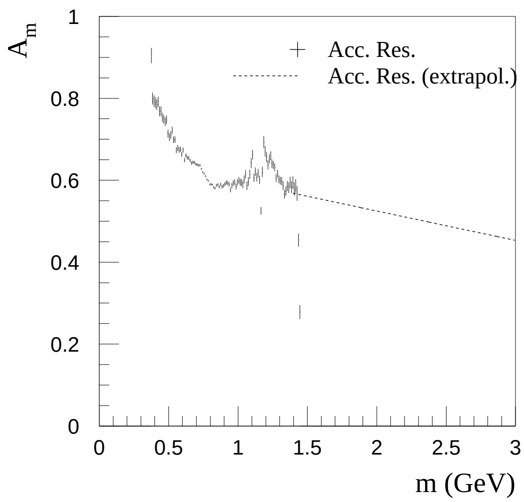

Figure 4.22: Resonance (x_p=0.05-0.1)

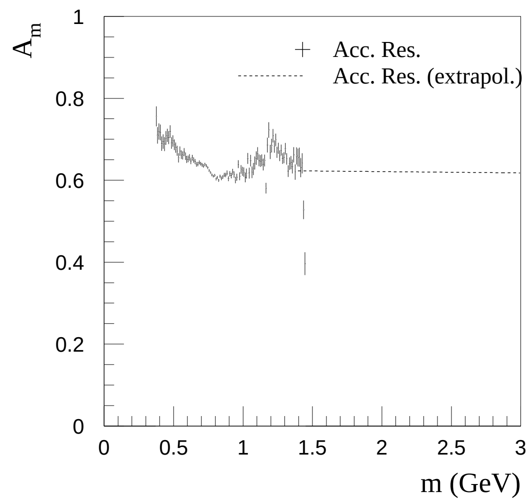

Figure 4.23: Resonance (x_p=0.1-0.15)

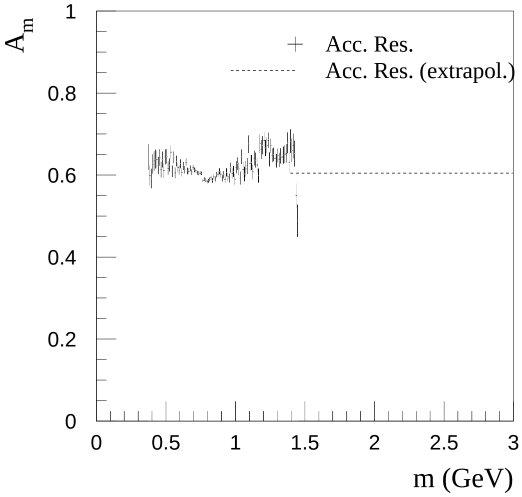

Figure 4.24: Resonance (x_p=0.15-0.2)

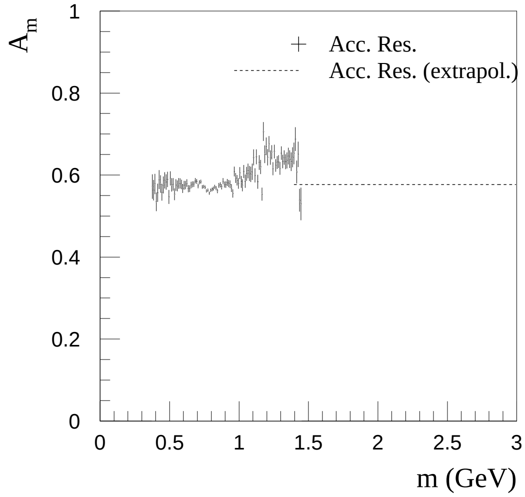

Figure 4.25: Resonance (x_p=0.2-0.3)

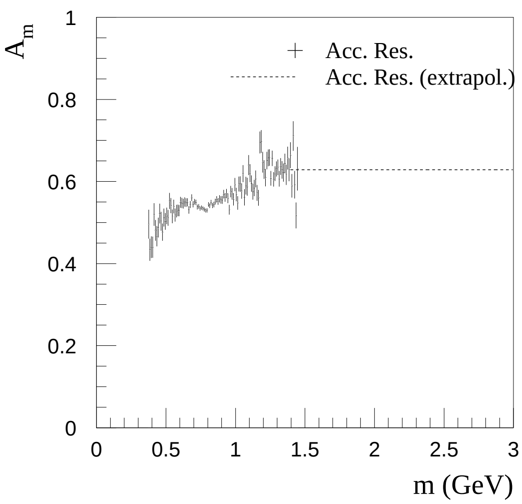

Figure 4.26: Resonance (x_p=0.3-0.5)

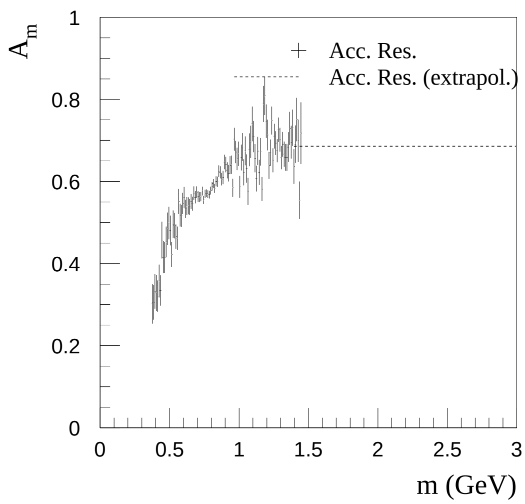

Figure 4.27: Resonance(x_p=0.5-1.0)

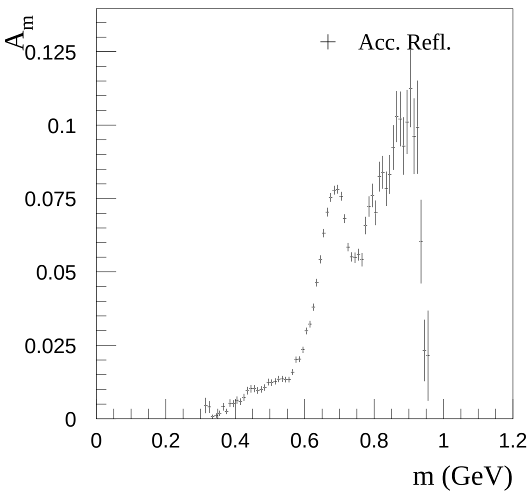

Figure 4.28: Reflection (x_p=0.005-0.025)

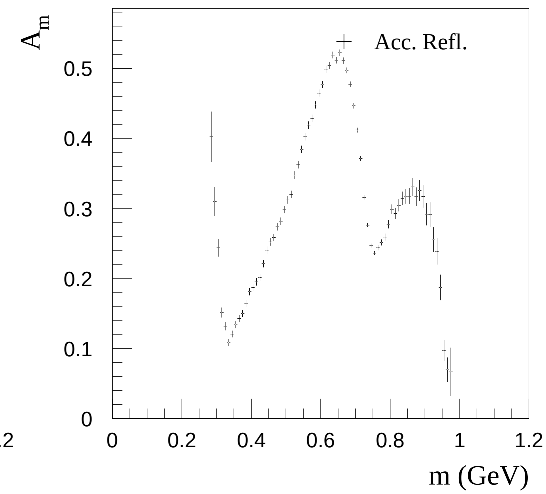

Figure 4.29: Reflection (x_p=0.025-0.05)

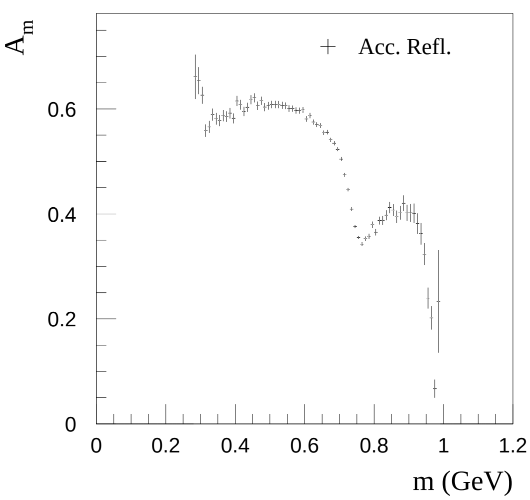

Figure 4.30: Reflection (x_p=0.05-0.1)

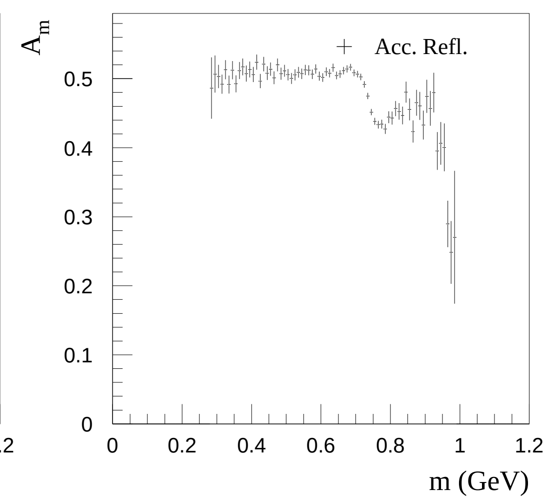

Figure 4.31: Reflection (x_p=0.1-0.15)

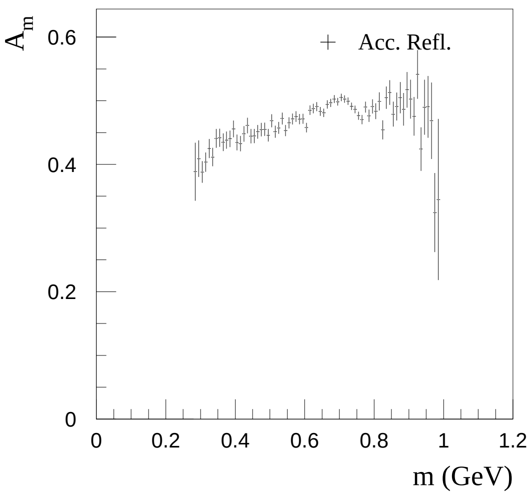

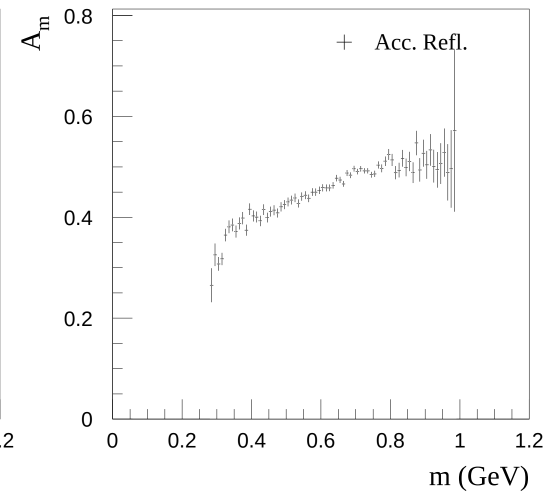

Figure 4.32: Reflection (x_p=0.15-0.2)

Figure 4.33: Reflection (x_p=0.2-0.3)

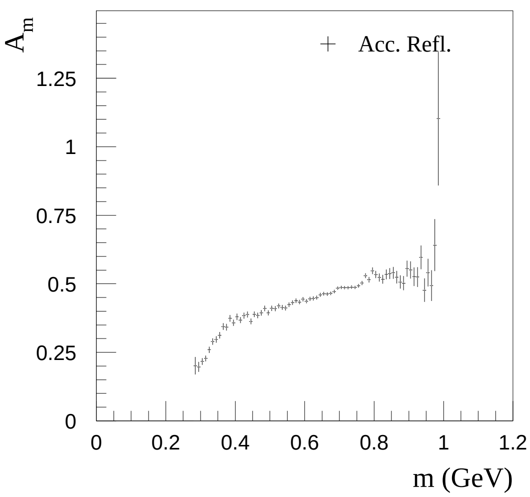

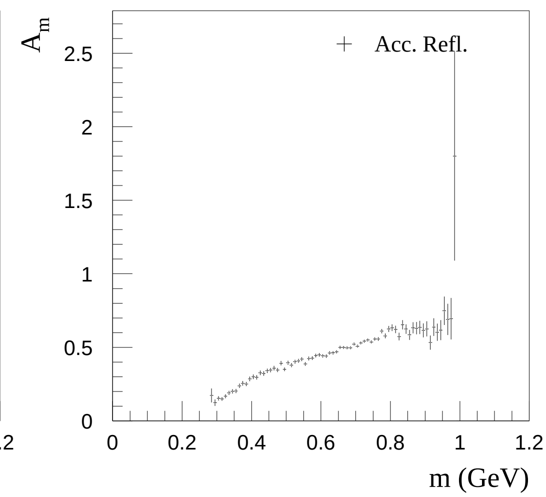

Figure 4.34: Reflection (x_p=0.3-0.5)

Figure 4.35: Reflection (x_p=0.5-1.0)

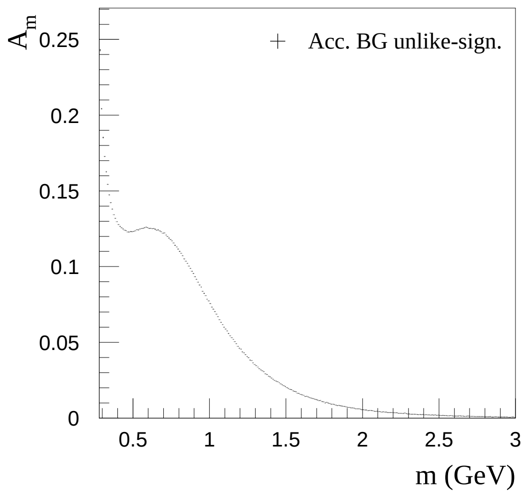

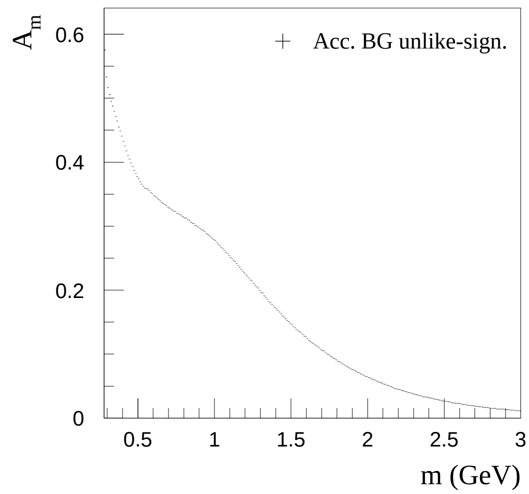

Figure 4.36: Unlike sign BG(x_p=0.005-0.025)

Figure 4.37: Unlike sign BG(x_p=0.025-0.05)

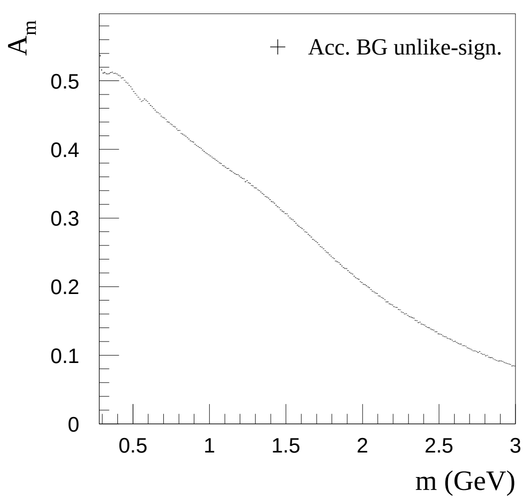

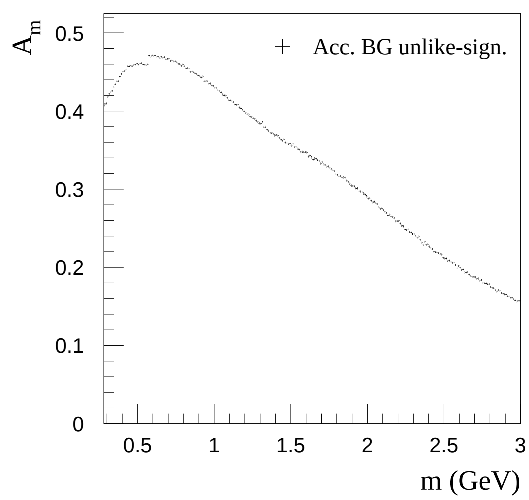

Figure 4.38: Unlike sign BG(x_p=0.05-0.1)

Figure 4.39: Unlike sign BG(x_p=0.1-0.15)

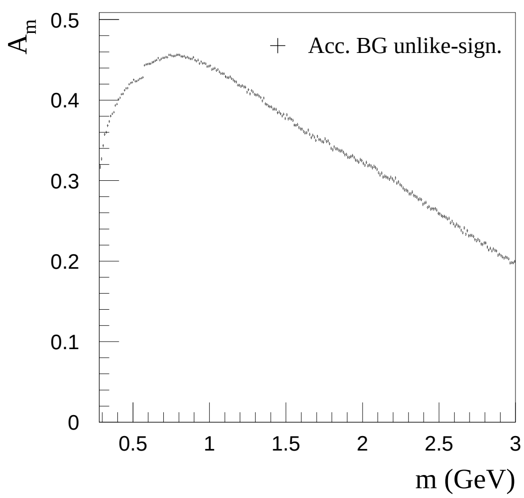

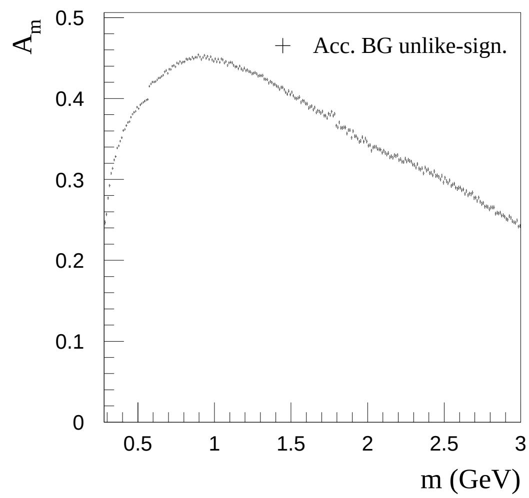

Figure 4.40: Unlike sign BG(x_p=0.15-0.2)

Figure 4.41: Unlike sign BG(x_p=0.2-0.3)

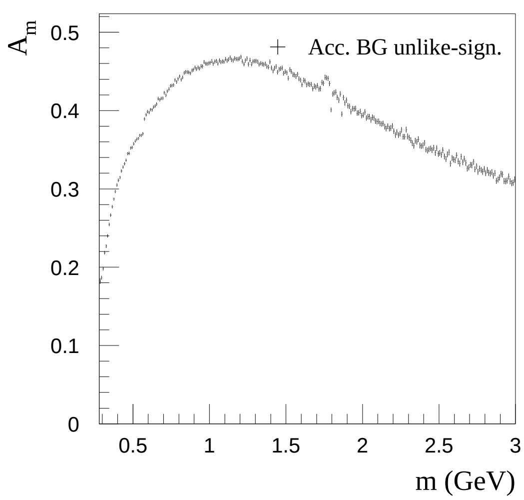

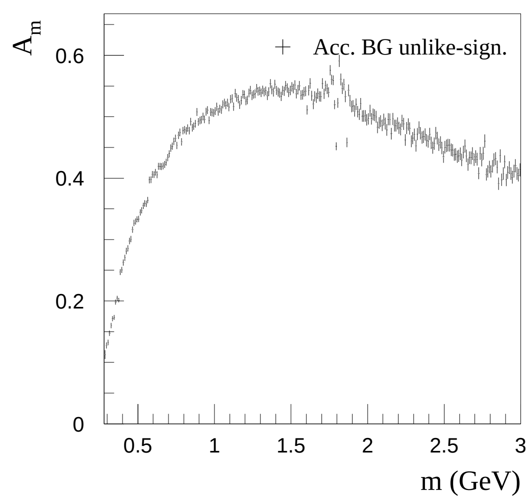

Figure 4.42: Unlike sign BG(x_p=0.3-0.5)

Figure 4.43: Unlike sign BG(x_p=0.5-1.0)

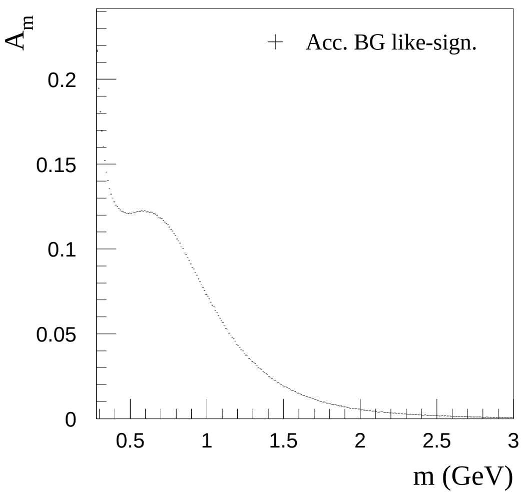

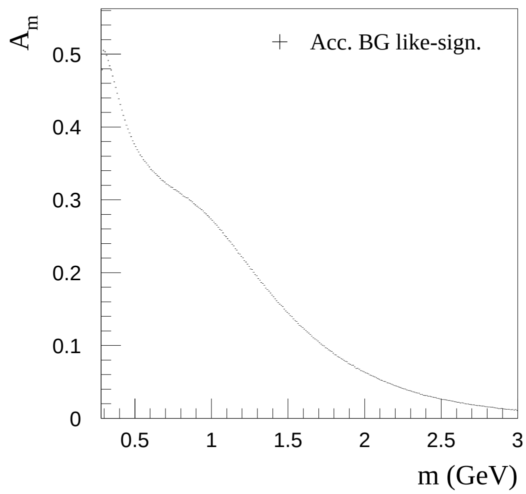

Figure 4.44: Like sign BG(x_p=0.005-0.025)

Figure 4.45: Like sign BG(x_p=0.025-0.05)

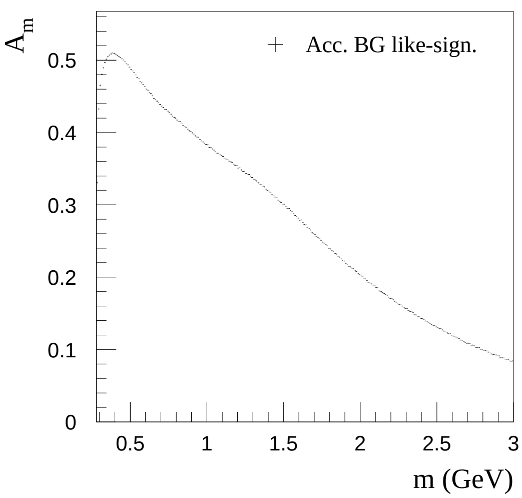

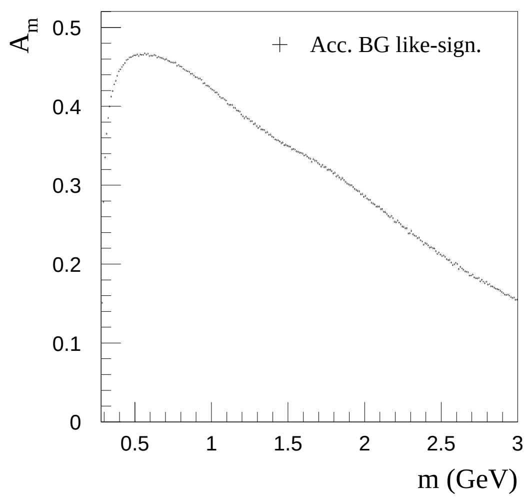

Figure 4.46: Like sign BG(x_p=0.05-0.1)

Figure 4.47: Like sign BG(x_p=0.1-0.15)

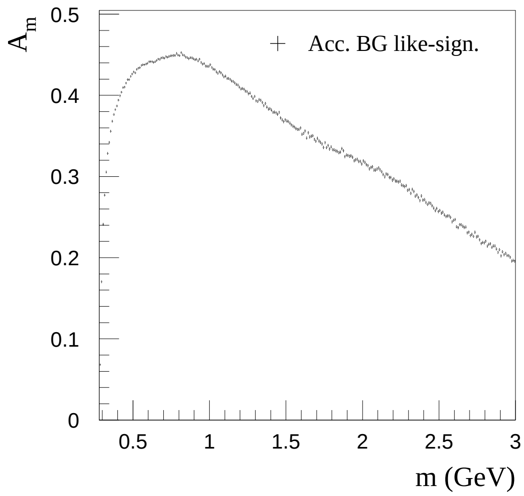

Figure 4.48: Like sign BG(x_p=0.15-0.2)

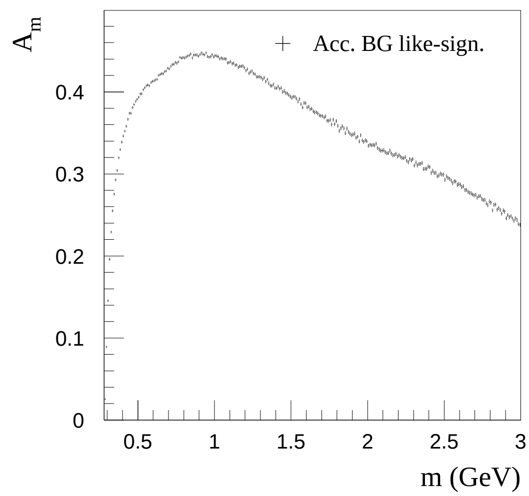

Figure 4.49: Like sign BG(x_p=0.2-0.3)

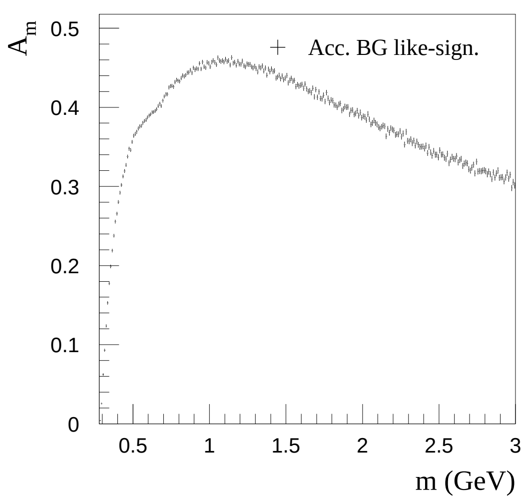

Figure 4.50: Like sign BG(x_p=0.3-0.5)

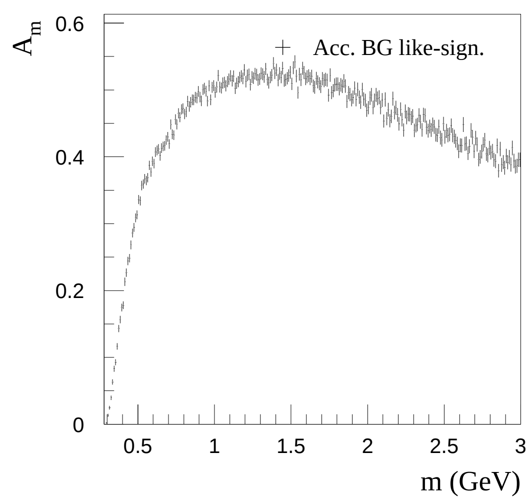

Figure 4.51: Like sign BG(x_p=0.5-1.0)

A wildly fluctuating shape of the acceptance function in combination with a narrow resonance reduces the chance of a successful fit.

To understand the behaviour of the acceptance function at least for the resonances a few simple consideration must be done. The overall normalization of the acceptance is given by the reconstruction probability of two single tracks. The single track reconstruction probability is ~ 0.9 [11] which result in a maximum probability for two tracks of ~ 0.8. Additionally it is reduced due to the cuts which have been applied. The more or less steep rise at the $\pi^+\pi^-$ threshold comes from the track angular resolution which has a minimum resolving angle of $\sim 2°$. This reduces the normalization in the first bins after the threshold for high momenta particles. The behaviour of the acceptance upper mass region is dominated by the hemisphere cut which reduces the acceptance for low momenta.

The shape of the acceptance function in the lower mass region is important for the analysis. Beyond 1.5 GeV the shape is rather unimportant which can be seen later on in the systematics section. Since the whole $\pi^+\pi^-$ mass spectrum is influenced by BEC's it is a correct question if the acceptance is also affected by these distortions. But it was found that these effects are negligible [2] and up to now a test of this fact is very time consuming since a complete full MC sample with BEC switched on does not exist and must have been generated.

4.7.1 The fit procedure

The fit has to take into account all resonances, reflections and the combinatorial background. Within this work all particles which are no $\pi^+\pi^-$ resonances and contain a $\pi^+\pi^-$ pair (e.g. 3 pion decay) or a misidentified K^+K^- or $K\pi$ in their decay chain are considered as reflections. Together with the background and the resonances they build the base for the definition of the fit function. The function used for the fit to the $\pi^+\pi^-$ mass spectrum is defined according to:

$$\begin{aligned} F(m,\lambda,1/\sigma) &= BG(m,\lambda,1/\sigma) + \\ & A_{reso}(m)(n_3 \cdot \rho^0(m,\lambda,1/\sigma) + n_4 \cdot f_2(m,\lambda,1/\sigma) + n_5 \cdot f_0(m)) + \\ & A_{refl}(m) \cdot Refl(K^{*0}, \omega^0, \eta, \eta', K^0_S) \end{aligned} \tag{4.14}$$

with

$$\begin{aligned} BG(m,\lambda,1/\sigma) &= A_{BG(+/-)}(m) BG^{\pm,\mp}(m,\lambda,1/\sigma) - \\ & n_1 \cdot (1 + n_2 \cdot Q) \cdot A_{BG(\pm\pm)}(m) BG^{\pm\pm}(m,\lambda,1/\sigma) \end{aligned} \tag{4.15}$$

where $Q = \sqrt{m_{\pi\pi} - 4m_\pi^2}$.

- $n_3 - n_5$ are the normalizations of the resonances implemented as free parameters in the fit. All signal shapes are normalized such that the total content of each shape is equal to 1. Due to the acceptance function multiplied to the signal shape the normalization can be directly interpreted as number of particles in all events except the normalization of the BG.

- The background is normalized to the the number of data events and so the number n_1 is always close to one. The correction for the long range BE effects (see theory section), controlled by the value of n_2 is small. ($n_2 \ll 1$). Both parameters together control the total size of the subtracted background in such a way that it is not necessary to introduce an additional parameter for the unlike- sign background. One can imagine that the subtracted background can get also negative which is not surprising if we recall the fact that BE effects alter the shape of the unlike-sign background differently compared to the like-sign one.

- Each reflection has its own normalization, but only the values of the ω and the K^{*0} are allowed to vary freely during the fit. This rule is valid as long as the momentum is higher than $x_p = 0.1$. For the two lowest x_p bins, previous measured values [12] have been used for the normalization. The restriction was necessary since the fit routine got in trouble due to less structure in the lowest x_p-bins. Without this restriction the two reflections together with the ρ^0 suppressed all other contribution which is specially critical for the f_0 and the f_2. Since the latter have their maximum of the fragmentation function in the lowest momentum bins it is necessary to force all non resonant signals to stay as close as possible to their measured values.

  For the ω an alternative idea exists. Instead of fixing the total number of the the ω the relationship between the ρ and ω has been used for the control of the ω-normalization.

- The normalization for the η and the η' has been taken from the full MC. This restriction was necessary since the the η and the η' have not been measured in the low momentum ranges with the required precision and the lower edge of the spectrum is very important for the stability, especially for low momentum. These shapes also come from the full MC (detector + cuts) and have normalized to number of data events.

  The same is valid for the K_S^0 - also this normalization has been frozen to the values from the full MC - corrected to the number of data events.

The production of the shapes of the resonances, BG and the K^{*0}-reflection has been described already in the previous section. For the other reflections (ω, η, ...) the shapes produced by the standard full MC have been used. These shapes include all detector effects and therefore they need no acceptance function. Again the history has been used to identify the correct particle. These shapes also have a statistics of $\sim 10^7$ since they have been produced by the same routine which provides the acceptance function.

For the fit the method of least squares minimization has been used. The algorithm tries to minimize the following function:

$$\chi^2 = \sum_{i=1}^{n} \left(\frac{N_i - f(i)}{\sigma_i} \right)^2 \rightarrow Minimum \tag{4.16}$$

where N_i represents the data and σ_i the corresponding statistical error; f(i) is the fit function at the i^{th} mass bin. The algorithm itself has been provided by PAW which uses the the minimizing package MINUIT. After the fit 4 criteria must have been fulfilled before a fit was accepted:

→ The χ^2/dof should be as close as possible to 1.

→ The extracted values of the reflections (ω, K^{*0}) should agree within 1σ with the earlier measurements.

→ The fit must also agree beyond the measured mass range.

→ The result should also be ok by eye.

A very critical point for the success of the fit is the implementation of the BEC into the fit routine. The BE effect is parameterized by two parameters which are both implemented as free factors. Since it is not possible to produce the shapes with the correct distortion in real time nor it is possible to generate them for each value in advance I have interpolated between a given set of shapes with different parameters. This interpolation happens during the fit and increases the computation time enormously. The interpolation is necessary since number of sets produced with JETSET is naturally limited by the computing power of the resources. (The production of $6 * 10^6$ events including BEC takes ~ 17 cpu hours on a machine with 70 cern units) The interpolation takes place for each shape affected by the BE correlations according to the following definitions:

$$Z(x_1, y) = Z(x_1, y_1) + \frac{Z(x_1, y_2) - Z(x_1, y_1)}{y_2 - y_1} \cdot (y - y_1) \tag{4.17}$$

$$Z(x_2, y) = Z(x_2, y_1) + \frac{Z(x_2, y_2) - Z(x_2, y_1)}{y_2 - y_1} \cdot (y - y_1) \tag{4.18}$$

$$Z(x,y) = Z(x_1,y) + \frac{Z(x_2,y) - Z(x_1,y)}{x_2 - x_1} \cdot (x - x_1)$$

It is a two dimensional linear interpolation where λ represents x and the y stands for the $1/\sigma$. Every fit must be started with different initial values to find a stable minimum. To allow also higher values as prepared by the parameter sets I included also an extrapolation feature which allows to extrapolate using the two last bases of the linear extrapolation. This whole interpolation procedure has been tested in a first fit series with only one parameter (λ) and it showed, that the routine can be extended to the full version without loosing stability.

The mass range, of the fit has been set to $0.38 - 2.5$ GeV. The lower limit is dictated by the acceptance function because it is only available down to the limit given above. Furthermore I tried to avoid the mass range of the two reflections η, η' to minimize the influence of them. The characteristic behaviour of these particles in the low momentum region are rather uncertain and thats why I avoid them. The upper limit is set by the fact that it should be avoided to include the upper end of the generated shapes since the inclusion of such an edge and the corresponding discontinousity endangers the stability of the fit routine. Furthermore beyond 2.5 GeV the spectrum is dominated by the background, and so no important information gets lost when the fit range is restricted. Finally this range reduction saves a lot of cpu time.

Remark: Since different parameterizations exist for the same particles, it must be defined what is the normalization for a shape. The ρ^0 and the f_2 are very broad and have long tails therefore the results of the fit for the three particles do not directly correspond to the number of particles per event. Following a previous analysis [12], a fix defined mass range will be used to determine if this signal can be accounted for this resonance.

$$n_S = n_{S'} \frac{\int_{m_0-2.5\Gamma}^{m_0+2.5\Gamma} f_S(m)dm}{\int_{min}^{max} f_S(m)dm} \tag{4.19}$$

where $n_{S'}$ is the number of particles measured with the fit; n_S is the final (corrected) number of particles; S stands for the signal type. The integration has been performed numerically since the BW-functions are hard to calculate analytically.

The fits have been performed in eight x_p intervals - each in the dedicated mass range.

To keep the fit routine stable was the most sophisticated problem. The more sources with strong fluctuating parts or discontinousities the more unstable gets the fit. In the following I present the most important distortions.

- The BE interpolation routine introduces some fluctuations which can be discarded as long as the initial values for the fit are not set to completely stupid numbers. But it is necessary to vary the initial values as already mentioned above to find the global minimum.

- A further source of instability is the acceptance function which heavily fluctuates in the mass range of the f_2 and for the K^{*0} respectively. Although the overall statistics are high due to the low multiplicity of the f_2 the signal is very small and incorporates large statistical errors. If one could increase the statistics which is nearly not possible since the whole generation process of an adequate number takes to much time one could improve the situation. But not only the statistics are the problem - since the acceptance function is the ratio of two fluctuating distribution we import further fluctuations. A possibility to cure the problem is to smooth the acceptance function which reduces the distortions but also removes some important characteristics of whole acceptance function.

As we will see in the systematics sections neither the BEC nor the acceptance function are critical.

To stabilize the fit I had to reduce the number of degrees of freedom. In a first step the BE parameters have been fixed to an average value known from earlier measurements. if the fit fails, the normalizations of the reflections have been fixed too. In all cases these restrictions stabilized the fit. The results from this fit have been taken as input for the fit routine but this time with released parameters. The fit routine is very sensitive to unphysical errors as it happens if a particle hasn't been included. This was the reason for finding the problem with the BEC parameter (look up section 4.4). But as long as the physics are correct the routine works fine. A further indicator for the quality of the fit can be defined with the following function.

$$Q_i = \sum_{n=i-1}^{n=i+1} \frac{(N_n - f(n))^2}{3} \tag{4.20}$$

This function measures the distance of the fit function to the data averaged over 3 bins. If the fit fails for specific bins this function would show a peak (discontiousity) at this position.

The background contains also other particles as we can see in Fig.4.59 where we find a charmed meson decay ($D^0 \rightarrow K\pi$) positioned just below 1.8 GeV.

The fits obtained with the fit routine described above with the smallest χ^2 for each x_p-bin are shown in Fig. 4.52-4.59. Each plot contains the data with the according fit, additionally the three resonances have been included in every picture. The errors are statistical only and disappear in the plots behind the data crosses for low momenta.

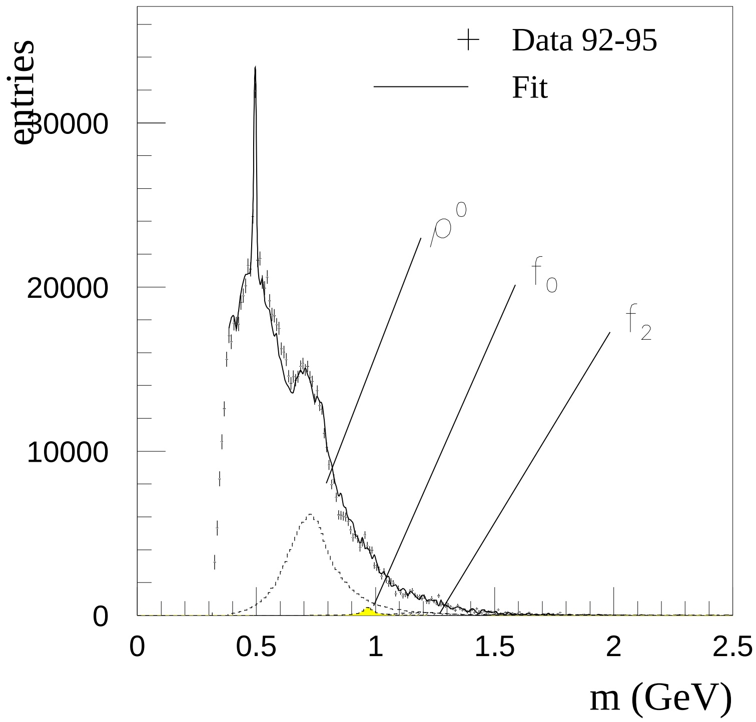

Figure 4.52: x_p=0.005-0.025

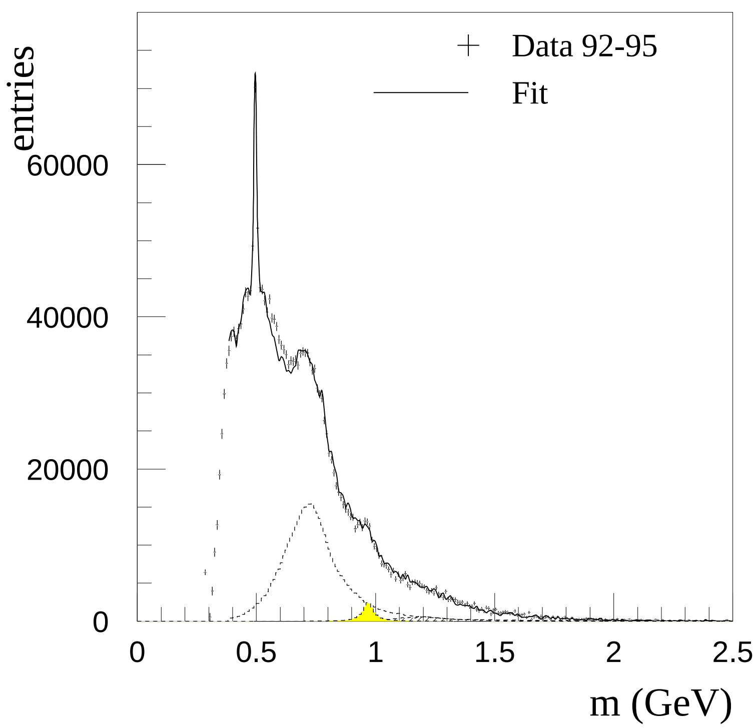

Figure 4.53: x_p=0.025-0.05

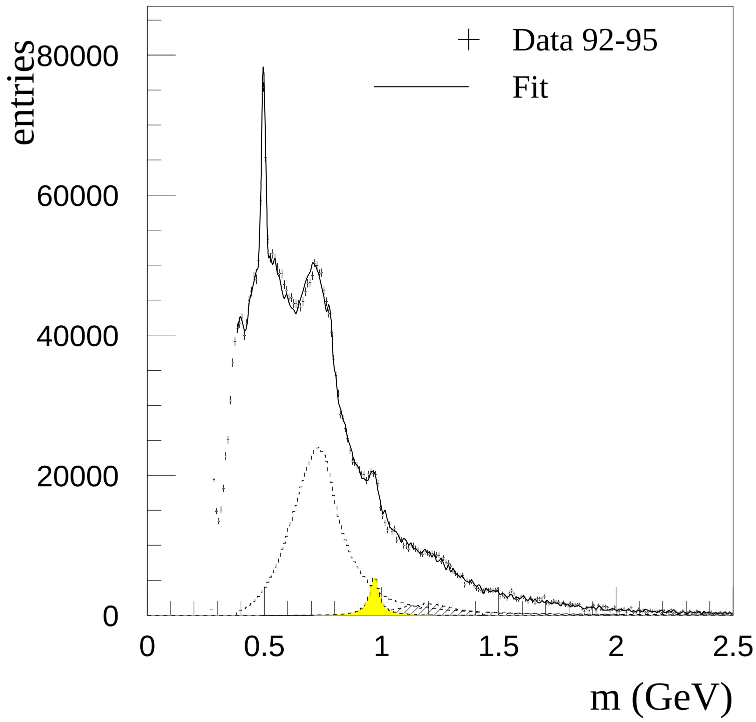

11

Figure 4.54: x_p=0.05-0.1

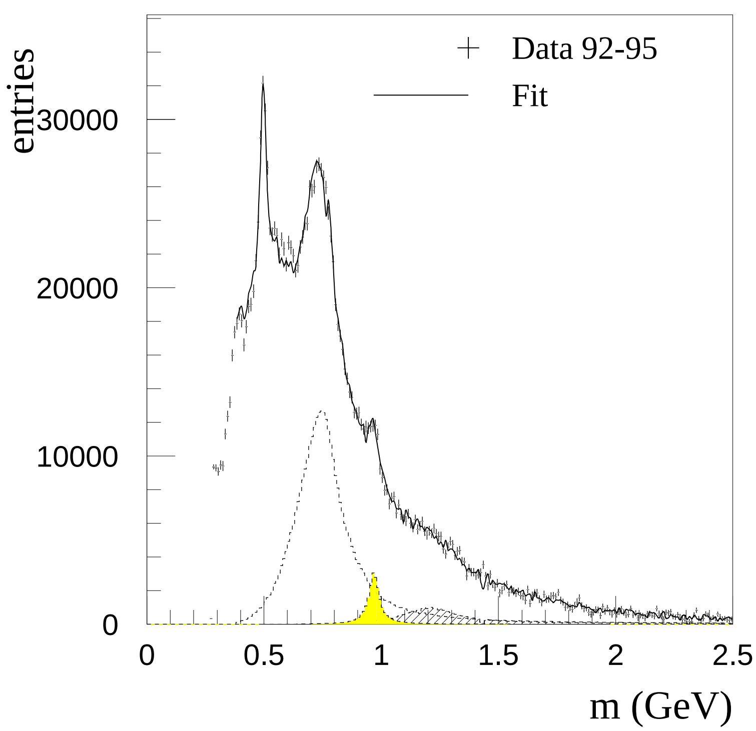

Figure 4.55: x_p=0.1-0.15

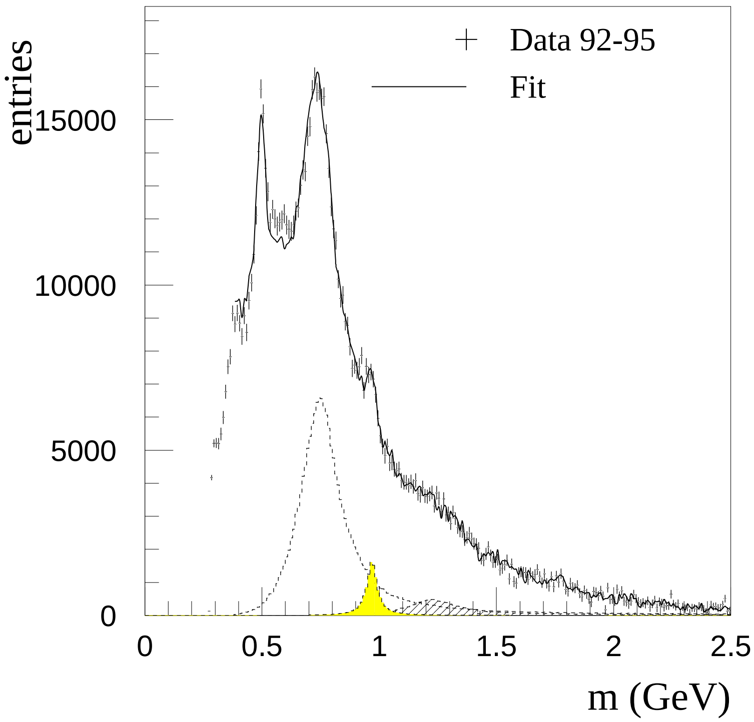

Figure 4.56: x_p=0.15-0.2

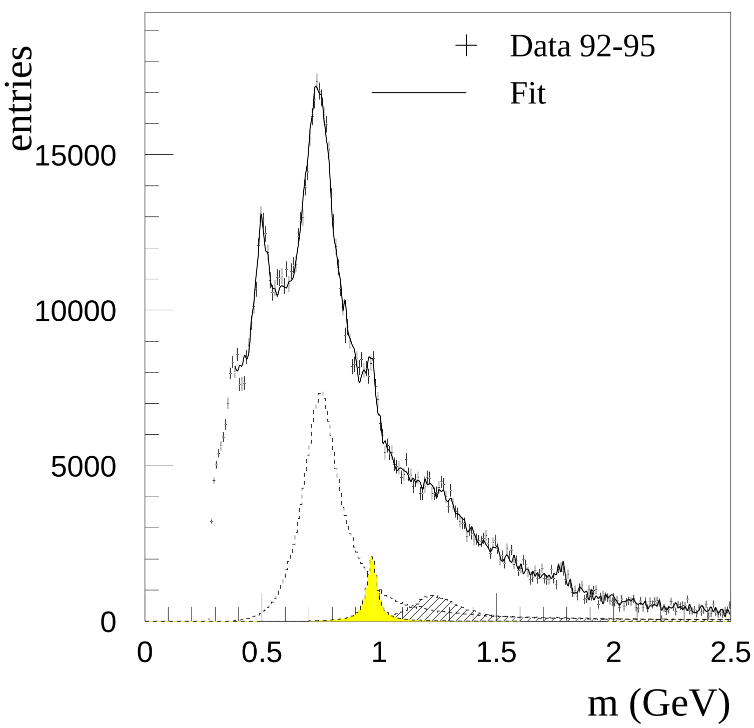

Figure 4.57: x_p=0.2-0.3

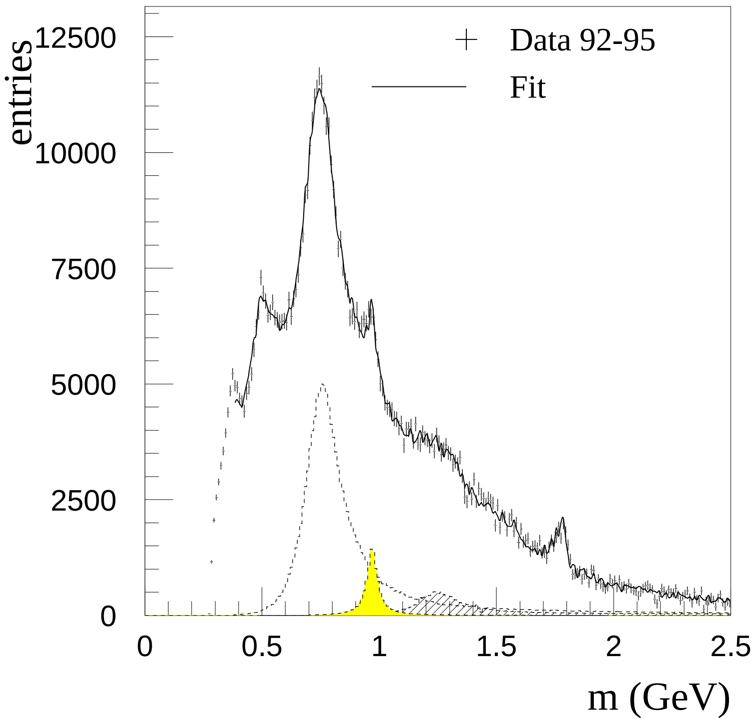

Figure 4.58: x_p=0.3-0.5

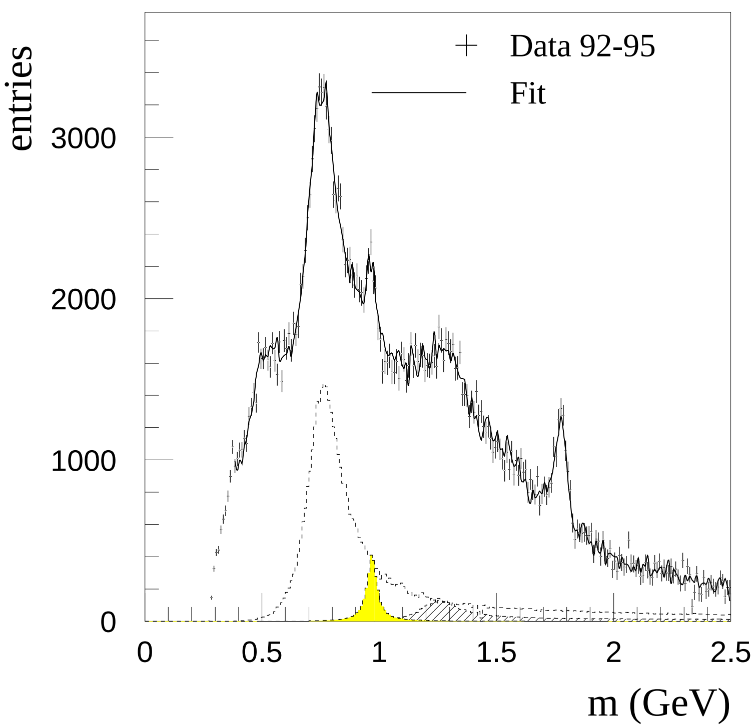

Figure 4.59: x_p=0.5-1.0

x_p-range	Multiplicity ρ^0 /Z decay	$1/\sigma_{had} d\sigma/dx_p$	χ^2/dof
0.005 - 0.025	0.240±0.0107±0.0101	12.62±0.53±0.51	2.69
0.025 - 0.05	0.330±0.0084±0.0257	13.20±0.34±1.03	2.36
0.05 - 0.1	0.387±0.008±0.0136	7.75±0.16±0.27	1.94
0.1 - 0.15	0.189±0.0050±0.0070	3.78±0.10±0.14	2.15
0.15 - 0.2	0.101±0.0032±0.0062	2.018±0.065±0.12	1.54
0.2 - 0.3	0.119±0.0021±0.0031	1.19±0.0205±0.03	1.67
0.3 - 0.5	0.084±0.0020±0.0041	0.42±0.01±0.02	1.54
0.5 - 1.0	0.021±0.0007±0.0013	0.04±0.00±0.00	1.47
0.005-1.00	1.4710±0.01781±0.0621		1.92
all x_p	1.478±0.018±0.0621		

Table 4.8: Measured multiplicities and differential cross sections for ρ^0 . (extrapolated to the full x_p range.)

4.8 Results and Discussion

The final values are presented in Table 4.8-4.8, for each measured momentum interval, in the form of the production rates per event and the differential cross section. The two quantities have been obtained as follows. The production rate has been extracted from the fit for each x_p interval. The recalculated number, according Eqn. 4.19 has been normalized to the number of data events (2.766.134 data events).

The numbers of f_2 and f_0 additionally have been corrected for their branching ratios and their isospin state [20].
Dividing the multiplicity by the size of the momentum interval we obtain the differential cross section for each x_p-interval. The first error is statistical the second is the systematical error. The errors of the total multiplicity have been calculated as the sum in quadrature of the intervals, assuming that the results of the intervals are uncorrelated to each other. The systematical errors are discussed in the next section.

At this stage one would expect further corrections due to the detector but since the acceptance functions incorporate all these effects this step can be discarded. The values should be corrected for an event selection bias which has been neglected up to now since the change is expected to be less than 1-2%.

x_p-range	Multiplicity f_0 /Z decay	$1/\sigma_{had} d\sigma/dx_p$	χ^2/dof
0.005 - 0.025	0.0117±0.0032±0.0061	0.59±0.16±0.31	2.69
0.025 - 0.05	0.0292±0.0032±0.0039	1.17±0.13±0.15	2.36
0.05 - 0.1	0.0497±0.0027±0.0035	0.99±0.05±0.07	1.94
0.1 - 0.15	0.0256±0.0019±0.0017	0.51±0.04±0.03	2.15
0.15 - 0.2	0.0155±0.0014±0.0014	0.31±0.03±0.03	1.54
0.2 - 0.3	0.0187±0.0011±0.0008	0.19±0.01±0.01	1.67
0.3 - 0.5	0.0136±0.00200±0.0008	0.07±0.01±0.00	1.54
0.5 - 1.0	0.0032±0.0004±0.0004	0.01±0.00±0.00	1.47
0.005-1.00	0.1618±0.006±0.0135		1.92
all x_p	0.1673±0.018±0.0135		

Table 4.9: Measured multiplicities and differential cross sections for the f_0 . (extrapolated to the full x_p range.)

x_p-range	Multiplicity f_2 /Z decay	$1/\sigma_{had} d\sigma/dx_p$	χ^2/dof
0.005 - 0.025	0.0163±0.0053±0.0051	0.82±0.27±0.26	2.69
0.025 - 0.05	0.0315±0.0070±0.0038	1.27±0.28±0.15	2.36
0.05 - 0.1	0.0632±0.0063±0.0064	1.28±0.13±0.13	1.94
0.1 - 0.15	0.0338±0.0038±0.0040	0.68±0.07±0.08	2.15
0.15 - 0.2	0.0195±0.0015±0.0021	0.39±0.03±0.04	1.54
0.2 - 0.3	0.0269±0.0014±0.0025	0.271±0.02±0.03	1.67
0.3 - 0.5	0.0145±0.0019±0.0015	0.14±0.01±0.01	1.54
0.5 - 1.0	0.0035±0.0008±0.0003	0.01±0.00±0.00	1.47
0.005-1.00	0.210±0.0118±0.0203		
all x_p	0.210±0.0118 ±0.0203		

Table 4.10: Measured multiplicities and differential cross sections for the f_2 . (extrapolated to the full x_p range.)

x_p- range	λ	$1/\sigma$
0.050-0.1	2.58±0.071	0.34± 0.0088
0.100-0.15	2.29±0.077	0.35±0.0088
0.15- 0.2	2.43±0.061	0.33±0.0065
0.2 - 0.3	1.74±0.040	0.35±0.0064
0.3 - 0.5	1.32±0.069	0.33±0.0068
0.5 - 1.0	1.67±0.058	0.33±0.0067

Table 4.11: The BE parameters which have been obtained by the fits to the $\pi^+\pi^-$ spectrum

Each fit (x_p-range) is given with its χ^2/dof[7] which decreases with higher momenta. This improvement of the fit for high momenta originates from the clear structure that can be found for this momentum range. (e.g. see Fig.4.59) In the low momentum region the differential cross sections of the ω and the ρ^0 are nearly the same and so they form one big bump that nearly hides all other contributions. Furthermore the statistical error for low momentum range is much smaller and this increases the χ^2 too. Nevertheless the indicator (χ^2) stays around 1-2 signaling a good quality of the fit.

As already mentioned the measurement covers the momentum range $x_p > 0.005$. To extract the total multiplicity an extrapolation for the lowest x_p has been applied. A calculation with JETSET delivers a missing multiplicity of 0.5 % for the ρ^0 and similar numbers for the f_2 and the f_0 . JETSET is also the tool to recover this missing part. The fragmentation functions of the JETSET model calculation describes real data well especially in the low momentum region and therefore they have been used for this extrapolation[12].

Each fit returns a pair of BE parameters listed in Table 4.11. For the two lowest x_p bins (x_2, x_3) the BE parameters have been fixed to the average values of all fits with higher momentum ($x_p = 0.05 - 1.0$).

4.8.1 Systematics

Every measurement incorporates errors of various sources. These errors can be subdivided into the statistical and the systematic errors. The first type can be reduced with increasing statistics and can be calculated with an adequate theory. The systematic errors are somehow more difficult

[7] dof...degrees of freedom

to include since they arise from incomplete knowledge of the characteristics of the experiment (e.g. electronical and mechanical distortions, incomplete knowledge about the detector,...) and also incomplete knowledge of the physics theories behind. Since no theory exists for the treatment of such errors the decision whether it is an error or not depends on the analysis.

Nevertheless in HEP one possible method to estimate such errors is to vary the parameters which have been used to select the events or tracks within a defined range and compared to the results obtained with the default set. This means that each analysis must be computed again several times with different options and the maximum difference of the results compared to the nominal result with the default cuts corresponds to the uncertainty due to this selection-criteria. Of course this error does not parameterize a certain source but is a mixture of different sources.

The computational efford of this method is enormous since the whole analysis often must be recomputed and all events (data and MC) must be analyzed more than once. Other systematic errors arise from the method of the analysis itself. (extraction functions, acceptance calculation, ...)

Within this analysis the following sources of systematical errors have been examined.

- The cuts for the event-selection and the selection criteria of the tracks have been varied.
  1. d_0: 0.2 cm to 2 cm
  2. z_0: 2 cm to 10 cm
  3. dE/dx selection: χ <2 and χ <4, minimum number of wires = 80
- The lower edge of the fit range has been varied from 0.38 to 0.5 and the upper limit from 2.2 to 2.8. It was not meaningful to lower the limit of 0.38 because no acceptance function exists for the resonances below this value.
- The masses and widths of the shapes used for the fit have been varied within their uncertainties given in the PDG [20].
- The normalizations of the acceptance functions in the extrapolated region have been varied by 15% and also different parameterizations (constant, polynomial) for the extrapolation have been used.
- The normalization of the K^{*0}, the ω and the K^0_S have been varied by 15% in the x_p ranges where they have been fixed.

x_p-range	fit-range	dE/dx	acc.	d_0, z_0	K^{*0}, ...	m_0,Γ_0	Syst. E
0.005 - 0.025	1.95	3.47	0.63	0.90	0.63	0.52	4.20
0.025 - 0.05	2.70	5.00	3.17	0.60	2.38	3.49	7.78
0.05 - 0.1	0.68	2.35	0.76	1.59	1.65	0.70	3.51
0.1 - 0.15	1.91	2.04	1.27	0.09	1.17	1.75	3.72
0.15 - 0.2	0.69	5.94	0.72	0.14	0.95	0.77	6.15
0.2 - 0.3	0.46	0.59	1.35	0.37	0.73	1.95	2.62
0.3 - 0.5	0.28	4.71	1.00	0.84	0.30	0.31	4.91
0.5 - 1.0	0.43	5.83	0.23	1.86	0.31	1.20	6.26
all x_p	0.96	1.27	1.09	0.55	3.40	1.50	4.22

Table 4.12: Systematic errors for the ρ^0 given in percent for each x_p interval.

- The shape of the f_0 and the f_2 have been parameterized differently. (Flatte for the f_0 ; Parameterization a la Allison Wright [44] for the f_2)
- Uncertainties due to the errors of the branching ratios also have been included.
- For the BE correlations no systematic studies have been done.

In the following tables the row titled with acc. corresponds to the acceptance; the title K^{*0},... includes the systematics of the K^{*0}, K^0_S and ω; the last row is the quadratic sum of all error sources;

In the Tables 4.12-4.14 all systematic errors are listed for each x_p interval and for each resonances with the errors in percent. The errors have been calculated as the maximum difference between the default multiplicity and the new calculated one. The total systematic error is the sum in quadrature of the errors from the different sources. For the values for all x_p the fit results have been summed up over all x_p and then the error has been calculated for each error source.

Table 4.15 shows the obtained results for each resonance with the different sources of error given in percent.

x_p-range	fit-range	dE/dx	acc.	d_0, z_0	K^{*0}, ...	m_0, Γ_0	br. ratio	Syst.E.
0.005 - 0.025	6.35	21.75	19.38	9.00	1.34	2.58	0.06	31.28
0.025 - 0.05	8.55	7.24	2.87	0.77	2.30	2.91	0.11	12.17
0.05 - 0.1	1.78	6.18	4.45	4.93	2.31	3.60	0.22	10.19
0.1 - 0.15	5.41	8.71	2.94	0.78	0.50	5.04	0.12	11.83
0.15 - 0.2	1.62	8.53	2.69	2.58	0.13	4.86	0.07	10.63
0.2 - 0.3	1.45	5.89	1.84	0.89	2.35	6.50	0.10	9.42
0.3 - 0.5	0.80	1.59	4.09	6.90	0.79	6.02	0.05	10.23
0.5 - 1.0	0.66	1.38	3.64	5.57	0.95	4.53	0.01	8.19
all x_p	2.23	7.24	3.81	1.49	1.81	3.93	0.60	9.65

Table 4.13: Systematic errors for the f_2 given in percent for each x_p interval.

x_p-range	fit-range	dE/dx	acc.	d_0, z_0	K^{*0}, ...	m_0, Γ_0	br. ratio	Syst.E.
0.005 - 0.025	4.65	41.7	5.11	29.89	2.84	7.31	0.04	52.36
0.025 - 0.05	2.23	10.1	0.81	0.63	3.82	7.50	0.09	13.37
0.05 - 0.1	0.31	1.04	0.54	3.80	3.92	4.32	0.15	7.07
0.1 - 0.15	2.61	4.59	3.03	1.46	2.69	2.62	0.08	7.30
0.15 - 0.2	2.02	8.84	0.41	1.22	0.78	0.82	0.05	9.23
0.2 - 0.3	1.92	3.47	0.72	1.06	1.29	0.92	0.06	4.46
0.3 - 0.5	0.68	3.22	2.82	3.37	2.35	1.27	0.04	6.11
0.5 - 1.0	1.25	3.22	3.78	10.30	4.80	1.86	0.01	12.60
all x_p	0.69	4.86	2.10	1.58	3.25	4.80	0.50	8.05

Table 4.14: Systematic errors for the f_0 given in percent for each x_p interval.

source of error	ρ^0	f_0	f_2
fit range	0.96	0.69	2.23
K^{0*} and other	3.40	3.25	1.81
acceptance	1.09	2.10	3.81
d_0, z_0	0.55	1.58	1.49
dE/dx	1.27	4.86	7.24
m_0,Γ_0	1.50	4.80	3.93
sum in quadrature	4.22	8.05	9.65

Table 4.15: Sources of systematic error. All of values are given in percent.

4.8.2 Discussion

In the Figures 4.60 - 4.62 the differential cross-sections are shown compared to the values obtained using the JETSET model. The errors in the plots are the total errors computed as the sum in quadrature from the statistical and the systematical error.
The parameters of the JETSET model have been tuned on ALEPH event shape and single charged particle distributions but also on ALEPH inclusive spectra of various particles [33]. The ρ^0 has been compared also to an older measurement which has been done with less statistics [12]. For the ρ^0 we find a good agreement to the values obtained by the earlier measurement over the full x_p-range. If we compare the total numbers of both measurements we also find an agreement within 1σ as well as for the number obtained from JETSET. The major difference is the smaller statistical error due to the 4 times higher statistics. The systematical error for the ρ^0 is dominated by the K^{*0} which is positioned just below the ρ^0 . A change of its normalization of 15% causes a change in the multiplicity for the ρ^0 . All other contribution are small. Also the shape of the acceptance function does not distort the results.

If one tries to compare the number obtained from BE correlation to the results of other measurements one has to compare first the fixed values (χ, number of participating particles) since other experiments use different assumptions. From this we can see that other experiments have different definitions. If we compare the results to the previous ALEPH measurement we find a good agreement.

For the f_0 the situation looks rather different, since no direct comparison can be made. The models have not been tuned yet to fit this resonance since it is difficult to measure - (no earlier measurements exist [8]) - so the overall data/MC normalization differs significantly. It should be remarked that the MC normalization of the f_0 has been calculated via a spin counting method for the p-wave mesons in JETSET. Nevertheless the slope agrees over almost the full momentum range and this supports the assumption that the f_0 can be described as a $q\bar{q}$ scalar meson. A further fact which indicates that the f_0 is scalar $q\bar{q}$ meson, is the parameterization with a BW function. Furthermore this parameterization delivers a mass and a width compatible with the PDG [20] values. It also was an interesting observation, that the f_0 is not affected by BEC, since this supports the idea that particles above a certain lifetime do not participate to this effect.
The reason for the rather large systematical error due to the K^{*0} is an indirect consequence since the distortion of the ρ^0 influences the f_0 . For the f_0 of course the influence of the extrapolation

[8] No ALEPH measurements!

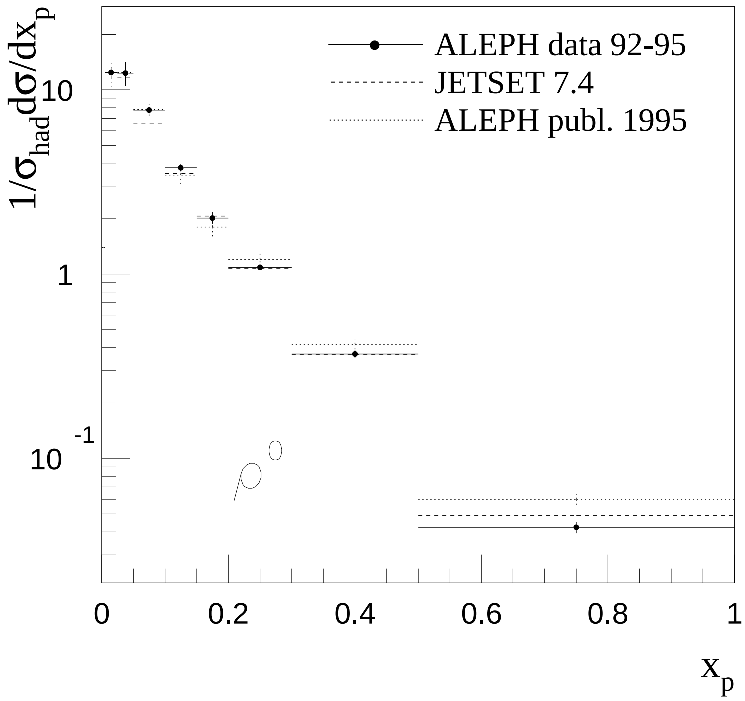

Figure 4.60: Fragmentation function for the ρ^0 .

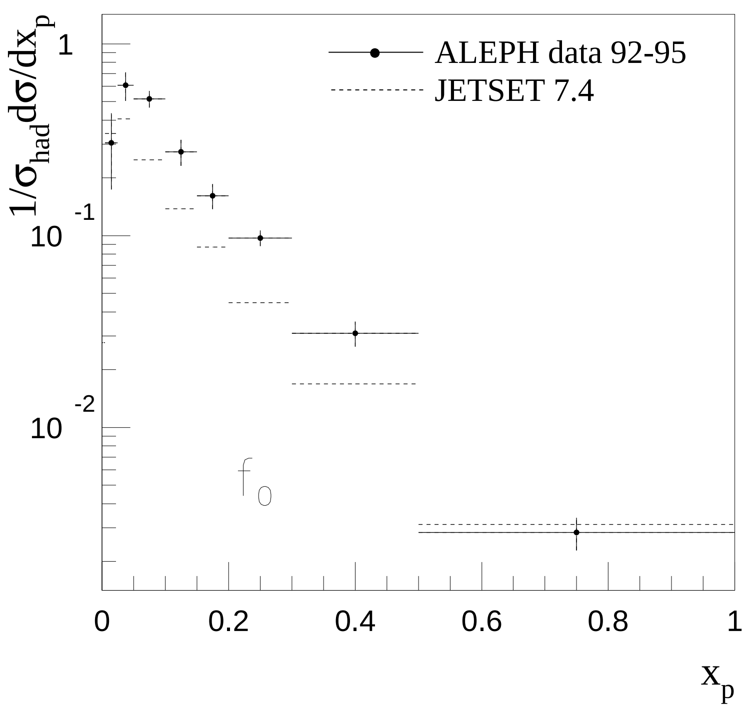

Figure 4.61: Fragmentation fumction for the f_0

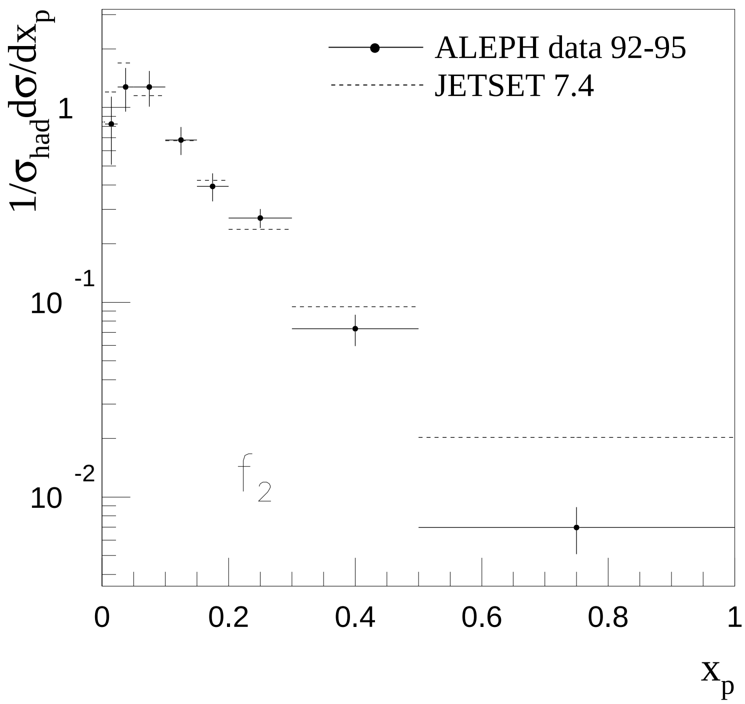

Figure 4.62: Fragmentation function for the f_2

of the acceptance function is more important than it has been for the ρ^0 . A large error arises from the large uncertainty of the width which ranges from 40 to 100 MeV [20].

The fragmentation function of the f_2 (Fig.4.62) fluctuates around the values of JETSET model with rather high errors. The picture indicates that the fragmentation function seems to be softer than expected from the JETSET. But due to large errors one must be careful. Again the fact that the f_2 is clearly affected by the BE effects indicates, that the parameterization model of the BEC can't be completely wrong. From the systematic errors it can be seen where the fit didn't succeed without reducing the dregrees of freedom. In this areas it was necessary to fix some of the degrees of freedom e.g. normalization of the K^{*0}. Whereas in the upper x_p intervals other resonances hide it (the tail of ρ^0), in the lower momentum ranges the f_2 nearly vanishes. Due to the distance in the spectrum of the f_2 to the K^{*0} this error is smaller compared to the ρ^0 and the f_0 . But on the other hand it is clear that the extrapolation of the acceptance function causes a larger error since the f_2 is closer to the extrapolated area. If we check the range of variation for the systematic-study of the fit range we see that mainly the tail of the f_2 is affected and this causes the increased error.

	$\rho^0(770)$	$f_0(980)$	$f_2(1270)$
ALEPH	1.478±0.018±0.0634	0.1673±0.018±0.0162	0.210±0.0118 ±0.0143
DELPHI	1.192±0.059±0.085	0.164±0.015±0.015	0.214±0.032±0.020
OPAL		0.141±0.007±0.011	0.155±0.011±0.018

Table 4.16: Measured average multiplicities for ρ^0 , f_0 , f_2 per hadronic Z decay, compared to the results from other LEP experiment.

If we compare the multiplicities of the resonances to other experiments (Table 4.16) we find some differences for the ρ^0 compared to DELPHI. Since their measurement used only a 2/3 of the available multiplicity and the BEC have treated differently one has to be careful comparing the results. The different implementation of the BEC in addition to their parameterization of the background makes it difficult to find out the reason for the different results. For the f_0 we find a good agreement (within 1σ) between the different experiments. The small difference observed by OPAL can originate from the different parameterization of the f_0 shape (Flatte). Furthermore OPAL neglected all effects concerning the ρ^0 since they included it only as background. (e.g. they didn't include a tail for the ρ^0 - resonances) For the f_2 we find a good agreement with DELPHI and the different result of OPAL could be again a consequence of the fact that they didn't investigate that much into the ρ^0 (no tail, no BEC for the ρ^0).

The inclusive spectra of particles with different spin states help us to understand the relative probabilities for spin state to be produced within the hadronization. A measurement of such a ratio can be used as an input for a MC generator. Two different ratios can be identified with the obtained results.

1. Tensor/Vector - Meson

It has been expected that the fragmentation function of tensor mesons is slightly harder than that of the vector mesons [27] From Table 4.17 where the ratio f_2 $/\rho^0$ for different x_p is presented, we can see that the fragmentation function agrees with the JETSET calculation. A slight rise in the fragmentation function can be observed (Figure 4.63) which indicates the harder production.

2. Scalar/Vector Meson

For this result no JETSET calculations are available. The fragmentation function behaves similar to the one of the f_2 as it is pointed out in Figure 4.64. This picture will be stressed by the next ratio.

3. Scalar/Tensor - Meson

x_p -range	f_2 / ρ^0 (measured)	f_2 / ρ^0 (JETSET)
0.005 - 0.025	0.0678±0.0266	0.0856
0.025 - 0.05	0.0955±0.0244	0.1696
0.05 - 0.1	0.1646±0.0203	0.1688
0.1 - 0.15	0.1803±0.0257	0.1818
0.15 - 0.2	0.1952±0.0341	0.2194
0.2 - 0.3	0.2284±0.0217	0.1981
0.3 - 0.5	0.1744±0.0271	0.2234
0.5 - 1.0	0.1653±0.0474	0.3471
average:	0.1591±0.0284	0.1992

Table 4.17: The ratio Tensormeson/Vectormeson with the f_2 and the ρ^0

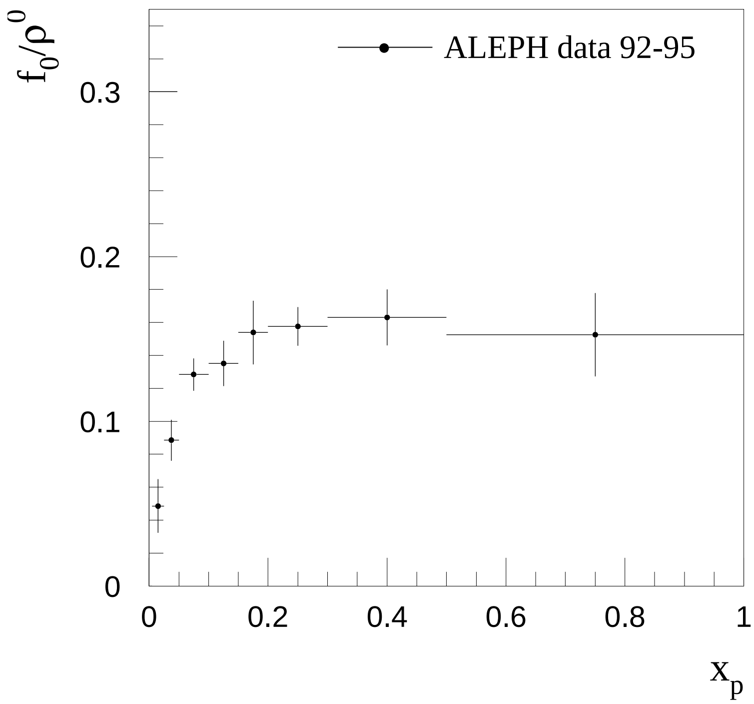

Figure 4.63: Comparison of the fragmentation functions for the ρ^0 and the f_0

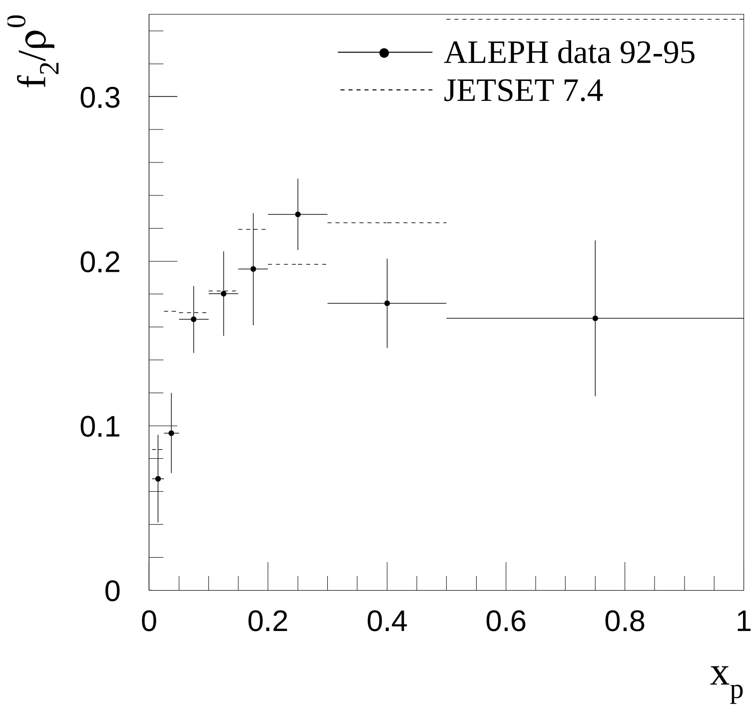

Figure 4.64: Comparison of the fragmentation functions for the ρ^0 and the f_2

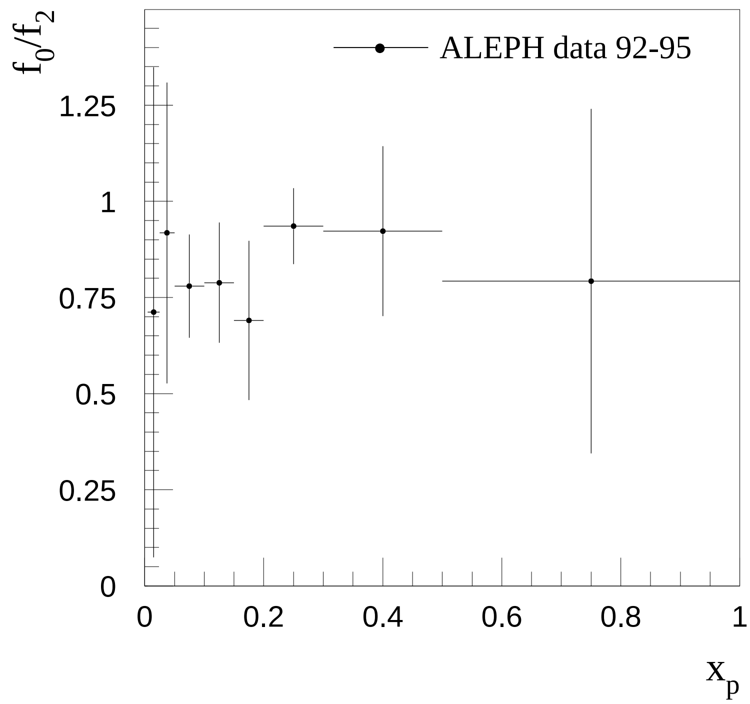

Figure 4.65: Comparison of the fragmentation functions for the f_0 and the f_2

x_p -range	f_0 / ρ^0 (measured)
0.005 - 0.025	0.0486±0.0163
0.025 - 0.05	0.0885±0.0124
0.05 - 0.1	0.1284±0.0098
0.1 - 0.15	0.1352±0.0138
0.15 - 0.2	0.1539±0.0193
0.2 - 0.3	0.1576±0.0118
0.3 - 0.5	0.1631±0.0170
0.5 - 1.0	0.1525±0.0253
average:	0.1285±0.0157

Table 4.18: The ratio Scalarmeson/Vectormeson with the f_0 and the ρ^0

x_p -range	f_0 / f_2 (measured)
0.005 - 0.025	0.7115±0.6369
0.025 - 0.05	0.9179±0.3910
0.05 - 0.1	0.7797±0.1341
0.1 - 0.15	0.7885±0.1561
0.15 - 0.2	0.6902±0.2069
0.2 - 0.3	0.9353±0.0988
0.3 - 0.5	0.9223±0.2208
0.5 - 1.0	0.7928±0.4480
average:	0.8119±0.2866

Table 4.19: The ratio Tensor-meson/Vector-meson with the f_2 and the ρ^0

Chapter 5

Conclusion

The fragmentation functions and total inclusive rates for the resonances ρ^0 , f_0 and f_2 , have been measured at the Z peak using most of the LEP1 statistics. The total multiplicity of the ρ^0 (1.478±0.018±0.0621) is close to the previous measured value and the value of the JETSET model.The discrepancy between the result and the value obtained by DELPHI should be mentioned although it is difficult to compare the numbers since DELPHI used a different parameterization for BEC and different BG shapes. For the two other resonances no JETSET calculations are available and also no earlier ALEPH measurements. But there is good agreement (1 σ)of the numbers of the f_2 (0.210±0.0118 ±0.0203) and f_0 (0.1673±0.018±0.0135with the results from DELPHI [5]. In order to explain discrepancies between data and Monte Carlo in the like sign subtracted $\pi^+\pi^-$ mass spectrum, Bose Einstein correlations have been taken into account. For the ρ^0 and the f_2 a distortion due to BE effects can be observed, but not for the f_0 . Also the fragmentation functions have been compared to model calculations where the overall shape agrees for all three. The results support the idea that BE effects are important in multihadronic production processes and confirms the JETSET model with its calculations for the resonances. Nevertheless it is necessary to retune the model to reproduce the new multiplicities.

5.0.3 Outlook

This work is one link in a long chain of studies on particle production and it is clear that also this work can be extended. Nevertheless it should form a solid base for further studies on these particles. In particular it would be of interest to do the study with a full MC with BE included. But also the background contains many particles which should be studied more in detail.

Bibliography

[1] Apsimon. Comparison of photon and hadron induced production of ρ^0 mesons in the energy range of 65 to 175 GeV. *Z. Phys. C*, 53, 1992. OMEGA.

[2] A. Böhrer. Private communication.

[3] A. Böhrer. The ρ^0 line shape confronting Bose Einstein correlations. ALEPH 94-045, 1994.

[4] Abreu et al. Bose Einstein Correlation in the hadronic decays of the Z^0. *Phys. Lett. B*, 286:201–210, 1992. DELPHI.

[5] Abreu et al. Measurement of inclusive production of light meson resonances in hadronic decays of the Z^0. *Phys. Lett. B*, 298:236–246, 1992. DELPHI.

[6] Abreu et al. Production characteristics of K^0 and light meson resonances in hadronic decays of the Z^0. *Z. Phys. C*, 65:587–602, 1994. DELPHI.

[7] Abreu et al. Production of K^0 und light meson resonances in hadronic decays of the Z^0. *Z. Phys. C*, 65:587–602, 1994. DELPHI.

[8] Ackerstaff et al. Production of f^0,f^2 and ϕ in hadronic Z^0 decays. *Eur. Phys. J. C*, 4:19–28, 1998. OPAL.

[9] Acton et al. A study of Bose Einstein correlations in e^+e^- annihilation at LEP. *Phys. Lett. B*, 267:143–153, 1991. OPAL.

[10] Acton et al. Inclusive neutral vector meson production in hadronic Z^0 decays. *Z. Phys. C*, 56:521–536, 1992. OPAL.

[11] Buskulic et al. Performance of the ALEPH detector at LEP. *Nucl. Instrum, Meth. A*, 360:481–506, 1994. ALEPH.

[12] Buskulic et al. Inclusive production of neutral mesons in hadronic Z^0 decays. *Z. Phys. C*, 69:379–392, 1996.

[13] Decamp et al. A study of bose- einstein correlations in e^+e^- annihilation at 91 gev. *Z. Phys. C*, 54:75, 1992. ALEPH.

[14] Juricic et al. Bose- Einstein correlations in e^+e^- collisions. *Phys. Rev. D*, 39:1, 1989.

[15] Buskulic et at. Properties of Hadronic Z decays and test of QCD Generators. *Z. Phys. C*, 55:209–234, 1992. ALEPH.

[16] S.M. Flatte. Coupled Channel Analysis of the $\pi\eta$ and $K\bar{K}$ systems near $k\bar{k}$ threshold. *Phys. Lett. B*, 63:224, 1976.

[17] Fritzsch H.Gell-Mann M.Leytwyler H. Advantages of the Color Octet Gluon picture. *Phys. Lett. B*, 47:365–368, 1973.

[18] GEIGER K.Ellis J.Heinz U.Wiedemann U.A. Bose-einstein correlations in a space-time approach to e^+e^- annihilation into hadrons. CERN-TH/98-345, 1998.

[19] Goldhaber. Influence of Bose Einstein statistics on the antiproton- proton annihilation process. *Phys. Rev.*, 120:300–312, 1995.

[20] Particle Data Group. Review of Particle Physics,. *Europ. Phys. J. C*, 3:94pp, 1998.

[21] Halzen F.Martin A.D. *Quarks & Leptons: An Introductory Course in Modern Particle Physics*. John Wiley & Sons, Inc., 1984.

[22] T. Hebbeker. Tests of Quantum Chromodynamics in hadronic decays of Z^0 bosons produced in e^+e^- annihilation. *Phys. Rept.*, 217:69–157, 1992.

[23] Hernandez R.Herrera G. An estimate of meson size effects on Bose-Einstein correlations. *Phys. Lett. B*, 332:448–450, 1992.

[24] J.D. Jackson. Remarks on the phenomenological analysis of resonances. *Il Nuovo Cimento*, XXXIV:1644–1666, 1964.

[25] Campagne J.E. *Z. Phys. C*, 53:469, 1989. ALEPH.

[26] Altarelli G. Kleiss R. Verzegnassi C. Z Physics at LEP1 - Vol.1 Standard Physics. CERN 89-08 (Yellow Report), 1989.

[27] Lafferty Knowles. Hadronization in z^0 decay. *J. Phys. G*, 23:731–789, 1997.

[28] G.D. Lafferty. Residual Bose Einstein Correlation in inclusive $\pi^+\pi-$ systems and the $\rho(770)^0$ line shape in multihadronic Z^0 decays. *Z. Phys. C*, 60:659–666, 1995.

[29] Gell-Mann M. *Acta Physica Austriaca Suppl.*, IX:733, 1972.

[30] Kobayashi M. and T. Maskawa. CP violation in the renormalizable theory of weak interaction. *Progr. Theor. Phys.*, 49:652–657, 1973.

[31] R. Muresan O. Smirnova, B.Lörstad. Tests of the JETSET Bose-Einstein correlation model in the e^+e^- annihilation process. hep-ex/9808032, 1998.

[32] J.A.M. Rodriguez. *Inclusive Production von K^{0*} Mesonen in hadronischen Zerfällen des Z^0*. PhD thesis, Universität-Gesamthochschule Siegen, 1995.

[33] G. Rudolph. Private communication.

[34] Haywood S. Where are we going with Bose- Einstein Correlation - a Mini Review. *RAL*, (074):40, 1994.

[35] Weinberg S. A model of leptons. *Phys. Rev. Lett.*, 19:1264–1266, 1967.

[36] Sjöstrand. High energy physics event generation with Phythia 5.7 and Jetset 7.4. 1993.

[37] Sjöstrand. Modelling BE-Correlation at lep2. hep-ph/9711460, 1997.

[38] Flatte S.M. On the Nature of 0^+ mesons. *Phys. Lett. B2*, 63:228, 1976.

[39] Suzuki. Bose Einstein Correlation and two body final state interaction of dipion. *Phys. Rev. D*, 35:11, 1987.

[40] Muta T. *Foundations of Quantum Chromodynamics*. World Scientific, 1987.

[41] B.R. Webber. Quantum Chromodynamics. In *1993 European School of High-Energy Physics*, 1994. CERN 94-04 (Yellow Report).

[42] U.A. Wiedemann. Multiparticle Bose-Einstein Correlation. *Phys.Rev. C*, 57:3324–3339, 1998.

[43] de E.A. Wolf. Bose Einstein Correlations and generating functions. IIHE-94.02,IISN0379-301X, 1998.

[44] A. Wright. Search for the glueball candidates $f_0(1500)$ and $f_j(1710)$ in $\gamma\gamma$ collisions. CERN-EP/99-153, 1999.

Lebenslauf

Name	Krebs-Florian Wolfgang
geboren	19.11.1973 in Innsbruck
wohnhaft in	A - 1190 Wien
	Flotowgasse 23/1/8
Eltern	Edvard Krebs
	Rosa Krebs geb. Wallner
Familienstand	verheiratet
Volksschule	1979-1983 in Innsbruck (Wörndlestr.)
Hauptschule	1983-1988 in Innsbruck (Pembaurstr.)
Höhere	1988-1993 in Innsbruck (Anichstr.)
techn. Lehranstalt	Nachrichtentechnik
Studium	1993 Immatrikulation an der
	Universität Innsbruck
	Inskription der Fächer
	Physik und Betriebs-
	wirtschaftslehre